NASA Technical Paper 2253

February 1984

Static Internal Performance Including Thrust Vectoring and Reversing of Two-Dimensional Convergent-Divergent Nozzles

Richard J. Re and
Laurence D. Leavitt

NASA

NASA
Technical
Paper
2253

1984

Static Internal Performance Including Thrust Vectoring and Reversing of Two-Dimensional Convergent-Divergent Nozzles

Richard J. Re and
Laurence D. Leavitt

Langley Research Center
Hampton, Virginia

NASA
National Aeronautics
and Space Administration

**Scientific and Technical
Information Branch**

SUMMARY

The effects of geometric design parameters on two-dimensional convergent-divergent nozzles were investigated at nozzle pressure ratios up to 12 in the static test facility adjacent to the Langley 16-Foot Transonic Tunnel. Forward-flight (dry and afterburning power settings), vectored-thrust (afterburning power setting), and reverse-thrust (dry power setting) nozzles were investigated. The nozzles had thrust vector angles from 0° to 20.26°, throat aspect ratios of 3.696 to 7.612, throat radii from sharp to 2.738 cm, expansion ratios from 1.089 to 1.797, and various sidewall lengths.

The results of this investigation indicate that two-dimensional convergent-divergent nozzles have static internal performance comparable to axisymmetric nozzles with similar expansion ratios. Nozzle expansion flap curvature (radius) at the throat had little effect on thrust ratio, but discharge coefficient decreased by as much as 3.5 percent when the radius was reduced to zero (sharp throat). Nozzle throat aspect ratio (throat width divided by throat height) had little effect on thrust ratio over the range of nozzle pressure ratio tested. A nozzle geometrically vectored at angles up to 20.26° turned the flow at least as much as the design vector angle once nozzle pressure ratio was high enough to eliminate separation on the lower expansion surface. The thrust-reverser nozzles (designed for 50-percent reverse thrust) produced reverse thrust of 50 percent or more when the reverser port passage rear wall was longer than the forward wall.

INTRODUCTION

Studies of expanded operational capabilities for turbofan- and turbojet-powered aircraft at various flight conditions, especially those associated with tactical situations, have given rise to consideration of propulsion system participation in the enhancement of aircraft maneuver, attitude control, landing approach, and landing ground-roll performance. Some of these studies have included propulsion systems with nonaxisymmetric nozzles having the ability to change the direction of the thrust vector to generate other forces and moments (refs. 1 to 7). Nozzles having essentially two-dimensional flow up to the exit have been projected to be competitive with axisymmetric nozzles for level flight and be more amenable to incorporation of thrust vectoring for installed-performance improvements (ref. 8). The emergence of the nonaxisymmetric nozzle as a candidate for these applications has created the need for research on a variety of nozzle types and for parametric data on the effect of component variations on the performance of each.

The three principal types of nonaxisymmetric nozzles on which research data are available include the two-dimensional convergent-divergent (2D-CD) nozzle (refs. 9 to 12), the single-expansion-ramp nozzle (SERN) (refs. 10 to 13), and the wedge nozzle (refs. 11, 12, and 14 to 17). Specific aircraft configurations have been modified and tested in wind tunnels with nonaxisymmetric nozzles (refs. 14, 15, and 18) to obtain installed-performance effects. However, the constraints presented by the location of aircraft components on existing designs can render the conversion to nonaxisymmetric nozzles a difficult task, especially for the in-flight

thrust-reversing mode (ref. 19). When aircraft configurations are initially designed to include multiple-function nozzles, many potential problems can be avoided by proper placement of components (refs. 20 to 22).

One type of nonaxisymmetric nozzle that has been extensively researched is the SERN. Initial development of this type nozzle came from a requirement for a vertical takeoff and landing (VTOL) aircraft, and the nozzle incorporated an exhaust deflector (refs. 20 to 25) to provide high thrust vector angles (up to 110°) at very low airspeeds. Considerable data on static (refs. 10 to 13) and installed (refs. 14, 15, 21, and 22) performance are available for versions of the SERN without a deflector (elimination of VTOL capability).

The 2D-CD nozzle did not receive significant attention as soon as the SERN but has now emerged as a competitive nonaxisymmetric nozzle design for multiple-function applications. (See, for example, ref. 26.) Investigations of specific 2D-CD nozzle designs have been made, although parametric static-performance data on the effect of nozzle component variation are limited (refs. 9 to 12). Reference 10 contains static data on the effect of nozzle parameters such as expansion ratio, sidewall length, flap length, and flap divergence angle. Reference 9 contains static data on the effect of flap radius at the nozzle throat at two expansion ratios as well as comparisons of measured flap surface pressure and nozzle thrust ratio with computational values obtained by the method of reference 27.

The present paper contains static internal performance data for 2D-CD nozzles having geometric variations representative of engine power setting (throat area), sidewall length, throat aspect ratio (throat width divided by throat height), thrust vector angle, and thrust reversing. Thrust-vectoring data were obtained for afterburning power setting at design thrust vector angles of 9.79°, 13.22°, and 20.26° with four sidewall configurations. Throat aspect ratio (3.696 to 7.612) was varied at nozzle expansion ratio of 1.089 and 1.797 by reducing throat height. Sidewall length effects were also determined for two nozzle configurations having large throat aspect ratios. Two nozzles with sharp throats (no radius of curvature at the intersection of the convergent and divergent flaps) were investigated to determine the effect (compared with typical throat radii) on nozzle discharge coefficient. The effect of expansion ratio (1.250 to 1.797) on the internal performance of unvectored dry-power nozzles having a nearly constant flap divergence angle (approximately 10.8°) was also investigated. A thrust-reverser concept for 2D-CD nozzles in which a flow blocker is deployed ahead of the throat while rectangular ports open symmetrically at the top and bottom of the nozzle was also investigated. The design thrust reversal angle of the blocker and port passage was 120° (measured forward from a horizontal reference plane). Reverser configuration variations consisted of port passage length and port door location (external).

The purpose of the investigation was to expand the available internal performance data base for 2D-CD nozzles over a range of nozzle geometries and nozzle design pressure ratios. Internal performance data (thrust ratio, vector angle, and discharge coefficient) were obtained from force balance and flow measurements. Flap internal surface static pressures were measured on some nozzle configurations. Nozzles having a throat area representative of a dry power setting and the thrust reverser were tested at nozzle pressure ratios from 2 to 9. Nozzles having a throat area representative of afterburning power setting were tested at nozzle pressure ratios from 2.0 to 5.5. The nozzles with higher throat aspect ratios (5.806 and 7.612) had smaller throat areas and were tested at nozzle pressure ratios from 2 to 12. This investigation was conducted in the static test facility adjacent to the Langley 16-Foot Transonic Tunnel.

SYMBOLS

All forces and moments (with the exception of resultant gross thrust) and angles are referred to the model centerline (body axis). Nozzle pitching moment is referred to the balance moment center, which is on the model centerline at station 74.65. A detailed discussion of the data-reduction and calibration procedures as well as definitions of forces, angles, and propulsion relationships used herein can be found in reference 11.

AR nozzle throat aspect ratio, w_t/h_t

A_e nozzle exit area, cm^2

A_t nozzle throat area, cm^2

d_{eq} diameter of circle having same area as throat of reheat nozzles, 8.131 cm

F measured thrust along body axis, N

F_i ideal isentropic gross thrust, $w_p\sqrt{RT_{t,j}\frac{2\gamma}{\gamma - 1}\left[1 - \left(\frac{p_\infty}{p_{t,j}}\right)^{\frac{\gamma-1}{\gamma}}\right]}$, N

F_r resultant gross thrust, $\sqrt{F^2 + N^2}$, N

h_b half-height of flow area in reverser before flow is turned into reverser ports (see fig. 7(a)), 3.226 cm

h_e vertical distance between tip of vectored upper flap and horizontal external surface of lower flap (see fig. 3(a)), cm

h_t nozzle throat height (see fig. 2), cm

k_d vertical distance between tip of lower divergent flap and horizontal external surface of lower flap (see fig. 3(a)), cm

k_s vertical distance between tip of lower end point of sidewall and horizontal external surface of lower flap (see. fig. 3(a)), cm

N measured normal force, N

p local static pressure, Pa

$p_{t,j}$ jet total pressure, Pa

p_∞ ambient pressure, Pa

R gas constant, 287.3 J/kg-K

R_t radius of curvature of nozzle flap surface at nozzle throat (see figs. 2 and 3), cm

Sta.	model station, cm
s	thrust-reverser port passage uncontained length (see fig. 7(b)), cm
$T_{t,j}$	jet total temperature, K
v	thrust-reverser port passage contained length (see fig. 7(b)), cm
w_i	ideal mass-flow rate, kg/sec
w_p	measured mass-flow rate, kg/sec
w_t	nozzle throat width, 10.157 cm
w_v	thrust-reverser port opening width (see fig. 7(a)), 1.664 cm
x	axial distance measured from nozzle connect station (Sta. 104.47), positive aft (see fig. 9), cm
x_e	axial distance measured from nozzle connect station to end of nozzle divergent flap (see figs. 2 and 3), cm
x_s	axial distance measured from nozzle connect station to end of nozzle sidewall (see figs. 2 and 3), cm
x_t	axial distance measured from nozzle connect station to nozzle throat (unvectored) station (see figs. 2 and 3), cm
y	lateral distance measured from model centerline, positive to left looking upstream (see fig. 9), cm
z	vertical distance measured from model centerline (see fig. 7(a)), cm
γ	ratio of specific heats, 1.3997 for air
Δ	incremental value
δ_j	resultant thrust vector angle, $\tan^{-1}\frac{N}{F}$, deg
δ_v	design or geometric thrust vector angle measured from horizontal reference line, positive in downward direction, deg
ρ	divergence angle of nozzle divergent flap surface (negative downward for upper flap and positive downward for lower flap), deg

Subscripts:

d	lower
i	internal

max maximum

u upper

Configuration designations:

A1,A2,A3,A4 nozzle configurations having throat aspect ratio 2.012

A1V10,A1V13,A1V20 vectored configurations of A1, where last two digits indicate approximate value of δ_v

A2V10,A2V13,A2V20 vectored configurations of A2, where last two digits indicate approximate value of δ_v

A3V10,A3V13,A3V20 vectored configurations of A3, where last two digits indicate approximate value of δ_v

A4V10,A4V13,A4V20 vectored configurations of A4, where last two digits indicate approximate value of δ_v

B1,B2 nozzle configurations having sharp throats

D1,D2,...,D10 nozzle configurations having throat aspect ratio 3.696

D11V5 nozzle configuration having throat aspect ratio 3.696 and vectored 5°

D12V5 configuration D11V5 with cutback sidewalls

E1,E2,E3,E4 nozzle configurations having throat aspect ratio 5.806

F1,F2,F3,F4 nozzle configurations having throat aspect ratio 7.612

F5V5 nozzle configuration having throat aspect ratio 7.612 and vectored 5°

S1,S2,S3,S4 sidewall configurations

R1,R2,...,R6 reverse-thrust configurations

2D-CD two-dimensional convergent-divergent

APPARATUS AND METHODS

Static-Test Facility

This investigation was conducted in the static-test facility adjacent to the Langley 16-Foot Transonic Tunnel. Test apparatus is installed in a room with a high ceiling. The jet exhausts to atmosphere through a large open doorway. The control room is remotely located from the test area, and a closed-circuit television camera is used to observe the model. This facility utilizes the same clean, dry-air supply as that used in the Langley 16-Foot Transonic Tunnel and a similar air-control system - including valving, filters, and a heat exchanger (to operate the jet flow at constant stagnation temperature).

Single-Engine Propulsion-Simulation System

A sketch of the single-engine air-powered nacelle model on which various nozzles were mounted is presented in figure 1(a) with a typical nozzle configuration installed. The body shell forward of station 52.07 was removed for this investigation.

An external high-pressure air system provided a continuous flow of clean, dry air at a controlled temperature of about 300 K. This high-pressure air was varied up to approximately 12 atm (1 atm = 101.3 kPa) and was brought through the dolly-mounted support strut by six tubes which connect to a high-pressure plenum chamber. As shown in figure 1(b), the air was then discharged perpendicularly into the model low-pressure plenum through eight multiholed sonic nozzles equally spaced around the high-pressure plenum. This method was designed to minimize any forces imposed by the transfer of axial momentum as the air was passed from the nonmetric high-pressure plenum to the metric (mounted on the force balance) low-pressure plenum. Two flexible metal bellows were used as seals and served to compensate for axial forces caused by pressurization. The air was then passed from the model low-pressure plenum (circular in cross section) through a transition section, a choke plate, and an instrumentation section, as shown in figure 1(a). The transition section provided a smooth flow path for the airflow from the round low-pressure plenum to the rectangular choke plate and instrumentation section. The instrumentation section had a flow path width-height ratio of 1.437 and was identical in geometry to the nozzle airflow entrance. The nozzles were attached to the instrumentation section at model station 104.47.

Nozzle Design and Models

Nozzle concept.- The two-dimensional convergent-divergent (2D-CD) nozzle is a nonaxisymmetric exhaust system in which a symmetric contraction and expansion process takes place internally in the vertical plane. Basic nozzle components consist of upper and lower flaps to regulate the contraction and expansion process and flat nozzle sidewalls to contain the flow laterally. The flap inner surface geometry can be varied or altered by actuators so that (1) engine power setting can be changed by varying the throat height (minimum area), and (2) expansion surface angle (flat surface downstream of the throat) can be varied for optimum expansion of the exhaust flow. The flatness of the flaps and sidewalls of the 2D-CD nozzle facilitates the incorporation of performance capabilities not readily amenable to axisymmetric designs. The 2D-CD nozzle can be designed to (1) vector the exhaust flow up or down by varying the geometry of the upper and lower flaps independently and (2) reverse or spoil the thrust by opening ports upstream of the throat while deploying internal blockers from the flaps to divert the flow to the thrust-reverser ports. Many practical mechanical schemes have been proposed to achieve some or all of the aforementioned capabilities but will not be described herein. However, development of a 2D-CD nozzle having multiple capabilities is described in reference 26.

Unvectored- and vectored-thrust nozzle models.- The nozzle models of the present investigation were attached to the propulsion simulation system (fig. 1) at model station 104.47 and had a constant flow path width of 10.157 cm. Parametric nozzle geometry changes were made by combining various interchangeable upper and lower flaps and sidewalls. The parameters for unvectored-thrust nozzles were expansion ratio (A_e/A_t), sidewall length (x_s), flap throat radius (R_t), expansion surface (flap) length, and throat aspect ratio (w_t/h_t). The parameters for the vectored-thrust nozzles were thrust vector angle (δ_v) and sidewall length. The values of the nozzle parameters selected for this investigation are presented in figure 2 for

unvectored-thrust nozzles and in figure 3 for vectored-thrust nozzles. Photographs of unvectored- and vectored-nozzle models with one sidewall removed for viewing are presented in figures 4 through 6.

Reverse-thrust nozzle models.- Conceptually, the thrust-reverser components for the 2D-CD nozzles would be deployed ahead of the throat at dry power settings. Flow would be blocked by components deployed from the flaps while ports would open on the top and bottom of the nozzle contraction section to allow flow to exit with a vector component in the reverse direction. The nozzle minimum area (throat) occurs in the port (exit) passages, which are constant in area along their length. The reverse-thrust angle designed into the hardware was 120° measured forward from a horizontal reference plane; that is, the blocker surface angle was 120°, the passage angle was 120°, and all external port door angles were 120°. Geometrically, 120° can provide a 50-percent component of thrust in the reverse direction.

Nozzle thrust-reverser configurations were built up from different combinations of blocker, flap, door, and sidewall combinations. Details of the six configurations tested are shown in figure 7(b). Configuration variables were port passage length and external port door location. A photograph of a typical thrust-reverser nozzle model with one sidewall removed for viewing is presented in figure 8.

Instrumentation

A three-component strain-gage balance was used to measure the forces and moments on the model downstream of station 52.07 cm. (See fig. 1.) Jet total pressure was measured at a fixed station in the instrumentation section (see fig. 1) by means of a four-probe rake through the upper surface, a three-probe rake through the side, and a three-probe rake through the corner. A thermocouple, also located in the instrumentation section, was used to measure jet total temperature. Mass flow of the high-pressure air supplied to the nozzle was determined from pressure and temperature measurements in the high-pressure plenum (located on top of the support strut) calibrated with standard axisymmetric nozzles. Internal static-pressure orifices were located on some of the nozzle upper and lower flaps (fig. 9) and on the blocker of reverse-thrust configurations (fig. 7(a)). Coordinates of the static-pressure orifices for each flap configuration are given in tables I through IX in nondimensional form as x/x_t and $y/(w_t/2)$.

Data Reduction

All data were recorded simultaneously on magnetic tape. Approximately 50 frames of data, taken at a rate of 10 frames per second, were used for each data point; average values were used in computations. Data were obtained in an ascending order of $p_{t,j}$. With the exception of resultant gross thrust F_r, all force data in this report are referenced to the model centerline.

The basic performance parameter used for the presentation of results is the internal thrust ratio F/F_i, which is the ratio of the actual nozzle thrust (along the body axis) to the ideal nozzle thrust, where ideal nozzle thrust is based on measured mass flow w_p, jet total pressure $p_{t,j}$, and jet total temperature $T_{t,j}$. The balance axial-force measurement, from which actual nozzle thrust is subsequently obtained, is initially corrected for model weight tares and balance interactions. Although the bellows arrangement was designed to eliminate pressure and momentum interactions with the balance, small bellows tares on axial, normal, and pitch

balance components still exist. These tares result from a small pressure difference between the ends of the bellows when internal velocities are high and from small differences in the forward and aft bellows spring constants when the bellows are pressurized. As discussed in reference 11, these bellows tares were determined by running calibration nozzles with known performance over a range of expected normal forces and pitching moments and were applied to the balance data to obtain actual nozzle thrust.

Nozzle discharge coefficient w_p/w_i is the ratio of measured mass flow to ideal mass flow, where ideal mass flow is based on jet total pressure $p_{t,j}$, jet total temperature $T_{t,j}$, and measured nozzle throat area. Nozzle discharge coefficient is, then, a measure of the ability of a nozzle to pass mass flow and is reduced by momentum and vena contracta losses.

PRESENTATION OF RESULTS

The basic nozzle internal performance data obtained in this investigation are presented in figures 10 through 31, which will not be discussed individually. However, reference will be made to the performance of those nozzles directly relevant to the discussion as the need arises. Local static pressures were measured on the nozzle internal expansion surfaces for various nozzle total pressure ratio settings and are presented in ratio form in tables I through IX. Those nozzles on which internal expansion surface static-pressure measurements were obtained are indicated in figures 2 and 3. Ratios of local pressures measured on the reverse-thrust blocker are presented in table X. Samples of pressure data are presented graphically and will be introduced as needed in a later section of this report.

Nozzle internal thrust ratio F/F_i, resultant thrust ratio F_r/F_i, and discharge coefficient w_p/w_i are presented graphically as a function of nozzle pressure ratio in figures 10 through 29. The resultant thrust ratio, shown only for vectored-thrust nozzles, is indicated by a dashed line in figures 27 to 29. Thrust vector angle and pitching-moment ratio are presented in figures 30(a) and (b), respectively, for the vectored-thrust nozzles. Figure 31 presents internal performance data for the thrust-reverser configurations. A negative value of thrust ratio indicates thrust in the reverse direction.

RESULTS AND DISCUSSION

The relative cross-sectional areas of the engine exhaust duct (or augmentor section) and nozzle throat for current axisymmetric nozzle installations at a given power setting establish a basis for selection of rectangular throat aspect ratios (ratio of width to height) for nonaxisymmetric nozzle applications. For example, current axisymmetric installations have nozzle-throat-area to engine-exhaust-duct-area ratios of about 1/3 for dry power setting and 2/3 for afterburning (reheat) power setting. For a simple application where the nonaxisymmetric nozzle is to be blended into the projected area behind the engine, the width of the rectangular nozzle can be assumed to be equal to the engine exhaust diameter. Therefore, throat aspect ratio for dry power nozzles should be about 3.8 and for afterburning nozzles, about 1.9. These numbers are presented merely as typical for a simple application. Other demands on the nozzle, such as a need to generate large amounts of supercirculation (or induced) lift, might make larger values of throat aspect ratio desirable.

With the previous discussion in mind, it can be noted from the nozzle geometric data in figures 2 and 3 that configuration designations starting with the letters "B" and "D" represent dry power configurations and that designations starting with the letter "A" represent afterburning power configurations. Nozzles having designations starting with letters "E" and "F" have larger throat aspect ratios and can be considered for use in more specialized applications.

Unvectored Nozzles

Sidewall geometry.- The effect of sidewall geometry on the internal performance of a throat aspect ratio 2.012 nozzle (representative of afterburning) having an expansion ratio of 1.300 is shown in figure 10. These data show similar effects of sidewall length (cutback) on thrust ratio as reported in reference 10 for aspect ratio 3.696 nozzles (representative of dry power) having expansion ratios of 1.089 and 1.797. That is, for the greatest amount of sidewall cutback (about 75 percent), there was only a small loss in maximum thrust ratio (approximately 1/2 percent for the present investigation). At low off-design nozzle pressure ratios, thrust ratio increased when the sidewalls were cut back. Closer examination of the sidewall cutback effects on maximum thrust ratio for three nozzle expansion ratios (1.089 (ref. 10), 1.300 (present study), and 1.797 (ref. 10)) indicates a trend of increased thrust ratio losses as expansion ratio is increased. (See unvectored nozzle thrust ratio increments in fig. 32 for AR = 2.012 and 3.696.) Maximum sidewall cutback (about 75 percent) resulted in maximum thrust-ratio losses of approximately 1/4 percent, 1/2 percent, and 1 percent, respectively, for the three expansion ratios. Discharge coefficient was unaffected when the sidewalls were cut back on any of the aforementioned nozzles.

The effects of sidewall cutback on thrust ratio for two nozzles with large throat aspect ratios (5.806 and 7.612) are summarized in figure 33. Results indicate sidewall cutback effects on thrust ratio are negligible on these high-aspect-ratio nozzles regardless of nozzle expansion ratio (which varied from 1.089 to 1.797). In fact, data trends indicate that the impact of sidewall cutback on thrust ratio decreases with increasing aspect ratio. One possible explanation for this might be that as aspect ratio increases, the area of sidewall containment relative to divergent flap area decreases. As a result, a smaller percentage of total exhaust flow is influenced by sidewall geometry changes. Unlike the trend noted for $AR < 3.7$ nozzles, discharge coefficients for the larger AR nozzles (see fig. 33) increased 1 to 1.5 percent at high nozzle pressure ratios when the sidewalls were cut back. The reason for this is not known.

A summary plot of the effect of sidewall cutback on the maximum value of nozzle thrust ratio from available static internal performance data is presented in figure 32 for unvectored and vectored nozzles.

The variation of local pressure (ratio) along the flap centerline of the unvectored afterburning nozzle with three different sidewalls is shown at the top of figures 34(a) and (b) for nozzle pressure ratios of 2.0 and 5.0, respectively. For a nozzle pressure ratio of 2.0 (fig. 34(a)), separation due to cutting back the sidewall was greater for configuration A4 (cut back to 22.7 percent). Away from the flap centerline (lateral pressure orifice rows), flow separation was more extensive for both A3 and A4. These increases in separation at conditions below the nozzle design pressure ratio increase flap static pressure in the separation region and effectively decrease the nozzle expansion ratio. This produces an increase in thrust

ratio with sidewall cutback and causes a small shift in peak thrust ratio to a lower nozzle pressure ratio. This effect of sidewall cutback, shown in figure 10, has been discussed previously in reference 10. Near the nozzle design pressure ratio (fig. 34(b)), the effect of sidewall cutback does not reach the centerline of the nozzle flap; however, flap static pressure near the sidewall (see lateral pressure distributions at the bottom of fig. 34(b)) is decreased. These lower pressures produce the small losses in thrust ratio noted earlier for sidewall cutback.

Throat radius.- The effects on internal performance of changes in flap curvature (throat radius) at the nozzle throat are summarized in figure 35. Although there is a large shift in the thrust ratio curve for configuration B1 (fig. 35(a)) relative to configurations D2, D7, and D8 because of a difference in nozzle design pressure ratio, it is apparent from the other configurations in figure 35(a) that throat curvature has little effect on nozzle thrust ratio.

The major effect of throat radius is on nozzle discharge coefficient (w_p/w_i) which is decreased by approximately 3.5 percent for a sharp throat (R_t = 0 cm) over the range of pressure ratios investigated with a nozzle expansion ratio of 1.797. A similar effect of throat radius on nozzle discharge coefficient is shown for low expansion ratios. The loss in discharge coefficient increases nonlinearly with decreasing throat radius as shown in incremental form in figure 35(b) for R_t/h_t = 0, 0.249, 0.578, and 0.996.

Pressure data for configurations D7 through D10 are contained in reference 9. Those data indicate that as throat radius decreases, static pressure values just downstream of the nozzle throat decrease, and static pressure values upstream of the throat increase. The lower pressures immediately downstream of the throat are believed to be the result of increased local flow overexpansion as throat radius is decreased. The sharp throats of nozzle configurations B1 and B2 may cause a local flow separation bubble to be formed just aft of the geometric throat as the exhaust flow is expanded over an infinitesimally small length (i.e., zero length). The pressure data of this investigation and of reference 9, along with analytical results from a two-dimensional inviscid code (ref. 9), indicate a tendency for the physical nozzle throat (location for $p/p_{t,j}$ = 0.528) to move slightly downstream of the nozzle geometric throat as throat radius is decreased. The local viscous effects (which become more significant as throat radius decreases) also act to reduce the effective nozzle throat area and, hence, reduce nozzle discharge coefficient w_p/w_i.

Expansion ratio.- The effect on nozzle internal performance of increasing expansion ratio by increasing flap length is shown by comparing the data obtained on configurations D3 through D6 which have approximately the same flap divergence angle of 10.8°. A summary plot of the data for these configurations (fig. 36) shows that a fixed-throat, fixed-divergence-angle (10.8°) nozzle, designed to increase expansion ratio by increasing flap length, would have an essentially constant thrust ratio of about 0.99 (locus of thrust-ratio peaks) over the pressure-ratio range investigated. The same result was obtained in reference 10 for a nozzle having a flap divergence angle of approximately 5.5° over the same ranges of expansion and pressure ratio. There was no significant effect of expansion-ratio variation on discharge coefficient (which ranged from 0.978 to 0.991 in the pressure-ratio range from 2 to 9) for either group of nozzles.

The peak thrust ratios and discharge coefficient levels obtained over the range of expansion ratios are comparable with those obtained with axisymmetric nozzles having similar expansion ratios. (See refs. 11 and 14.) The internal performance of

the current test nozzles is well behaved, in that peak thrust ratio occurs very near the design nozzle pressure ratio for each expansion ratio tested. (See fig. 36.)

Throat aspect ratio.- Nozzle throat aspect ratio (w_t/h_t) was varied between 3.696 and 7.612 for two expansion ratios by changing throat height and holding nozzle width constant; that is, nozzle area decreased as nozzle throat aspect ratio increased. The ratio of throat radius to throat height R_t/h_t was held nearly constant; hence as aspect ratio increased, both h_t and R_t decreased. A summary of the effect on internal performance of increasing throat aspect ratio for nozzle expansion ratios of 1.089 and 1.797 is presented in figure 37. For the range of throat aspect ratios investigated, there is little effect of throat aspect ratio on nozzle thrust ratio. However, discharge coefficient decreased significantly with increased aspect ratio. These decreases are thought to be partly a result of the relative increase in the influence of the viscous effects resulting from the reduced throat height and increased throat width and partly a result of the decreased throat radius. Unfortunately, the separate effects could not be isolated with the available data. For both higher throat aspect ratios (5.806 and 7.612), discharge coefficient increased with increasing pressure ratio by as much as 1 percent between nozzle pressure ratios of 2 and 9. This increase in discharge coefficient with increasing nozzle pressure ratio was even greater (as much as 1.6 percent) when the sidewalls were cut back. Reasons for these increases in discharge coefficient are not known at present, but similar increases have been obtained for other nozzles with moderate-to-high throat aspect ratios.

Vectored-Thrust Nozzles

Vectoring the thrust from a 2D-CD nozzle can be done in a number of different ways. For example, to obtain the highest internal performance, the whole nozzle can be gimbaled about an axis system upstream of the convergent section so that the flow would turn at low speed with no turning losses. In such an arrangement, the internal performance along the vectored nozzle axis would be identical to the unvectored-nozzle performance, and the resulting vector angle would equal the geometric design vector angle. However, such a nozzle would have drawbacks from a practical standpoint, in that it would require a set of actuation hardware (extra weight) to gimbal the nozzle downward as well as the actuators necessary to change nozzle power setting and expansion ratio. In addition, the gimbaled-type nozzle has the potential for relatively high increases in drag during vectored operation at maneuver speeds, as reported in reference 8. As the nozzle is gimbaled, excessive boattail angles on the nozzle top surface are created while the bottom surface protrudes into the free-stream flow field. Both can result in significant drag increases. A more practical arrangement is to incorporate the vectoring functions into the system that changes power setting and expansion ratio by arranging for the upper and lower flaps to be independently actuated so that they can be deflected independently (ref. 26). This is the type of thrust vectoring represented by the nozzles described in figure 3. One disadvantage of this arrangement is that the throat orientation remains about the same for the vectored-thrust configurations as it did for the forward-thrust configurations. This means that supersonic flow downstream of the throat must be turned by the nozzle divergent flaps. Previous studies (for example, refs. 8, 11, and 12) have shown a potential for thrust losses when this is done.

Thrust vector angle.- The incremental effect on resultant thrust ratio of vectoring an afterburning nozzle (with an expansion ratio of 1.300) 9.79° and 20.26° with each of four sidewall configurations is shown in figure 38. These increments

were obtained by subtracting resultant thrust ratio for the unvectored nozzles (with the appropriate sidewalls) from the resultant thrust ratio of the vectored nozzles (figs. 27 and 29) and hence represent internal turning gains (positive increments) or losses (negative increments). In general, vectoring the nozzles resulted in an increase in resultant thrust ratio at low nozzle pressure ratios and a decrease in resultant thrust ratio over a range of nozzle pressure ratios in the vicinity of the design pressure ratio (approximately 1 percent for $\delta_v = 9.79°$ and 3 percent for $\delta_v = 20.26°$).

All the nozzles were effective in vectoring the thrust (fig. 30(a)) when the nozzle pressure ratio was large enough to reduce the amount of flow separation from the lower flap. The largest thrust vector angles were obtained with full sidewalls. Thrust vector angles were equal to or greater than the geometric vector angle with full-length sidewalls for all three nozzles when extensive lower-flap flow separation was not present. The maximum measured vector angle for each nozzle with full-length sidewalls was reached below the design pressure ratio and decreased as pressure ratio was increased. This effect of thrust angularity varying with pressure ratio is common in nonaxisymmetric nozzles whenever one flap is longer than the other relative to the exhaust flow centerline. It occurs for both unvectored and vectored single-expansion-ramp nozzles (see, for example, refs. 10 and 13) and some vectored 2D-CD nozzles where rotation of the individual flaps takes place about axes near the throat. This type nozzle geometry presents expansion surfaces of unequal length for the flow to work against, so that one side of the exhaust flow is contained longer by a flap (in this investigation, the lower flap) while the other side of the exhaust flow is unbounded.

Comparisons of the variation of flap centerline pressure (ratio) with x/x_t with full-length sidewalls at nozzle geometric vector angles of 0°, 9.79°, 13.22°, and 20.26° for a nozzle pressure ratio of 5.0 are shown in figure 39. Sonic flow occurs at $x/x_t = 0.94$ (just upstream of the geometric throat) on both upper and lower flaps for the range of vector angles tested. The nozzles with a geometric vector angle of 13.22° were obtained by combining the upper and lower flaps of the 20.26° and 9.79° configurations, respectively. These data show that the pressure distributions on the upper flap for the 13.22° and 20.26° configurations (same piece of model hardware) are identical, even though the lower flaps (and therefore geometric vector angle and nozzle expansion ratio) are different. As discussed in reference 13, this is because the Mach wave, which originates at the throat from flow turning over the lower flaps, is acute enough in both cases (at $p_{t,j}/p_\infty = 5.0$) so that it passes out the nozzle exit without impinging on the surface of the upper flap. The x/x_t coordinate used in the tables and as the abscissa in the pressure distribution plots is along the model centerline ($\delta_v = 0°$). However, downstream of $x/x_t = 1.0$, an x/x_t coordinate, transformed by using δ_v, may be a more appropriate abscissa if detailed comparisons of pressure distributions at different vector angles are to be made.

Although there was no effect on discharge coefficient of vectoring the nozzle from 0° to 9.79°, there was a 1-percent decrease due to vectoring the nozzle from 9.79° to 20.26° (figs. 10, 27, and 29).

Sidewall cutback.- The effect of sidewall cutback on the internal performance and vectoring characteristics for three vectored nozzles at afterburning power setting is shown in figures 27 through 30. Incremental effects of sidewall cutback on peak resultant thrust ratio are shown at the top of figure 32. These data indicate slightly larger losses in peak thrust ratio because of sidewall cutback for vectored nozzles than for unvectored nozzles.

Examples of the effect of sidewall cutback on the variation of nozzle (δ_v = 20.26°) surface pressure (ratio) along the flap centerline and laterally from the flap centerline are shown in figures 40 and 41 for nozzle pressure ratios below and near the unvectored-nozzle design pressure ratio. The upper-flap centerline pressure variations with x/x_t are identical in shape and magnitude for both nozzle pressure ratios (figs. 40(a) and 41(a)) and indicate attached flow. Some separation occurs laterally towards the edge of the upper flaps with cutback sidewalls. However, the pressures on the lower flap indicate that the flow is almost completely separated up to the nozzle throat at the low nozzle pressure ratio for three sidewall configurations (fig. 40(b)). With the fourth sidewall configuration (most cutback), separation of the lower-flap flow is less severe along the centerline; however, extensive separation still occurs laterally toward the edge of the flap. Separation along the lower-flap centerline was eliminated at the higher nozzle pressure ratios, but was still evident laterally toward the edge of the flap when the sidewall was cut back (fig. 41(b)).

The effect of sidewall cutback on nozzle thrust vector angle is shown in figure 30(a). In all cases when extensive flow separation was not present, increases in sidewall cutback produced decreases in thrust vector angle up to as much as 6°. When significant flow separation existed on the lower flap, sidewall cutback had only small effects on thrust vector angle.

Nozzle discharge coefficient was unaffected by sidewall cutback (figs. 27 through 29) for all three geometric vector angles.

Thrust-Reverser Nozzles

Deployment of a thrust blocker upstream of a forward-thrust nozzle throat necessitates careful consideration of the discharge coefficient of the thrust-reverser nozzle relative to that of the forward-thrust nozzle. For example, if the discharge coefficient of the thrust-reverser nozzle is significantly lower than that of the forward-thrust nozzle, engine operation can be adversely affected by an increase in back pressure unless there has been a compensating increase in reverser port area. If, on the other hand, reverser port area has been overcompensated for (port area too large), the resulting decrease in back pressure can result in engine overspeed.

The thrust-reverser nozzles of this investigation are related to the dry power ("D") nozzle configurations, in that the reverser port area was sized to approximate the dry power (cruise) throat area adjusted to compensate for an expected decrease in discharge coefficient during reverse-thrust operation. That is, an attempt was made to make the reverser port large enough (approximately 21 percent larger than the dry power nozzle area) to allow engine mass flow to remain the same at a given nozzle pressure ratio for the forward-thrust dry power and the reverse-thrust configurations. The results indicate that reverser nozzle discharge coefficients were low (0.755 or less based on actual reverser port area) relative to typical forward-thrust nozzle discharge coefficients (0.985). Performance data for the six thrust-reverser configurations are presented in figure 31.

Port passage length.- The effect of port passage length (see fig. 7(b) for definition) on the internal performance of three thrust-reverser configurations having similar port exit geometries is shown in figure 42. Best reverse-thrust performance occurred for the midpassage length of v/w_v = 0.600. Reasons for the losses associated with both the short and long passage are not known. Nozzle discharge coefficient is also seen to vary with port passage length. Once the curves "flatten

out" above a nozzle pressure ratio of 3.5, the reverser configuration with the shortest passage length provided the highest values of discharge coefficient. Reasons for this are also unknown.

Perhaps the largest effects shown in figure 42 are those associated with variation of nozzle pressure ratio. Above a nozzle pressure ratio of 4.0, levels of reverse thrust are seen to decrease as nozzle pressure ratio increases. The decrease in reverse-thrust ratio with increasing nozzle pressure ratio is probably due to the greater length of the forward port passage wall relative to the rear passage wall, in that part of the forward passage wall acts as an external expansion surface. (See fig. 7(b) for sketches of ports for configurations R1, R2, and R3.) This forward surface outside the contained passage is pressurized by the port exhaust flow and develops a force component in the thrust (forward) direction at the higher nozzle pressure ratios. This force component in the thrust direction varies with nozzle pressure ratio in the same manner as the normal-force component on the external portion of the ramp of a single-expansion-ramp nozzle. Examples of the variation of normal force with nozzle pressure ratio for single-expansion-ramp nozzles can be found in reference 13 where δ_j is presented as a function of nozzle pressure ratio.

The reverse-thrust ratios for nozzle pressure ratios below 4.0 vary widely. Reasons for this wide variation at low nozzle pressure ratios are thought to be a result of varying amounts of separation at the port lip as well as nonlinear effects on the external expansion surface.

The low values of discharge coefficient for all the thrust-reverser nozzles of this investigation are probably related to the sharp corner at the entrance to the port passage. That is, the flow has to negotiate a sharp-cornered 120° turn to enter the port passage. Some evidence of this influence can be seen in the pressure measurements on the surface of the blocker (table X and fig. 43), which indicate that the passage flow at the blocker surface is not choked until it approaches or reaches the port exit (somewhere downstream of the last pressure orifice). The pressure data also show that changes in port exit geometry did not affect the blocker pressure distribution.

A separate investigation conducted on configuration R2 with additional pressure orifices installed on the blocker, sidewall, and passage surface of the forward flap is reported in reference 28. The sidewall static pressures measured during that investigation indicate that the sonic line on the passage sidewall extends from the sharp corner of the forward flap at the port entrance to the corner of the blocker at the port exit and is slightly curved. That is, the sharp corner at the port entrance greatly influences the flow entering the port, and choking does not occur at the geometric minimum.

External doors.- Configuration R2 was used as a baseline to examine the effects of the location of external port exit doors on internal performance. (See fig. 44.) The most significant effects were obtained when a single port exit door was mounted in the aft position (configuration R5) so that the aft passage wall was longer than the forward passage wall. This arrangement allows pressurization of the door, as previously discussed for the forward uncontained port wall. However, in this case, the door force component is in the reverse-thrust direction and is therefore additive to the passage force component. This configuration attained a nearly constant reverse-thrust-ratio level equal to or greater than the geometric design value (cos 120°) over the nozzle-pressure-ratio range. The addition of a sector-type port sidewall (configuration R6) to the aft door configuration (R5) had only a small favorable effect on reverse-thrust ratio.

CONCLUSIONS

The effects of geometric design parameters on the internal performance of two-dimensional convergent-divergent nozzles were investigated at nozzle pressure ratios up to 12 in the static test facility adjacent to the Langley 16-Foot Transonic Tunnel. Forward-flight (dry and afterburning power settings), vectored-thrust (afterburning power setting), and reverse-thrust (dry power setting) nozzles were investigated. Results of this study lead to the following conclusions:

1. Unvectored two-dimensional convergent-divergent nozzles have static internal performance comparable with unvectored axisymmetric nozzles with similar expansion ratios.

2. An unvectored nozzle (representing afterburning power setting) lost only 1/2 percent in maximum thrust ratio when the sidewalls were cut back about 75 percent of the distance between the exit and throat.

3. Nozzle expansion flap curvature (radius) at the throat had little effect on thrust ratio over the nozzle-pressure-ratio range tested, but discharge coefficient decreased as much as 3.5 percent when the radius was reduced to zero (sharp throat).

4. Nozzle throat aspect ratio (throat width/throat height), which was varied between 3.696 and 7.612, had little effect on thrust ratio.

5. A nozzle (representing afterburning power setting) geometrically vectored at angles up to 20.26° turned the flow at least as much as the design vector angle once nozzle pressure ratio was high enough to eliminate separation on the lower expansion flap.

6. The thrust-reverser nozzles (representing a dry power nozzle in the reverse mode) had low discharge coefficients ranging from 0.67 to 0.76. Above a nozzle pressure ratio of 3.5, discharge coefficient for each reverser configuration remained constant with increasing nozzle pressure ratio.

7. The thrust-reverser nozzles (designed for 50-percent reverse thrust) produced reverse thrust of 50 percent or more when the reverser port passage rear wall was longer than the forward wall.

Langley Research Center
National Aeronautics and Space Administration
Hampton, VA 23665
December 14, 1983

REFERENCES

1. F-15 2-D Nozzle System Integration Study. Volume I - Technical Report. NASA CR-145295, 1978.

2. Stevens, H. L.: F-15/Nonaxisymmetric Nozzle System Integration Study Support Program. NASA CR-135252, 1978.

3. Bergman, D.; Mace, J. L.; and Thayer, E. B.: Non-Axisymmetric Nozzle Concepts for an F-111 Test Bed. AIAA Paper No. 77-841, July 1977.

4. Wasson, H. R.; Hall, G. R.; and Palcza, J. L.: Results of a Feasibility Study To Add Canards and ADEN Nozzle to the YF-17. AIAA Paper 77-1227, Aug. 1977.

5. Goetz, G. F.; Petit, J. E.; and Sussman, M. B.: Non-Axisymmetric Nozzle Design and Evaluation for F-111 Flight Demonstration. AIAA Paper 78-1025, July 1978.

6. Hiley, P. E.; Wallace, H. W.; and Booz, D. E.: Nonaxisymmetric Nozzles Installed in Advanced Fighter Aircraft. J. Aircr., vol. 13, no. 12, Dec. 1976, pp. 1000-1006.

7. Hiley, P. E.; and Bowers, D. L.: Advanced Nozzle Integration for Supersonic Strike Fighter Application. AIAA-81-1441, July 1981.

8. Berrier, B. L.; and Re, R. J.: A Review of Thrust-Vectoring Schemes for Fighter Aircraft. AIAA Paper No. 78-1023, July 1978.

9. Mason, Mary L.; Putnam, Lawrence E.; and Re, Richard J.: The Effect of Throat Contouring on Two-Dimensional Converging-Diverging Nozzles at Static Conditions. NASA TP-1704, 1980.

10. Berrier, Bobby L; and Re, Richard J.: Effect of Several Geometric Parameters on the Static Internal Performance of Three Nonaxisymmetric Nozzle Concepts. NASA TP-1468, 1979.

11. Capone, Francis J.: Static Performance of Five Twin-Engine Nonaxisymmetric Nozzles With Vectoring and Reversing Capability. NASA TP-1224, 1978.

12. Willard, C. M.; Capone, F. J.; Konarski, M.; and Stevens, H. L.: Static Performance of Vectoring/Reversing Non-Axisymmetric Nozzles. AIAA Paper 77-840, July 1977.

13. Re, Richard J.; and Berrier, Bobby L.: Static Internal Performance of Single Expansion-Ramp Nozzles With Thrust Vectoring and Reversing. NASA TP-1962, 1982.

14. Capone, Francis J.; and Berrier, Bobby L.: Investigation of Axisymmetric and Nonaxisymmetric Nozzles Installed on a 0.10-Scale F-18 Prototype Airplane Model. NASA TP-1638, 1980.

15. Capone, Francis J.; Hunt, Brian L.; and Poth, Greg E.: Subsonic/Supersonic Nonvectored Aeropropulsive Characteristics of Nonaxisymmetric Nozzles Installed on an F-18 Model. AIAA-81-1445, July 1981.

16. Maiden, Donald L.; and Petit, John E.: Investigation of Two-Dimensional Wedge Exhaust Nozzles for Advanced Aircraft. J. Aircr., vol. 13, no. 10, Oct. 1976, pp. 809-816.

17. Capone, Francis J.; and Maiden, Donald L.: Performance of Twin Two-Dimensional Wedge Nozzles Including Thrust Vectoring and Reversing Effects at Speeds up to Mach 2.20. NASA TN D-8449, 1977.

18. Pendergraft, O. C.: Comparison of Axisymmetric and Nonaxisymmetric Nozzles Installed on the F-15 Configuration. AIAA Paper 77-842, July 1977.

19. Bare, E. Ann; Berrier, Bobby L.; and Capone, Francis J.: Effect of Simulated In-Flight Thrust Reversing on Vertical-Tail Loads of F-18 and F-15 Airplane Models. NASA TP-1890, 1981.

20. Hutchinson, R. A.; Petit, J. E.; Capone, F. J.; and Whittaker, R. W.: Investigation of Advanced Thrust Vectoring Exhaust Systems for High Speed Propulsive Lift. AIAA-80-1159, June/July 1980.

21. Schnell, W. C.; and Grossman, R. L.: Vectoring Non-Axisymmetric Nozzle Jet Induced Effects on a V/STOL Fighter Model. AIAA Paper 78-1080, July 1978.

22. Schnell, W. C.; Grossman, R. L.; and Hoff, G. E.: Comparison of Non-Axisymmetric and Axisymmetric Nozzles Installed on a V/STOL Fighter Model. [Preprint] 770983, Soc. Automot. Eng., Nov. 1977.

23. Lander, J. A.; and Palcza, J. Lawrence: Exhaust Nozzle Deflector Systems for V/STOL Fighter Aircraft. AIAA Paper No. 74-1169, Oct. 1974.

24. Lander, J. A.; Nash, D. O.; and Palcza, J. Lawrence: Augmented Deflector Exhaust Nozzle (ADEN) Design for Future Fighters. AIAA Paper No. 75-1318, Sept.-Oct. 1975.

25. Nash, D. O.; Wakeman, T. G.; and Palcza, J. L.: Structural and Cooling Aspects of the ADEN Nonaxisymmetric Exhaust Nozzle. Paper No. 77-GT-110, American Soc. Mech. Eng., Mar. 1977.

26. Stevens, H. L.; Thayer, E. B.; and Fullerton, J. F.: Development of the Multi-Function 2-D/C-D Nozzle. AIAA-81-1491, July 1981.

27. Cline, Michael C.: NAP: A Computer Program for the Computation of Two-Dimensional, Time-Dependent, Inviscid Nozzle Flow. LA-5984 (Contract W-7405-ENG. 36), Los Alamos Sci. Lab., Univ. of California, Jan. 1977.

28. Putnam, Lawrence E.; and Strong, Edward G.: Internal Pressure Distributions for a Two-Dimensional Thrust-Reversing Nozzle Operating at a Free-Stream Mach Number of Zero. NASA TM-85655, 1983.

TABLE I.- RATIO OF INTERNAL STATIC PRESSURE TO JET TOTAL PRESSURE FOR UNVECTORED-NOZZLE CONFIGURATIONS

(a) $p/p_{t,j}$ for configuration A1

	$y/w_t/2 = 0.0$							
	x/x_t							
$P_{t,j}/P_\infty$	0.638	0.745	0.851	0.957	1.000	1.064	1.117	1.170
2.000	.641	.800	.728	.472	.332	.256	.283	.305
2.998	.641	.802	.727	.469	.335	.257	.282	.305
4.014	.841	.802	.728	.467	.335	.257	.281	.304
5.029	.841	.802	.728	.466	.336	.256	.279	.303
5.627	.642	.802	.729	.466	.337	.255	.279	.303

	$y/w_t/2 = 0.0$						
	x/x_t						
$P_{t,j}/P_\infty$	1.277	1.383	1.489	1.596	1.702	1.809	1.872
2.000	.332	.335	.322	.300	.434	.468	.478
2.998	.331	.335	.320	.298	.273	.251	.236
4.014	.330	.334	.319	.296	.273	.250	.236
5.029	.329	.333	.319	.295	.271	.248	.236
5.627	.329	.333	.319	.294	.271	.247	.236

	$x/x_t = 1.064$					$x/x_t = 1.489$				
	$y/w_t/2$					$y/w_t/2$				
$P_{t,j}/P_\infty$	0.250	0.500	0.750	0.875	0.950	0.250	0.500	0.750	0.875	0.950
2.000	.259	.255	.252	.256	.257	.321		.322	.321	.334
2.998	.260	.258	.259	.260	.261	.321		.320	.319	.319
4.014	.259	.258	.260	.259	.260	.320		.318	.317	.318
5.029	.258	.256	.259	.258	.260	.320		.317	.316	.317
5.627	.257	.256	.259	.257	.260	.320		.317	.316	.316

	$x/x_t = 1.809$				
	$y/w_t/2$				
$P_{t,j}/P_\infty$	0.250	0.500	0.750	0.875	0.950
2.000	.469	.471	.497	.488	.489
2.998	.252	.250	.251	.246	.250
4.014	.252	.250	.250	.251	.244
5.029	.251	.250	.248	.250	.244
5.627	.251	.249	.248	.250	.243

TABLE I.- Continued

(b) $p/p_{t,j}$ for configuration A3

$p_{t,j}/p_\infty$	$y/w_t/2 = 0.0$							
	x/x_t							
	0.638	0.745	0.851	0.957	1.000	1.064	1.117	1.170
1.985	.841	.800	.728	.472	.331	.256	.282	.305
2.987	.840	.801	.726	.470	.334	.257	.281	.305
3.994	.840	.801	.727	.469	.335	.257	.280	.305
3.954	.840	.801	.727	.469	.335	.257	.280	.305
4.974	.841	.802	.726	.468	.335	.256	.279	.304
5.722	.841	.801	.728	.468	.335	.255	.278	.303

$p_{t,j}/p_\infty$	$y/w_t/2 = 0.0$						
	x/x_t						
	1.277	1.383	1.489	1.596	1.702	1.809	1.872
1.985	.331	.334	.323	.300	.417	.476	.492
2.987	.330	.334	.320	.297	.273	.250	.233
3.994	.329	.334	.321	.297	.271	.243	.226
3.954	.329	.334	.321	.297	.271	.243	.226
4.974	.328	.332	.319	.293	.270	.246	.232
5.722	.327	.332	.318	.292	.270	.246	.232

$p_{t,j}/p_\infty$	$x/x_t = 1.064$					$x/x_t = 1.489$				
	$y/w_t/2$					$y/w_t/2$				
	0.250	0.500	0.750	0.875	0.950	0.250	0.500	0.750	0.875	0.950
1.985	.258	.255	.250	.274	.232	.325	.308	.449	.475	.496
2.987	.262	.258	.257	.266	.230	.321	.322	.321	.329	.337
3.994	.260	.256	.276	.230	.166	.318	.320	.319	.303	.276
3.954	.260	.258	.277	.236	.197	.320	.315	.319	.302	.279
4.974	.258	.259	.259	.264	.260	.319	.335	.317	.297	.249
5.722	.257	.254	.259	.261	.260	.319	.337	.316	.296	.239

$p_{t,j}/p_\infty$	$x/x_t = 1.809$				
	$y/w_t/2$				
	0.250	0.500	0.750	0.875	0.950
1.985	.483	.496	.490	.498	.500
2.987	.253	.253	.302	.298	.339
3.994	.252	.246	.231	.201	.243
3.954	.251	.246	.233	.202	.246
4.974	.251	.245	.212	.171	.193
5.722	.250	.244	.206	.158	.175

TABLE I.- Continued

(c) $p/p_{t,j}$ for configuration A4

$p_{t,j}/p_\infty$	$y/w_t/2 = 0.0$						
	x/x_t						
	0.745	0.851	0.957	1.000	1.064	1.117	1.170
1.985	.800	.728	.472	.331	.256	.282	.305
2.990	.801	.727	.469	.334	.257	.281	.306
3.984	.801	.727	.467	.335	.257	.280	.305
5.003	.801	.728	.466	.335	.256	.279	.304
5.036	.801	.728	.467	.335	.256	.279	.304
4.976	.801	.728	.467	.335	.256	.279	.304
5.582	.801	.728	.467	.335	.256	.279	.304

$p_{t,j}/p_\infty$	$y/w_t/2 = 0.0$						
	x/x_t						
	1.277	1.383	1.489	1.596	1.702	1.809	1.872
1.985	.331	.335	.324	.484	.535	.555	.544
2.990	.331	.335	.322	.299	.274	.252	.235
3.984	.329	.334	.320	.296	.271	.248	.233
5.003	.328	.332	.319	.294	.270	.245	.233
5.036	.328	.333	.319	.294	.270	.245	.233
4.976	.328	.333	.319	.294	.270	.245	.233
5.582	.328	.332	.319	.293	.270	.245	.233

$p_{t,j}/p_\infty$	$x/x_t = 1.064$					$x/x_t = 1.489$				
	$y/w_t/2$					$y/w_t/2$				
	0.250	0.500	0.750	0.875	0.950	0.250	0.500	0.750	0.875	0.950
1.985	.261	.256	.257	.246	.267	.370	.442	.481	.511	.505
2.990	.264	.259	.265	.246	.260	.322	.328	.330	.342	.345
3.984	.260	.256	.263	.248	.259	.319	.330	.265	.254	.256
5.003	.258	.254	.262	.244	.258	.318	.333	.251	.205	.204
5.036	.258	.255	.262	.244	.258	.319	.334	.251	.204	.203
4.976	.258	.255	.262	.244	.258	.319	.334	.251	.206	.205
5.582	.257	.254	.262	.243	.256	.318	.336	.251	.186	.183

$p_{t,j}/p_\infty$	$x/x_t = 1.809$				
	$y/w_t/2$				
	0.250	0.500	0.750	0.875	0.950
1.985	.557	.542	.518	.510	.501
2.990	.256	.267	.309	.353	.343
3.984	.247	.209	.220	.253	.250
5.003	.246	.203	.169	.198	.200
5.036	.246	.203	.168	.197	.199
4.976	.246	.203	.170	.199	.202
5.582	.245	.203	.152	.175	.180

TABLE I.- Continued

(d) $p/p_{t,j}$ for configuration D1

$p_{t,j}/p_\infty$	$y/w_t/2 = 0.0$										
	x/x_t										
	0.651	0.724	0.796	0.868	0.941	0.969	0.998	1.027	1.056	1.085	1.114
1.969	.942	.921	.891	.837	.631	.475	.376	.348	.352	.355	.375
2.470	.944	.923	.892	.837	.631	.474	.374	.347	.350	.352	.364
2.865	.944	.922	.891	.837	.631	.473	.374	.346	.350	.353	.366
2.929	.944	.922	.891	.837	.630	.473	.374	.345	.350	.353	.366
2.998	.943	.922	.891	.837	.631	.474	.373	.345	.350	.353	.366
3.453	.942	.922	.891	.836	.628	.473	.373	.345	.350	.352	.365
3.933	.942	.922	.891	.836	.616	.472	.373	.345	.350	.350	.364
3.956	.942	.922	.891	.836	.616	.473	.373	.345	.350	.350	.363
4.436	.942	.922	.891	.836	.605	.471	.373	.345	.349	.349	.363
4.915	.942	.922	.891	.836	.596	.470	.374	.347	.348	.348	.363
5.408	.941	.922	.890	.835	.587	.467	.373	.345	.348	.346	.362
5.911	.941	.922	.890	.835	.611	.470	.373	.344	.347	.346	.361
6.386	.941	.922	.890	.835	.610	.469	.372	.344	.347	.345	.361
6.873	.941	.921	.890	.835	.607	.468	.372	.343	.346	.344	.360
7.362	.941	.922	.890	.835	.609	.468	.372	.343	.345	.343	.360
7.848	.941	.921	.890	.835	.605	.467	.371	.343	.345	.342	.360
8.363	.940	.921	.890	.834	.603	.466	.371	.342	.344	.342	.360
9.363	.940	.921	.890	.834	.599	.463	.371	.342	.344	.340	.360

$p_{t,j}/p_\infty$	$x/x_t = 1.027$					$x/x_t = 1.114$				
	$y/w_t/2$					$y/w_t/2$				
	0.250	0.500	0.750	0.875	0.950	0.250	0.500	0.750	0.875	0.950
1.969	.341	.344	.344	.346	.358	.392	.386	.394	.391	.446
2.470	.340	.340	.341	.344	.354	.380	.380	.387	.380	.362
2.865	.339	.340	.341	.344	.353	.381	.381	.389	.380	.357
2.929	.339	.340	.341	.344	.353	.381	.381	.389	.380	.356
2.998	.339	.341	.341	.344	.354	.382	.380	.390	.380	.356
3.453	.343	.344	.344	.345	.356	.380	.379	.388	.378	.355
3.933	.345	.344	.346	.345	.356	.378	.378	.386	.377	.353
3.956	.345	.344	.346	.345	.356	.378	.378	.386	.377	.353
4.436	.345	.344	.346	.344	.356	.378	.377	.385	.376	.352
4.915	.345	.344	.347	.344	.356	.377	.376	.385	.377	.351
5.408	.344	.343	.346	.344	.355	.377	.375	.384	.376	.349
5.911	.343	.343	.345	.343	.354	.376	.375	.383	.384	.337
6.386	.343	.342	.344	.343	.354	.376	.375	.383	.383	.337
6.873	.343	.342	.343	.343	.353	.375	.374	.382	.381	.348
7.362	.342	.341	.343	.342	.353	.375	.374	.382	.381	.349
7.848	.342	.341	.343	.342	.353	.375	.374	.382	.381	.347
8.363	.341	.341	.342	.342	.352	.375	.373	.382	.380	.348
9.363	.341	.340	.342	.342	.352	.374	.372	.381	.380	.348

TABLE I.- Continued

(e) $p/p_{t,j}$ for configuration D2

$p_{t,j}/p_\infty$	$y/w_t/2 = 0.0$									
	x/x_t									
	0.791	0.901	1.011	1.077	1.143	1.286	1.429	1.560	1.736	1.890
1.996	.805	.631	.422	.476	.487	.408	.420	.403	.382	.365
2.495	.804	.630	.421	.474	.485	.407	.419	.401	.381	.363
2.902	.804	.630	.421	.473	.483	.406	.419	.400	.380	.362
2.958	.805	.630	.421	.473	.483	.406	.419	.400	.379	.362
3.023	.805	.630	.420	.473	.483	.406	.419	.400	.379	.362
3.040	.805	.630	.420	.473	.483	.406	.419	.400	.379	.361
3.493	.805	.631	.420	.473	.482	.405	.418	.399	.378	.360
3.474	.804	.630	.420	.473	.482	.405	.418	.399	.378	.360
3.980	.804	.630	.419	.472	.481	.405	.418	.399	.377	.359
4.486	.804	.630	.419	.472	.482	.403	.418	.398	.376	.359
4.980	.804	.630	.419	.472	.482	.403	.418	.398	.375	.358
5.467	.804	.630	.419	.471	.482	.403	.418	.398	.374	.358
5.954	.804	.630	.419	.471	.482	.403	.417	.398	.374	.357
5.966	.803	.630	.419	.471	.482	.403	.417	.398	.373	.357
6.476	.803	.630	.419	.471	.482	.402	.417	.398	.373	.357
6.965	.803	.630	.419	.471	.482	.403	.417	.398	.372	.357
7.447	.803	.630	.419	.471	.483	.403	.417	.398	.371	.357
7.955	.800	.630	.419	.471	.483	.403	.417	.398	.371	.356
8.428	.796	.630	.419	.471	.483	.403	.417	.398	.370	.356
8.444	.796	.630	.419	.471	.483	.403	.417	.398	.370	.356
8.719	.793	.630	.419	.471	.483	.403	.417	.398	.369	.356

$p_{t,j}/p_\infty$	$y/w_t/2 = 0.450$									
	x/x_t									
	0.791	0.901	1.011	1.077	1.143	1.286	1.429	1.560	1.736	1.890
1.996	.804	.632	.426	.480	.487	.410	.427	.392	.380	.357
2.495	.804	.632	.425	.472	.484	.410	.427	.391	.380	.355
2.902	.804	.631	.425	.466	.483	.409	.425	.390	.379	.355
2.958	.804	.631	.425	.466	.483	.409	.425	.390	.379	.354
3.023	.804	.631	.425	.465	.483	.409	.425	.390	.379	.354
3.040	.804	.631	.425	.464	.482	.409	.425	.390	.379	.354
3.493	.804	.630	.424	.460	.482	.409	.424	.389	.379	.353
3.474	.804	.631	.424	.460	.482	.409	.424	.389	.378	.353
3.980	.803	.630	.423	.456	.482	.409	.423	.389	.378	.352
4.486	.803	.630	.423	.453	.481	.409	.422	.389	.378	.351
4.980	.803	.630	.423	.451	.481	.409	.422	.389	.377	.351
5.467	.802	.630	.423	.442	.481	.409	.422	.389	.377	.350
5.954	.803	.630	.423	.439	.481	.409	.422	.389	.377	.350
5.966	.803	.630	.423	.439	.481	.409	.422	.389	.377	.349
6.476	.803	.630	.423	.438	.481	.409	.422	.389	.377	.349
6.965	.802	.630	.423	.446	.481	.409	.422	.389	.376	.349
7.447	.802	.630	.423	.445	.482	.409	.422	.389	.376	.348
7.955	.802	.630	.423	.444	.482	.409	.422	.389	.376	.349
8.428	.802	.630	.423	.444	.482	.409	.423	.389	.376	.349
8.444	.802	.630	.423	.443	.482	.409	.422	.389	.376	.348
8.719	.802	.630	.424	.443	.482	.410	.423	.389	.376	.348

TABLE I.- Continued

(e) Concluded

$p_{t,j}/p_\infty$	$y/w_t/2 = 0.875$								
	x/x_t								
	0.901	1.011	1.077	1.143	1.286	1.429	1.560	1.736	1.890
1.996	.638	.427	.483	.488	.431	.419	.378	.381	.360
2.495	.637	.428	.483	.485	.432	.418	.388	.380	.360
2.902	.636	.427	.482	.484	.430	.416	.393	.379	.359
2.958	.636	.427	.482	.484	.430	.416	.394	.379	.359
3.023	.636	.427	.481	.484	.430	.416	.395	.379	.359
3.040	.635	.427	.481	.484	.430	.416	.395	.379	.359
3.493	.636	.428	.481	.483	.428	.414	.398	.378	.358
3.474	.637	.428	.481	.483	.428	.414	.398	.378	.358
3.980	.638	.428	.480	.482	.426	.414	.401	.377	.357
4.486	.636	.428	.479	.483	.425	.413	.404	.376	.356
4.980	.636	.429	.479	.483	.424	.412	.405	.374	.356
5.467	.636	.429	.479	.482	.423	.412	.407	.374	.355
5.954	.636	.429	.479	.482	.423	.411	.408	.373	.355
5.966	.636	.429	.479	.482	.423	.411	.408	.373	.355
6.476	.635	.429	.479	.482	.422	.411	.409	.372	.355
6.965	.636	.430	.479	.482	.421	.411	.410	.372	.354
7.447	.636	.430	.479	.482	.421	.411	.411	.371	.354
7.955	.636	.430	.479	.482	.420	.411	.412	.371	.354
8.428	.635	.430	.479	.482	.419	.410	.412	.371	.353
8.444	.636	.430	.479	.482	.419	.410	.412	.371	.353
8.719	.635	.430	.479	.482	.419	.411	.413	.371	.353

$p_{t,j}/p_\infty$	$y/w_t/2 = 0.225$					$y/w_t/2 = 0.662$			
	x/x_t					x/x_t			
	0.791	1.011	1.286	1.560	1.890	1.011	1.286	1.560	1.890
1.996	.801	.428	.408	.389	.362	.422	.416	.390	.356
2.495	.801	.429	.410	.389	.361	.423	.416	.390	.356
2.902	.800	.431	.408	.389	.360	.423	.415	.390	.356
2.958	.800	.431	.408	.389	.360	.423	.415	.389	.355
3.023	.800	.431	.408	.389	.360	.423	.415	.389	.355
3.040	.800	.431	.408	.389	.360	.423	.415	.389	.355
3.493	.800	.431	.406	.388	.359	.423	.414	.389	.354
3.474	.799	.431	.406	.388	.359	.424	.414	.389	.354
3.980	.799	.430	.405	.388	.358	.424	.413	.388	.353
4.486	.795	.430	.405	.387	.357	.424	.413	.388	.352
4.980	.790	.430	.404	.387	.356	.423	.412	.388	.352
5.467	.787	.430	.404	.387	.356	.423	.412	.388	.351
5.954	.798	.430	.403	.387	.355	.424	.412	.387	.350
5.966	.798	.430	.403	.387	.355	.424	.412	.387	.350
6.476	.799	.430	.404	.386	.354	.424	.411	.387	.350
6.965	.799	.430	.403	.386	.354	.424	.411	.387	.349
7.447	.799	.430	.404	.386	.353	.424	.411	.387	.349
7.955	.798	.430	.404	.386	.353	.424	.411	.387	.348
8.428	.797	.430	.404	.386	.352	.424	.411	.387	.348
8.444	.797	.430	.404	.386	.352	.424	.410	.387	.348
8.719	.797	.430	.404	.386	.352	.424	.411	.387	.348

TABLE I.- Continued

(f) $p/p_{t,j}$ for configuration D3

$p_{t,j}/p_\infty$	$y/w_t/2 = 0.0$											
	x/x_t											
	0.624	0.702	0.780	0.858	0.920	0.967	0.998	1.029	1.061	1.107	1.154	1.201
1.958	.946	.919	.888	.834	.708	.479	.380	.300	.278	.286	.303	.448
2.458	.947	.921	.888	.834	.707	.478	.381	.298	.276	.284	.281	.263
2.939	.945	.921	.889	.835	.707	.478	.381	.298	.274	.284	.282	.263
3.433	.944	.921	.889	.834	.701	.477	.380	.298	.273	.285	.281	.263
3.926	.944	.921	.889	.834	.694	.477	.381	.298	.273	.284	.280	.262
4.400	.943	.921	.889	.834	.682	.476	.381	.298	.274	.283	.280	.262
4.907	.943	.921	.889	.834	.677	.474	.381	.298	.273	.282	.279	.261
5.380	.943	.921	.889	.834	.675	.473	.381	.297	.272	.282	.278	.261
5.385	.943	.921	.889	.834	.672	.472	.381	.297	.272	.282	.278	.260
5.894	.942	.921	.889	.833	.670	.470	.381	.297	.270	.282	.277	.260
6.365	.942	.921	.889	.833	.668	.469	.380	.296	.270	.281	.276	.259
6.868	.942	.921	.889	.833	.671	.468	.380	.295	.270	.281	.276	.259
7.360	.941	.921	.889	.833	.671	.467	.380	.295	.269	.280	.275	.258
7.826	.941	.921	.889	.833	.672	.467	.380	.295	.269	.280	.275	.258
8.378	.940	.920	.889	.833	.674	.467	.379	.294	.268	.279	.274	.257
8.597	.940	.920	.889	.833	.675	.467	.379	.294	.268	.279	.274	.257
8.660	.940	.920	.889	.833	.676	.467	.379	.294	.268	.279	.274	.257
8.751	.940	.920	.889	.832	.677	.467	.379	.294	.268	.279	.274	.257
9.296	.940	.920	.889	.832	.676	.467	.378	.294	.268	.279	.274	.257

$p_{t,j}/p_\infty$	$x/x_t = 1.029$					$x/x_t = 1.201$				
	$y/w_t/2$					$y/w_t/2$				
	0.250	0.500	0.750	0.875	0.950	0.250	0.500	0.750	0.875	0.950
1.958	.304	.305	.310	.314	.333	.439	.437	.443	.439	.462
2.458	.303	.302	.309	.312	.332	.273	.258	.275	.259	.326
2.939	.303	.301	.311	.313	.334	.273	.259	.276	.258	.268
3.433	.306	.302	.313	.314	.336	.273	.258	.275	.258	.266
3.926	.308	.303	.314	.315	.335	.272	.257	.274	.258	.265
4.400	.308	.303	.316	.316	.336	.272	.256	.274	.257	.265
4.907	.308	.302	.315	.316	.336	.272	.256	.273	.256	.264
5.380	.307	.302	.314	.318	.331	.272	.255	.272	.256	.264
5.385	.307	.302	.314	.318	.330	.272	.255	.272	.256	.264
5.894	.307	.301	.313	.316	.341	.271	.254	.274	.256	.259
6.365	.306	.300	.313	.315	.339	.271	.254	.275	.255	.260
6.868	.306	.300	.312	.313	.336	.271	.254	.275	.255	.255
7.360	.305	.299	.312	.313	.339	.270	.253	.274	.254	.258
7.826	.304	.299	.312	.313	.337	.270	.253	.273	.254	.257
8.378	.304	.299	.311	.312	.337	.270	.253	.273	.253	.256
8.597	.304	.298	.311	.312	.339	.270	.252	.273	.253	.256
8.660	.304	.298	.311	.312	.339	.270	.252	.273	.253	.256
8.751	.304	.298	.311	.311	.338	.270	.252	.273	.253	.254
9.296	.304	.298	.311	.310	.338	.270	.252	.273	.253	.254

TABLE I.- Continued

(g) $p/p_{t,j}$ for configuration D4

$p_{t,j}/p_\infty$	$y/w_t/2 = 0.0$										
	x/x_t										
	0.595	0.670	0.744	0.819	0.893	0.967	0.997	1.034	1.071	1.116	1.191
1.971	.952	.934	.910	.872	.790	.480	.398	.295	.281	.292	.289
2.467	.954	.936	.911	.872	.790	.478	.398	.294	.280	.292	.274
2.963	.953	.935	.910	.872	.787	.478	.397	.294	.280	.293	.275
3.446	.952	.935	.911	.871	.782	.479	.397	.293	.281	.293	.274
3.946	.953	.935	.911	.871	.776	.479	.397	.292	.280	.292	.274
4.423	.953	.935	.912	.871	.763	.479	.397	.292	.280	.291	.274
4.915	.953	.935	.911	.871	.758	.478	.397	.292	.279	.291	.273
5.402	.953	.935	.911	.871	.764	.478	.397	.291	.279	.290	.273
5.874	.953	.935	.911	.871	.758	.477	.397	.291	.279	.290	.273
5.886	.953	.935	.911	.871	.757	.477	.397	.291	.279	.290	.273
6.391	.952	.935	.911	.871	.759	.476	.396	.291	.279	.289	.273
6.875	.952	.935	.911	.870	.757	.475	.396	.290	.278	.289	.272
7.344	.952	.935	.911	.870	.755	.474	.396	.290	.278	.289	.272
7.845	.953	.935	.911	.870	.756	.474	.396	.290	.277	.288	.272
8.325	.952	.935	.911	.870	.756	.473	.396	.290	.277	.288	.272
8.584	.952	.935	.911	.870	.756	.473	.395	.290	.277	.288	.272
8.660	.952	.934	.911	.870	.758	.473	.395	.289	.277	.288	.272
8.751	.952	.934	.911	.870	.755	.473	.395	.290	.277	.288	.272
9.041	.952	.934	.911	.869	.754	.473	.395	.289	.277	.287	.272

$p_{t,j}/p_\infty$	$y/w_t/2 = 0.0$		$x/x_t = 1.034$				
	x/x_t		$y/w_t/2$				
	1.265	1.310	0.250	0.500	0.750	0.875	0.950
1.971	.433	.461	.297	.307	.295	.302	.307
2.467	.230	.353	.296	.304	.294	.300	.305
2.963	.230	.211	.296	.303	.292	.300	.303
3.446	.230	.211	.298	.307	.292	.299	.302
3.946	.230	.211	.300	.307	.293	.300	.301
4.423	.230	.211	.299	.307	.293	.299	.301
4.915	.229	.211	.299	.307	.292	.299	.300
5.402	.228	.211	.299	.306	.291	.299	.300
5.874	.228	.211	.299	.306	.289	.299	.300
5.886	.228	.210	.299	.306	.289	.298	.300
6.391	.227	.210	.298	.305	.289	.298	.300
6.875	.227	.210	.298	.305	.288	.298	.300
7.344	.227	.209	.298	.305	.288	.297	.300
7.845	.227	.209	.298	.305	.288	.297	.301
8.325	.227	.209	.298	.304	.288	.297	.301
8.584	.227	.209	.297	.304	.288	.297	.301
8.660	.227	.209	.297	.304	.287	.297	.300
8.751	.227	.209	.297	.304	.288	.297	.300
9.041	.227	.209	.296	.304	.288	.297	.300

$p_{t,j}/p_\infty$	$x/x_t = 1.191$					$x/x_t = 1.310$				
	$y/w_t/2$					$y/w_t/2$				
	0.250	0.500	0.750	0.875	0.950	0.250	0.500	0.750	0.875	0.950
1.971	.296	.298	.281	.298	.382	.455	.452	.476	.502	.495
2.467	.267	.271	.277	.275	.282	.324	.307	.332	.297	.339
2.963	.268	.273	.278	.276	.282	.214	.219	.220	.230	.256
3.446	.267	.273	.278	.276	.282	.214	.219	.221	.230	.226
3.946	.266	.273	.277	.276	.281	.214	.219	.221	.230	.225
4.423	.266	.272	.277	.274	.282	.214	.219	.222	.230	.226
4.915	.265	.272	.276	.275	.280	.213	.219	.221	.230	.226
5.402	.265	.272	.276	.275	.280	.213	.218	.221	.229	.225
5.874	.264	.271	.276	.275	.281	.213	.219	.221	.230	.225
5.886	.264	.271	.276	.274	.280	.213	.218	.221	.230	.225
6.391	.264	.271	.275	.275	.281	.212	.218	.221	.230	.225
6.875	.264	.271	.275	.274	.280	.212	.218	.221	.230	.225
7.344	.263	.270	.275	.274	.280	.212	.219	.221	.227	.224
7.845	.263	.270	.275	.274	.280	.212	.219	.221	.229	.224
8.325	.262	.270	.275	.274	.280	.212	.219	.221	.229	.224
8.584	.262	.270	.275	.274	.280	.212	.219	.221	.228	.224
8.660	.262	.270	.275	.274	.280	.212	.219	.221	.228	.224
8.751	.262	.270	.275	.274	.280	.212	.219	.221	.229	.223
9.041	.262	.269	.275	.274	.279	.211	.219	.221	.229	.223

TABLE I.- Continued

(h) $p/p_{t,j}$ for configuration D5

$p_{t,j}/p_\infty$	$y/w_t/2 = 0.0$									
	x/x_t									
	0.626	0.716	0.805	0.895	0.966	1.002	1.047	1.092	1.163	1.253
1.952	.929	.902	.853	.744	.452	.371	.310	.286	.296	.288
2.442	.928	.904	.853	.745	.452	.368	.306	.286	.296	.270
2.941	.927	.903	.854	.745	.452	.366	.304	.286	.296	.271
3.426	.927	.903	.853	.745	.448	.363	.301	.287	.295	.270
3.930	.926	.903	.853	.745	.441	.363	.300	.287	.293	.269
4.403	.926	.903	.853	.745	.433	.362	.299	.287	.292	.269
4.864	.926	.902	.853	.745	.428	.362	.298	.286	.291	.268
4.903	.926	.903	.853	.745	.429	.362	.298	.286	.291	.268
5.381	.926	.902	.853	.745	.421	.361	.297	.286	.290	.268
5.864	.926	.902	.853	.745	.423	.361	.297	.286	.290	.267
6.355	.926	.902	.852	.744	.422	.360	.297	.286	.290	.267
6.895	.925	.902	.852	.744	.420	.360	.297	.285	.289	.267
6.846	.925	.902	.852	.744	.421	.360	.297	.285	.289	.267
7.323	.925	.901	.852	.744	.427	.359	.296	.285	.289	.267
7.827	.925	.902	.852	.744	.426	.359	.296	.285	.289	.267
8.311	.925	.901	.852	.744	.423	.359	.296	.285	.288	.267
8.586	.925	.901	.852	.744	.423	.358	.295	.285	.289	.267
8.600	.925	.901	.852	.744	.425	.359	.296	.285	.289	.267
8.631	.925	.901	.852	.744	.425	.358	.295	.285	.289	.267
8.668	.925	.901	.852	.744	.427	.359	.296	.285	.289	.267
9.561	.925	.901	.851	.744	.427	.358	.295	.284	.288	.267

$p_{t,j}/p_\infty$	$y/w_t/2 = 0.0$				$x/x_t = 1.047$				
	x/x_t				$y/w_t/2$				
	1.342	1.432	1.521	1.575	0.250	0.500	0.750	0.875	0.950
1.952	.406	.430	.447	.464	.298	.309	.308	.304	.312
2.442	.225	.348	.366	.378	.296	.305	.305	.301	.310
2.941	.225	.197	.308	.323	.296	.304	.303	.301	.307
3.426	.225	.197	.164	.220	.296	.306	.304	.303	.305
3.930	.225	.197	.165	.151	.296	.306	.304	.303	.303
4.403	.225	.197	.166	.151	.294	.306	.303	.305	.302
4.864	.225	.197	.166	.152	.294	.305	.302	.304	.301
4.903	.225	.197	.166	.152	.294	.305	.302	.304	.301
5.381	.224	.197	.167	.152	.293	.305	.301	.303	.299
5.864	.224	.197	.167	.152	.293	.304	.301	.303	.295
6.355	.223	.196	.167	.152	.292	.304	.301	.303	.292
6.895	.223	.196	.167	.152	.293	.304	.301	.301	.292
6.846	.223	.196	.167	.152	.293	.303	.300	.301	.292
7.323	.223	.196	.167	.152	.293	.303	.300	.301	.289
7.827	.223	.196	.167	.152	.292	.303	.300	.301	.290
8.311	.223	.196	.167	.152	.292	.303	.299	.301	.291
8.586	.223	.196	.167	.152	.292	.303	.299	.301	.291
8.600	.223	.196	.168	.152	.292	.303	.300	.301	.290
8.631	.223	.196	.167	.152	.292	.302	.299	.301	.290
8.668	.223	.196	.168	.152	.292	.303	.299	.301	.291
9.561	.222	.195	.168	.152	.291	.302	.299	.300	.292

$p_{t,j}/p_\infty$	$x/x_t = 1.342$					$x/x_t = 1.575$				
	$y/w_t/2$					$y/w_t/2$				
	0.250	0.500	0.750	0.875	0.950	0.250	0.500	0.750	0.875	0.950
1.952	.380	.325	.359	.442	.478	.470	.505	.516	.506	.499
2.442	.233	.249	.241	.238	.256	.381	.377	.395	.412	.408
2.941	.233	.248	.241	.238	.249	.325	.323	.322	.319	.316
3.426	.232	.247	.241	.238	.248	.218	.197	.225	.265	.266
3.930	.232	.247	.241	.238	.248	.154	.143	.153	.213	.234
4.403	.231	.247	.241	.238	.244	.154	.146	.152	.178	.209
4.864	.231	.247	.241	.238	.245	.154	.148	.152	.166	.182
4.903	.231	.247	.241	.238	.245	.154	.148	.152	.166	.179
5.381	.230	.246	.241	.238	.246	.154	.150	.151	.162	.147
5.864	.230	.246	.241	.238	.246	.154	.152	.151	.162	.143
6.355	.230	.246	.241	.238	.244	.154	.153	.151	.162	.146
6.895	.230	.247	.241	.238	.244	.154	.155	.151	.162	.146
6.846	.230	.247	.241	.238	.240	.154	.155	.151	.162	.143
7.323	.230	.247	.241	.237	.240	.154	.156	.151	.157	.155
7.827	.229	.247	.241	.238	.241	.154	.157	.151	.157	.154
8.311	.229	.247	.242	.237	.240	.154	.157	.150	.156	.158
8.586	.229	.247	.241	.237	.240	.154	.158	.150	.158	.156
8.600	.229	.247	.242	.237	.240	.154	.158	.150	.158	.157
8.631	.229	.247	.241	.237	.240	.154	.158	.150	.158	.156
8.668	.229	.247	.242	.237	.236	.154	.158	.150	.158	.156
9.561	.229	.247	.241	.237	.239	.154	.159	.150	.158	.157

TABLE I.- Continued

(i) $p/p_{t,j}$ for configuration D6

$p_{t,j}/p_\infty$	$y/w_t/2 = 0.0$									
	x/x_t									
	0.791	0.901	1.011	1.077	1.143	1.286	1.429	1.560	1.736	1.890
1.969	.779	.615	.367	.284	.294	.276	.435	.435	.439	.464
2.219	.778	.613	.366	.283	.294	.276	.393	.418	.421	.429
2.470	.778	.616	.365	.282	.294	.277	.231	.377	.385	.388
2.712	.778	.615	.364	.282	.295	.277	.231	.300	.351	.354
2.951	.777	.616	.363	.282	.295	.277	.231	.191	.318	.324
3.197	.777	.616	.363	.281	.295	.277	.231	.191	.284	.296
3.444	.777	.616	.362	.281	.295	.278	.231	.191	.201	.274
3.941	.776	.616	.362	.281	.295	.277	.231	.191	.145	.231
4.420	.774	.616	.362	.280	.295	.276	.231	.191	.145	.121
4.908	.774	.617	.362	.280	.295	.275	.231	.191	.145	.117
5.386	.773	.617	.362	.280	.295	.275	.231	.191	.145	.117
5.881	.772	.617	.361	.279	.295	.274	.231	.190	.145	.117
6.373	.774	.617	.361	.279	.295	.274	.231	.190	.145	.117
6.866	.774	.617	.361	.279	.295	.274	.231	.190	.145	.117
7.334	.774	.617	.361	.280	.295	.273	.230	.190	.145	.117
7.828	.773	.617	.361	.279	.295	.273	.230	.190	.145	.117
8.310	.774	.617	.361	.279	.294	.273	.230	.190	.145	.117
8.592	.773	.617	.361	.279	.294	.273	.230	.190	.145	.117
8.654	.774	.617	.361	.279	.294	.273	.230	.190	.145	.117
8.753	.773	.617	.361	.279	.294	.273	.230	.190	.145	.117
9.209	.774	.617	.361	.279	.294	.273	.230	.190	.145	.117

$p_{t,j}/p_\infty$	$y/w_t/2 = 0.450$									
	x/x_t									
	0.791	0.901	1.011	1.077	1.143	1.286	1.429	1.560	1.736	1.890
1.969	.784	.619	.378	.285	.292	.277	.329	.418	.463	.500
2.219	.782	.618	.374	.283	.292	.278	.379	.416	.420	.428
2.470	.783	.618	.371	.282	.293	.278	.216	.375	.384	.387
2.712	.783	.618	.369	.281	.294	.278	.219	.275	.346	.350
2.951	.782	.618	.368	.280	.295	.278	.222	.193	.316	.322
3.197	.783	.618	.366	.280	.295	.278	.225	.193	.281	.294
3.444	.783	.618	.365	.279	.295	.277	.227	.192	.179	.272
3.941	.782	.617	.363	.278	.295	.277	.231	.192	.146	.228
4.420	.782	.617	.361	.278	.294	.277	.233	.192	.146	.117
4.908	.782	.617	.360	.278	.294	.276	.235	.192	.146	.116
5.386	.782	.616	.359	.278	.294	.276	.237	.192	.146	.117
5.881	.781	.616	.358	.278	.293	.276	.239	.192	.146	.117
6.373	.782	.616	.358	.277	.294	.276	.239	.191	.146	.117
6.866	.781	.616	.357	.277	.293	.276	.240	.191	.146	.116
7.334	.781	.616	.357	.277	.293	.276	.241	.191	.146	.116
7.828	.781	.617	.356	.277	.293	.276	.242	.191	.146	.116
8.310	.781	.616	.356	.277	.293	.276	.243	.191	.146	.116
8.592	.781	.616	.356	.277	.293	.276	.243	.191	.146	.116
8.654	.781	.616	.356	.277	.293	.276	.243	.191	.146	.116
8.753	.781	.616	.356	.277	.293	.276	.243	.191	.146	.116
9.209	.781	.617	.355	.277	.293	.276	.244	.191	.145	.116

TABLE I.- Continued

(i) Concluded

$p_{t,j}/p_\infty$	$y/w_t/2 = 0.875$								
	x/x_t								
	0.791	0.901	1.077	1.143	1.286	1.429	1.560	1.736	1.890
1.969	.785	.623	.282	.305	.305	.430	.478	.482	.489
2.219	.784	.622	.282	.306	.282	.333	.404	.411	.423
2.470	.785	.622	.282	.307	.282	.235	.366	.373	.381
2.712	.784	.621	.282	.307	.281	.235	.192	.337	.348
2.951	.784	.622	.283	.307	.282	.234	.190	.305	.313
3.197	.784	.622	.283	.307	.282	.234	.190	.271	.286
3.444	.783	.621	.283	.307	.282	.234	.191	.153	.268
3.941	.783	.622	.283	.307	.281	.234	.191	.148	.224
4.420	.783	.622	.282	.307	.281	.233	.192	.149	.121
4.908	.783	.621	.282	.306	.280	.233	.192	.148	.119
5.386	.783	.621	.282	.307	.280	.232	.192	.148	.120
5.881	.782	.621	.281	.306	.280	.232	.192	.148	.120
6.373	.782	.620	.281	.307	.280	.231	.192	.148	.120
6.866	.782	.620	.281	.307	.279	.231	.192	.148	.120
7.334	.782	.620	.281	.307	.279	.231	.192	.148	.120
7.828	.782	.620	.281	.307	.279	.231	.192	.148	.120
8.310	.782	.620	.281	.307	.279	.230	.192	.148	.119
8.592	.782	.620	.281	.307	.279	.230	.192	.148	.119
8.654	.782	.620	.281	.307	.279	.230	.192	.148	.119
8.753	.781	.620	.281	.307	.279	.230	.192	.148	.119
9.209	.781	.620	.281	.307	.279	.230	.192	.148	.119

$p_{t,j}/p_\infty$	$y/w_t/2 = 0.225$					$y/w_t/2 = 0.662$			
	x/x_t					x/x_t			
	0.791	1.011	1.286	1.560	1.890	0.791	1.286	1.560	1.890
1.969	.785	.368	.278	.418	.466	.782	.280	.456	.509
2.219	.785	.367	.279	.418	.429	.782	.280	.413	.427
2.470	.785	.367	.279	.377	.388	.782	.280	.373	.386
2.712	.784	.367	.279	.300	.353	.782	.280	.211	.342
2.951	.785	.366	.278	.190	.323	.783	.279	.192	.321
3.197	.786	.366	.278	.190	.296	.782	.279	.192	.295
3.444	.785	.365	.278	.190	.273	.782	.279	.192	.273
3.941	.784	.365	.277	.190	.231	.782	.279	.192	.229
4.420	.784	.364	.277	.190	.118	.782	.279	.191	.120
4.908	.784	.364	.277	.190	.116	.782	.279	.191	.120
5.386	.784	.364	.277	.190	.116	.781	.279	.191	.120
5.881	.784	.363	.277	.190	.116	.781	.279	.190	.120
6.373	.784	.363	.276	.190	.116	.781	.279	.190	.119
6.866	.783	.363	.276	.190	.116	.781	.279	.189	.119
7.334	.783	.363	.276	.189	.116	.781	.279	.189	.119
7.828	.782	.363	.276	.189	.116	.781	.279	.189	.119
8.310	.778	.362	.276	.189	.116	.781	.279	.189	.119
8.592	.775	.362	.276	.189	.116	.781	.279	.189	.119
8.654	.775	.362	.276	.189	.116	.781	.279	.189	.119
8.753	.774	.362	.276	.189	.116	.781	.279	.188	.119
9.209	.768	.362	.276	.189	.116	.781	.279	.188	.119

TABLE I.- Continued

(j) $p/p_{t,j}$ for configurations E1, E3, and F1

Configuration E1

$p_{t,j}/p_\infty$	$y/w_t/2 = 0.0$				
	x/x_t				
	0.889	1.000	1.127	1.246	1.365
1.971	.865	.412	.406	.391	.367
2.481	.865	.411	.407	.395	.370
2.959	.863	.409	.405	.393	.371
3.464	.863	.407	.404	.391	.373
3.452	.863	.407	.404	.392	.373
3.942	.859	.405	.404	.390	.372
4.432	.856	.405	.404	.389	.372
4.926	.860	.405	.404	.389	.371
5.403	.851	.405	.404	.388	.371
5.905	.844	.404	.403	.388	.371
6.390	.841	.404	.403	.388	.370
6.858	.851	.404	.404	.388	.370
7.371	.856	.404	.404	.387	.369
7.805	.854	.404	.404	.387	.369
8.827	.853	.403	.404	.387	.367
9.805	.851	.403	.404	.386	.366
9.842	.852	.403	.404	.386	.366
9.831	.851	.403	.404	.386	.366
11.690	.843	.403	.405	.386	.363

Configuration E3

$p_{t,j}/p_\infty$	$y/w_t/2 = 0.0$				
	x/x_t				
	0.889	1.000	1.127	1.246	1.365
1.975	.864	.375	.263	.415	.448
2.470	.863	.375	.264	.315	.354
2.956	.863	.374	.271	.194	.311
3.456	.863	.374	.277	.194	.273
3.951	.862	.373	.281	.194	.176
4.451	.862	.373	.283	.194	.130
4.442	.862	.373	.283	.194	.130
4.933	.862	.372	.285	.191	.130
5.409	.861	.372	.286	.191	.130
5.912	.861	.372	.288	.190	.130
6.377	.861	.372	.289	.190	.130
6.915	.861	.372	.290	.191	.130
6.888	.861	.372	.290	.190	.130
7.416	.861	.372	.291	.189	.130
7.886	.861	.372	.292	.190	.130
7.839	.861	.372	.292	.190	.130
8.363	.860	.372	.293	.189	.130
8.837	.861	.371	.293	.189	.130
9.833	.860	.371	.294	.190	.130
11.737	.860	.370	.296	.189	.130

Configurat_ F1

$p_{t,j}/p_\infty$	$y/w_t/2 = 0.0$				
	x/x_t				
	0.943	1.000	1.086	1.157	1.229
1.994	.823	.407	.407	.401	.363
2.485	.821	.406	.409	.406	.363
2.989	.819	.405	.408	.406	.362
3.485	.819	.403	.407	.404	.365
3.969	.818	.402	.406	.402	.369
4.460	.817	.401	.406	.400	.370
4.961	.816	.401	.406	.400	.369
5.454	.811	.400	.406	.399	.367
5.949	.814	.400	.406	.399	.365
6.444	.806	.399	.406	.399	.362
6.934	.814	.399	.406	.398	.360
7.446	.812	.399	.407	.398	.357
7.939	.812	.399	.407	.398	.354
8.844	.811	.398	.407	.398	.351
8.918	.810	.398	.407	.398	.351
9.889	.809	.398	.407	.398	.347
11.876	.807	.398	.408	.397	.342

TABLE I.- Concluded

(k) $p/p_{t,j}$ for configuration F3

$p_{t,j}/p_\infty$	$y/w_t/2 = 0.0$							
	x/x_t							
	0.943	1.000	1.043	1.086	1.121	1.157	1.193	1.229
1.981	.818	.382	.292	.302	.391	.421	.429	.441
2.232	.817	.381	.291	.280	.325	.393	.405	.409
2.475	.818	.380	.290	.275	.275	.349	.366	.366
2.716	.819	.379	.289	.275	.245	.289	.334	.342
2.973	.818	.377	.288	.275	.239	.214	.286	.311
3.232	.817	.376	.287	.274	.239	.205	.188	.272
3.203	.817	.376	.287	.274	.239	.205	.192	.276
3.453	.817	.375	.287	.274	.239	.205	.171	.224
3.963	.818	.374	.285	.273	.239	.205	.170	.133
4.434	.817	.373	.284	.273	.239	.206	.170	.134
4.912	.817	.372	.284	.273	.240	.206	.171	.134
5.435	.817	.372	.283	.273	.240	.206	.171	.134
5.904	.817	.371	.283	.273	.240	.206	.171	.134
6.380	.816	.371	.283	.273	.239	.206	.171	.134
6.885	.816	.371	.283	.272	.239	.206	.171	.135
7.383	.816	.371	.282	.272	.239	.206	.170	.135
7.850	.816	.370	.282	.271	.239	.206	.171	.135
8.370	.816	.370	.282	.271	.239	.206	.170	.135
8.840	.816	.370	.281	.270	.239	.206	.171	.135
9.795	.816	.369	.281	.271	.239	.206	.171	.135
9.831	.816	.369	.281	.271	.239	.206	.171	.135
11.783	.815	.368	.279	.272	.239	.207	.171	.136

$p_{t,j}/p_\infty$	$y/w_t/2 = 0.450$							
	x/x_t							
	0.943	1.000	1.043	1.086	1.121	1.157	1.193	1.229
1.981	.824	.340	.290	.287	.387	.421	.430	.440
2.232	.822	.341	.289	.278	.275	.377	.391	.394
2.475	.823	.341	.288	.278	.242	.286	.335	.346
2.716	.822	.341	.288	.277	.241	.204	.243	.309
2.973	.823	.341	.287	.277	.242	.204	.261	.309
3.232	.822	.341	.286	.277	.242	.204	.171	.283
3.203	.822	.340	.285	.277	.242	.204	.172	.288
3.453	.822	.340	.285	.277	.242	.205	.171	.227
3.963	.821	.340	.284	.276	.242	.205	.171	.143
4.434	.821	.339	.284	.276	.242	.205	.171	.143
4.912	.821	.340	.284	.277	.242	.205	.171	.143
5.435	.821	.340	.283	.277	.241	.204	.171	.143
5.904	.821	.341	.283	.277	.241	.204	.171	.143
6.380	.820	.341	.283	.276	.241	.204	.171	.143
6.885	.820	.340	.283	.276	.241	.204	.171	.143
7.383	.820	.340	.283	.276	.241	.204	.171	.143
7.850	.820	.340	.282	.276	.241	.204	.171	.143
8.370	.820	.341	.282	.276	.241	.204	.171	.143
8.840	.820	.340	.282	.276	.241	.204	.171	.143
9.795	.819	.340	.281	.276	.241	.204	.171	.143
9.831	.819	.340	.281	.276	.241	.204	.171	.142
11.783	.818	.338	.280	.276	.242	.204	.171	.143

$p_{t,j}/p_\infty$	$y/w_t/2 = 0.662$			$y/w_t/2 = 0.875$							
	x/x_t			x/x_t							
	1.086	1.157	1.229	0.943	1.000	1.043	1.086	1.121	1.157	1.193	1.229
1.981	.320	.433	.445	.806	.357	.295	.303	.393	.419	.429	.441
2.232	.290	.386	.395	.803	.357	.294	.279	.265	.337	.364	.386
2.475	.270	.334	.360	.802	.357	.293	.279	.241	.215	.312	.375
2.716	.270	.227	.313	.800	.357	.293	.279	.242	.205	.226	.303
2.973	.270	.203	.275	.799	.357	.292	.279	.242	.205	.176	.265
3.232	.271	.203	.239	.799	.357	.292	.279	.243	.205	.174	.241
3.203	.271	.203	.246	.799	.357	.292	.279	.243	.205	.174	.245
3.453	.274	.203	.147	.798	.356	.292	.279	.243	.205	.174	.171
3.963	.275	.203	.141	.797	.355	.291	.279	.243	.206	.174	.150
4.434	.275	.204	.142	.797	.355	.290	.279	.243	.206	.173	.150
4.912	.275	.204	.142	.797	.354	.289	.279	.243	.207	.174	.150
5.435	.275	.203	.143	.796	.354	.289	.279	.243	.206	.174	.150
5.904	.275	.203	.143	.796	.353	.289	.279	.243	.206	.173	.149
6.380	.275	.203	.144	.796	.353	.289	.279	.243	.206	.173	.150
6.885	.275	.203	.144	.796	.352	.289	.279	.242	.205	.173	.149
7.383	.274	.203	.144	.797	.352	.289	.279	.242	.205	.173	.149
7.850	.274	.202	.144	.796	.352	.289	.279	.242	.205	.173	.149
8.370	.274	.202	.145	.796	.352	.289	.280	.242	.205	.172	.148
8.840	.274	.202	.145	.796	.351	.289	.280	.242	.205	.172	.148
9.795	.274	.202	.145	.796	.351	.288	.280	.242	.205	.172	.146
9.831	.274	.202	.145	.796	.351	.288	.280	.242	.205	.172	.146
11.783	.273	.203	.146	.796	.350	.287	.282	.243	.205	.172	.147

TABLE II.- RATIO OF INTERNAL STATIC PRESSURE TO JET TOTAL PRESSURE FOR NOZZLE CONFIGURATION A1V10

(a) $p/p_{t,j}$ for upper flap

$p_{t,j}/p_\infty$	$y/w_t/2 = 0.0$							
	x/x_t							
	0.638	0.745	0.851	0.957	1.000	1.064	1.117	1.170
1.983	.842	.799	.731	.471	.351	.378	.449	.493
2.973	.841	.801	.731	.467	.354	.379	.451	.492
3.962	.841	.801	.733	.464	.355	.377	.448	.489
4.948	.843	.801	.733	.465	.357	.378	.448	.488
5.445	.845	.802	.733	.466	.357	.378	.448	.488

$p_{t,j}/p_\infty$	$y/w_t/2 = 0.0$					
	x/x_t					
	1.277	1.383	1.489	1.596	1.702	1.809
1.983	.510	.472	.431	.388	.348	.351
2.973	.509	.470	.428	.386	.347	.313
3.962	.508	.469	.427	.385	.346	.311
4.948	.509	.469	.428	.384	.346	.310
5.445	.510	.469	.428	.384	.346	.310

$p_{t,j}/p_\infty$	$x/x_t = 1.064$					$x/x_t = 1.489$				
	$y/w_t/2$					$y/w_t/2$				
	0.250	0.500	0.750	0.875	0.950	0.250	0.500	0.750	0.875	0.950
1.983	.381	.377	.365	.357	.408	.429	.421	.435	.424	.422
2.973	.391	.383	.375	.360	.416	.428	.438	.438	.423	.421
3.962	.389	.381	.372	.362	.413	.427	.445	.439	.422	.421
4.948	.388	.381	.371	.364	.412	.427	.450	.440	.422	.420
5.445	.387	.381	.371	.365	.412	.427	.453	.439	.422	.421

$p_{t,j}/p_\infty$	$x/x_t = 1.809$				
	$y/w_t/2$				
	0.250	0.500	0.750	0.875	0.950
1.983	.357	.362	.360	.367	.381
2.973	.310	.310	.315	.309	.308
3.962	.309	.307	.313	.309	.307
4.948	.309	.306	.313	.309	.308
5.445	.309	.306	.313	.309	.308

TABLE II.- Concluded

(b) $p/p_{t,j}$ for lower flap

$p_{t,j}/p_\infty$	$y/w_t/2 = 0.0$							
	x/x_t							
	0.638	0.745	0.851	0.957	1.000	1.064	1.117	1.170
1.983	.840	.795	.735	.483	.351	.346	.373	.377
2.973	.839	.794	.735	.481	.344	.194	.159	.169
3.962	.838	.793	.734	.481	.343	.194	.157	.168
4.948	.839	.793	.734	.481	.342	.193	.156	.167
5.445	.840	.794	.734	.480	.342	.193	.155	.167

$p_{t,j}/p_\infty$	$y/w_t/2 = 0.0$						
	x/x_t						
	1.277	1.383	1.489	1.596	1.702	1.809	1.915
1.983	.397	.422	.436	.450	.463	.475	.480
2.973	.188	.198	.195	.186	.221	.305	.326
3.962	.187	.196	.193	.185	.172	.157	.214
4.948	.166	.195	.193	.184	.171	.156	.177
5.445	.186	.193	.193	.185	.172	.157	.176

$p_{t,j}/p_\infty$	$x/x_t = 1.064$					$x/x_t = 1.489$				
	$y/w_t/2$					$y/w_t/2$				
	0.250	0.500	0.750	0.875	0.950	0.250	0.500	0.750	0.875	0.950
1.983	.312	.335	.350	.338	.331	.439	.435	.436	.437	.441
2.973	.201	.195	.187	.191	.203	.192	.193	.192	.189	.184
3.962	.201	.195	.188	.191	.204	.192	.193	.192	.190	.184
4.948	.201	.195	.187	.191	.203	.192	.191	.192	.190	.184
5.445	.200	.195	.187	.191	.201	.191	.191	.192	.190	.184

$p_{t,j}/p_\infty$	$x/x_t = 1.809$				
	$y/w_t/2$				
	0.250	0.500	0.750	0.875	0.950
1.983	.475	.471	.473	.472	.474
2.973	.307	.306	.301	.295	.312
3.962	.159	.162	.159	.167	.175
4.948	.160	.162	.159	.166	.168
5.445	.160	.160	.159	.165	.168

TABLE III.- RATIO OF INTERNAL STATIC PRESSURE TO JET TOTAL PRESSURE FOR NOZZLE CONFIGURATION A1V13

(a) $p/p_{t,j}$ for upper flap

$p_{t,j}/p_\infty$	$y/w_t/2 = 0.0$							
	x/x_t							
	0.638	0.745	0.851	0.957	1.000	1.064	1.117	1.170
1.986	.646	.630	.746	.588	.622	.632	.623	.611
2.978	.645	.630	.745	.584	.622	.630	.620	.609
3.979	.644	.630	.746	.582	.623	.630	.619	.608
4.942	.645	.630	.748	.581	.623	.632	.620	.608
5.007	.645	.631	.749	.581	.624	.632	.620	.609
5.500	.645	.630	.749	.580	.625	.632	.620	.608

$p_{t,j}/p_\infty$	$y/w_t/2 = 0.0$					
	x/x_t					
	1.277	1.383	1.489	1.596	1.702	1.809
1.986	.575	.526	.477	.437	.387	.350
2.978	.574	.524	.476	.434	.386	.347
3.979	.573	.522	.475	.432	.385	.344
4.942	.573	.522	.475	.431	.385	.343
5.007	.572	.522	.475	.431	.385	.343
5.500	.572	.522	.475	.431	.385	.342

$p_{t,j}/p_\infty$	$x/x_t = 1.064$					$x/x_t = 1.489$				
	$y/w_t/2$					$y/w_t/2$				
	0.250	0.500	0.750	0.875	0.950	0.250	0.500	0.750	0.875	0.950
1.986	.628	.629	.635	.637	.641	.476	.469	.478	.479	.476
2.978	.625	.627	.635	.635	.640	.474	.485	.476	.478	.474
3.979	.624	.627	.634	.633	.636	.473	.492	.475	.476	.473
4.942	.623	.627	.634	.633	.636	.472	.497	.474	.475	.472
5.007	.623	.627	.633	.633	.636	.472	.498	.474	.475	.472
5.500	.623	.627	.634	.633	.636	.471	.499	.474	.475	.472

$p_{t,j}/p_\infty$	$x/x_t = 1.809$				
	$y/w_t/2$				
	0.250	0.500	0.750	0.875	0.950
1.986	.347	.347	.346	.357	.395
2.978	.346	.346	.344	.348	.342
3.979	.344	.345	.341	.347	.338
4.942	.343	.345	.340	.346	.337
5.007	.343	.344	.340	.346	.337
5.500	.343	.344	.340	.346	.337

TABLE III.- Concluded

(b) $p/p_{t,j}$ for lower flap

$p_{t,j}/p_\infty$	$y/w_t/2 = 0.0$							
	x/x_t							
	0.638	0.745	0.851	0.957	1.000	1.064	1.117	1.170
1.986	.845	.803	.743	.498	.360	.211	.180	.192
2.978	.845	.801	.743	.498	.356	.209	.175	.189
3.979	.845	.801	.742	.498	.355	.208	.173	.187
4.942	.845	.801	.742	.497	.354	.207	.171	.186
5.007	.846	.802	.742	.497	.354	.207	.171	.186
5.500	.845	.801	.742	.497	.354	.207	.170	.186

$p_{t,j}/p_\infty$	$y/w_t/2 = 0.0$						
	x/x_t						
	1.277	1.383	1.489	1.596	1.702	1.809	1.915
1.986	.225	.253	.294	.394	.450	.482	.503
2.978	.222	.245	.261	.268	.270	.267	.280
3.979	.220	.242	.259	.267	.269	.267	.264
4.942	.218	.240	.258	.266	.269	.266	.262
5.007	.218	.240	.257	.265	.268	.266	.262
5.500	.218	.239	.256	.265	.268	.266	.262

$p_{t,j}/p_\infty$	$x/x_t = 1.064$					$x/x_t = 1.489$				
	$y/w_t/2$					$y/w_t/2$				
	0.250	0.500	0.750	0.875	0.950	0.250	0.500	0.750	0.875	0.950
1.986	.214	.208	.197	.208	.223	.273	.297	.378	.376	.383
2.978	.215	.209	.199	.209	.221	.257	.259	.253	.256	.261
3.979	.215	.208	.199	.207	.221	.256	.258	.255	.256	.260
4.942	.214	.208	.199	.204	.213	.255	.257	.254	.254	.257
5.007	.214	.207	.199	.204	.213	.255	.256	.253	.254	.257
5.500	.214	.207	.199	.205	.209	.254	.256	.253	.254	.256

$p_{t,j}/p_\infty$	$x/x_t = 1.809$				
	$y/w_t/2$				
	0.250	0.500	0.750	0.875	0.950
1.986	.489	.491	.476	.480	.477
2.978	.272	.275	.271	.278	.280
3.979	.273	.273	.270	.275	.273
4.942	.272	.272	.269	.273	.271
5.007	.272	.272	.269	.272	.271
5.500	.271	.272	.269	.272	.271

TABLE IV.- RATIO OF INTERNAL STATIC PRESSURE TO JET TOTAL PRESSURE FOR NOZZLE CONFIGURATION A1V20

(a) $p/p_{t,j}$ for upper flap

$p_{t,j}/p_\infty$	$y/w_t/2 = 0.0$								
	x/x_t								
	0.638	0.745	0.851	0.957	1.000	1.064	1.117	1.170	1.277
2.008	.846	.803	.750	.589	.619	.637	.629	.618	.591
2.524	.844	.801	.747	.582	.611	.628	.618	.605	.569
3.027	.845	.802	.747	.583	.611	.629	.619	.605	.569
3.532	.846	.803	.747	.583	.613	.630	.620	.606	.570
4.053	.848	.803	.747	.583	.612	.629	.620	.606	.570
4.553	.850	.804	.747	.583	.613	.629	.620	.607	.570
5.037	.848	.804	.747	.582	.613	.629	.620	.607	.570
5.552	.847	.805	.747	.582	.614	.630	.621	.607	.570

$p_{t,j}/p_\infty$	$y/w_t/2 = 0.0$					$x/x_t = 1.064$				
	x/x_t					$y/w_t/2$				
	1.383	1.489	1.596	1.702	1.809	0.250	0.500	0.750	0.875	0.950
2.008	.558	.524	.508	.489	.474	.633	.631	.635	.631	.629
2.524	.518	.472	.432	.385	.396	.624	.622	.626	.622	.620
3.027	.518	.472	.432	.385	.345	.624	.622	.626	.623	.620
3.532	.519	.472	.432	.385	.345	.624	.622	.627	.623	.620
4.053	.519	.472	.432	.385	.345	.624	.623	.627	.623	.621
4.553	.519	.472	.432	.385	.345	.624	.623	.628	.623	.621
5.037	.520	.472	.432	.384	.345	.624	.624	.628	.623	.621
5.552	.521	.472	.432	.384	.345	.625	.624	.629	.624	.622

$p_{t,j}/p_\infty$	$x/x_t = 1.489$					$x/x_t = 1.809$				
	$y/w_t/2$					$y/w_t/2$				
	0.250	0.500	0.750	0.875	0.950	0.250	0.500	0.750	0.875	0.950
2.008	.524	.520	.525	.525	.528	.472	.470	.470	.478	.477
2.524	.471	.467	.474	.473	.478	.400	.400	.389	.396	.385
3.027	.471	.467	.474	.473	.478	.347	.343	.338	.346	.333
3.532	.471	.467	.475	.473	.479	.347	.342	.338	.346	.330
4.053	.471	.468	.475	.473	.479	.347	.342	.338	.346	.330
4.553	.471	.468	.475	.473	.480	.347	.341	.337	.346	.329
5.037	.471	.468	.475	.473	.480	.346	.341	.337	.346	.329
5.552	.472	.468	.475	.474	.480	.346	.341	.337	.346	.329

TABLE IV.- Concluded

(b) $p/p_{t,j}$ for lower flap

$p_{t,j}/p_\infty$	$y/w_t/2 = 0.0$								
	x/x_t								
	0.638	0.745	0.851	0.957	1.000	1.064	1.117	1.170	1.277
2.008	.839	.800	.734	.477	.351	.452	.470	.473	.473
2.524	.837	.798	.733	.474	.345	.308	.372	.379	.380
3.027	.838	.799	.733	.473	.343	.204	.305	.312	.314
3.532	.839	.800	.734	.473	.343	.204	.256	.268	.268
4.053	.839	.800	.734	.473	.343	.204	.114	.080	.091
4.553	.841	.800	.734	.472	.343	.204	.114	.080	.091
5.037	.842	.800	.734	.472	.343	.204	.114	.081	.092
5.552	.842	.800	.735	.472	.343	.204	.115	.081	.092

$p_{t,j}/p_\infty$	$y/w_t/2 = 0.0$					$x/x_t = 1.064$				
	x/x_t					$y/w_t/2$				
	1.383	1.489	1.596	1.702	1.809	0.250	0.500	0.750	0.875	0.950
2.008	.475	.476	.478	.480	.475	.400	.419	.432	.429	.429
2.524	.381	.381	.382	.382	.377	.291	.292	.289	.293	.292
3.027	.314	.315	.315	.316	.311	.211	.199	.196	.199	.201
3.532	.267	.266	.266	.267	.264	.211	.200	.196	.200	.202
4.053	.108	.117	.121	.127	.170	.211	.201	.197	.200	.201
4.553	.108	.117	.121	.127	.128	.211	.201	.197	.200	.201
5.037	.108	.117	.121	.127	.127	.210	.201	.197	.200	.201
5.552	.108	.116	.122	.127	.127	.210	.201	.197	.200	.201

$p_{t,j}/p_\infty$	$x/x_t = 1.489$					$x/x_t = 1.809$				
	$y/w_t/2$					$y/w_t/2$				
	0.250	0.500	0.750	0.875	0.950	0.250	0.500	0.750	0.875	0.950
2.008	.475	.473	.470	.467	.472	.477	.476	.480	.483	.486
2.524	.381	.378	.373	.371	.375	.376	.376	.381	.383	.387
3.027	.314	.311	.306	.304	.307	.311	.311	.315	.314	.319
3.532	.266	.263	.258	.255	.259	.266	.265	.264	.266	.270
4.053	.117	.114	.114	.127	.151	.190	.209	.199	.235	.234
4.553	.116	.114	.113	.110	.119	.123	.129	.130	.181	.191
5.037	.115	.114	.112	.110	.116	.122	.129	.125	.128	.155
5.552	.115	.114	.112	.110	.114	.122	.129	.125	.125	.143

TABLE V.- RATIO OF INTERNAL STATIC PRESSURE TO JET TOTAL PRESSURE FOR NOZZLE CONFIGURATION A2V20

(a) $p/p_{t,j}$ for upper flap

$p_{t,j}/p_\infty$	$y/w_t/2 = 0.0$								
	x/x_t								
	0.638	0.745	0.851	0.957	1.000	1.064	1.117	1.170	1.277
2.018	.846	.803	.749	.589	.620	.635	.629	.618	.591
2.521	.844	.800	.745	.582	.612	.627	.619	.605	.568
3.019	.845	.801	.745	.582	.613	.627	.619	.605	.569
3.534	.844	.802	.746	.582	.613	.628	.619	.606	.569
4.048	.845	.803	.746	.582	.613	.628	.620	.606	.569
4.540	.845	.804	.746	.582	.613	.629	.620	.607	.569
5.032	.845	.804	.747	.582	.613	.629	.620	.607	.570
5.034	.845	.804	.747	.582	.613	.629	.620	.607	.570
5.553	.845	.805	.747	.582	.614	.630	.621	.607	.570

$p_{t,j}/p_\infty$	$y/w_t/2 = 0.0$					$x/x_t = 1.064$				
	x/x_t					$y/w_t/2$				
	1.383	1.489	1.596	1.702	1.809	0.250	0.500	0.750	0.875	0.950
2.018	.558	.520	.506	.486	.471	.634	.631	.635	.628	.623
2.521	.518	.467	.432	.385	.394	.624	.622	.626	.619	.614
3.019	.518	.463	.432	.385	.345	.623	.621	.625	.620	.615
3.534	.518	.462	.432	.385	.346	.623	.621	.626	.620	.615
4.048	.518	.462	.432	.385	.345	.623	.622	.626	.621	.616
4.540	.519	.462	.432	.384	.345	.624	.623	.627	.621	.617
5.032	.519	.462	.432	.384	.345	.624	.623	.627	.621	.617
5.034	.519	.462	.432	.384	.345	.624	.623	.627	.622	.617
5.553	.520	.462	.432	.384	.345	.624	.624	.628	.622	.618

$p_{t,j}/p_\infty$	$x/x_t = 1.489$					$x/x_t = 1.809$				
	$y/w_t/2$					$y/w_t/2$				
	0.250	0.500	0.750	0.875	0.950	0.250	0.500	0.750	0.875	0.950
2.018	.522	.518	.523	.523	.521	.468	.469	.472	.471	.451
2.521	.471	.467	.475	.473	.473	.394	.375	.350	.362	.343
3.019	.471	.467	.475	.473	.472	.346	.343	.342	.352	.311
3.534	.471	.467	.475	.473	.473	.346	.342	.341	.352	.308
4.048	.471	.467	.475	.473	.473	.347	.342	.341	.352	.309
4.540	.471	.468	.475	.474	.473	.347	.342	.341	.352	.309
5.032	.471	.468	.475	.474	.473	.346	.342	.341	.351	.310
5.034	.471	.468	.475	.474	.473	.346	.342	.341	.351	.310
5.553	.471	.468	.476	.474	.473	.346	.342	.340	.351	.308

TABLE V.- Concluded

(b) $p/p_{t,j}$ for lower flap

$p_{t,j}/p_\infty$	$y/w_t/2 = 0.0$								
	x/x_t								
	0.638	0.745	0.851	0.957	1.000	1.064	1.117	1.170	1.277
2.018	.840	.800	.734	.477	.352	.451	.471	.475	.476
2.521	.838	.798	.732	.473	.345	.310	.373	.379	.380
3.019	.838	.799	.732	.473	.343	.204	.310	.316	.317
3.534	.839	.799	.733	.472	.343	.204	.261	.270	.270
4.048	.840	.800	.733	.472	.343	.204	.115	.080	.090
4.540	.840	.800	.734	.472	.344	.204	.115	.080	.091
5.032	.841	.800	.734	.471	.344	.204	.115	.080	.092
5.034	.841	.800	.734	.471	.344	.204	.115	.080	.092
5.553	.841	.800	.734	.471	.344	.204	.115	.081	.092

$p_{t,j}/p_\infty$	$y/w_t/2 = 0.0$					$x/x_t = 1.064$				
	x/x_t					$y/w_t/2$				
	1.383	1.489	1.596	1.702	1.809	0.250	0.500	0.750	0.875	0.950
2.018	.477	.479	.482	.483	.481	.425	.438	.411	.410	.413
2.521	.381	.383	.384	.385	.384	.285	.295	.276	.275	.269
3.019	.317	.318	.320	.320	.320	.211	.199	.195	.199	.199
3.534	.269	.269	.270	.271	.271	.211	.200	.196	.201	.199
4.048	.108	.117	.121	.127	.203	.211	.201	.197	.201	.199
4.540	.108	.117	.121	.127	.128	.210	.200	.197	.201	.199
5.032	.108	.117	.122	.126	.128	.210	.200	.197	.201	.199
5.034	.108	.117	.121	.127	.128	.210	.200	.197	.201	.199
5.553	.108	.116	.122	.127	.127	.210	.200	.197	.201	.199

$p_{t,j}/p_\infty$	$x/x_t = 1.489$					$x/x_t = 1.809$				
	$y/w_t/2$					$y/w_t/2$				
	0.250	0.500	0.750	0.875	0.950	0.250	0.500	0.750	0.875	0.950
2.018	.479	.474	.456	.456	.465	.479	.479	.481	.489	.485
2.521	.382	.378	.361	.362	.369	.383	.383	.378	.391	.388
3.019	.317	.313	.295	.299	.305	.319	.320	.321	.326	.325
3.534	.267	.262	.246	.250	.256	.272	.272	.272	.278	.278
4.048	.117	.119	.170	.210	.225	.211	.191	.256	.245	.242
4.540	.116	.114	.120	.166	.188	.123	.185	.217	.222	.218
5.032	.116	.114	.112	.146	.165	.122	.166	.183	.203	.197
5.034	.116	.114	.112	.146	.165	.122	.166	.184	.203	.197
5.553	.115	.114	.112	.122	.148	.122	.142	.171	.183	.179

TABLE VI.- RATIO OF INTERNAL STATIC PRESSURE TO JET TOTAL PRESSURE FOR NOZZLE CONFIGURATION A3V20

(a) $p/p_{t,j}$ for upper flap

$p_{t,j}/p_\infty$	$y/w_t/2 = 0.0$								
	x/x_t								
	0.638	0.745	0.851	0.957	1.000	1.064	1.117	1.170	1.277
2.004	.846	.803	.749	.589	.621	.636	.631	.620	.593
2.520	.844	.800	.745	.582	.612	.627	.619	.605	.569
3.037	.844	.801	.745	.582	.612	.628	.619	.606	.569
3.533	.845	.802	.746	.582	.612	.628	.620	.606	.569
4.050	.846	.803	.746	.582	.613	.629	.620	.607	.570
4.546	.845	.804	.747	.582	.613	.629	.620	.607	.570
5.055	.845	.805	.747	.582	.613	.629	.620	.607	.570
5.552	.845	.805	.747	.582	.614	.630	.621	.608	.570

$p_{t,j}/p_\infty$	$y/w_t/2 = 0.0$					$x/x_t = 1.064$				
	x/x_t					$y/w_t/2$				
	1.383	1.489	1.596	1.702	1.809	0.250	0.500	0.750	0.875	0.950
2.004	.560	.525	.510	.494	.475	.635	.632	.636	.632	.630
2.520	.518	.472	.433	.386	.390	.624	.622	.627	.622	.621
3.037	.518	.472	.433	.386	.345	.624	.622	.627	.623	.621
3.533	.518	.472	.433	.386	.345	.624	.622	.627	.623	.621
4.050	.519	.472	.433	.386	.345	.624	.622	.627	.623	.622
4.546	.519	.472	.433	.386	.345	.624	.623	.628	.624	.622
5.055	.520	.472	.433	.385	.344	.624	.624	.628	.624	.623
5.552	.521	.472	.433	.385	.344	.625	.624	.629	.625	.624

$p_{t,j}/p_\infty$	$x/x_t = 1.489$					$x/x_t = 1.809$				
	$y/w_t/2$					$y/w_t/2$				
	0.250	0.500	0.750	0.875	0.950	0.250	0.500	0.750	0.875	0.950
2.004	.526	.522	.526	.526	.527	.474	.479	.494	.505	.499
2.520	.472	.468	.476	.472	.472	.392	.366	.345	.383	.391
3.037	.471	.467	.476	.472	.472	.348	.344	.300	.310	.319
3.533	.471	.467	.476	.472	.472	.348	.343	.292	.265	.271
4.050	.472	.468	.476	.472	.473	.348	.343	.290	.234	.233
4.546	.472	.468	.476	.472	.473	.347	.343	.289	.215	.205
5.055	.472	.468	.476	.472	.473	.347	.342	.288	.206	.182
5.552	.472	.468	.476	.473	.474	.347	.342	.288	.203	.163

TABLE VI.- Concluded

(b) $p/p_{t,j}$ for lower flap

$p_{t,j}/p_\infty$	$y/w_t/2 = 0.0$								
	x/x_t								
	0.638	0.745	0.851	0.957	1.000	1.064	1.117	1.170	1.277
2.004	.840	.800	.734	.477	.352	.457	.477	.481	.483
2.520	.837	.798	.732	.473	.345	.313	.373	.380	.381
3.037	.838	.798	.732	.473	.343	.204	.305	.311	.312
3.533	.839	.799	.733	.472	.343	.204	.116	.079	.089
4.050	.840	.800	.734	.472	.343	.204	.120	.080	.090
4.546	.840	.800	.734	.472	.343	.204	.119	.080	.091
5.055	.841	.800	.734	.472	.343	.204	.119	.080	.092
5.552	.842	.800	.735	.472	.343	.204	.118	.081	.092

$p_{t,j}/p_\infty$	$y/w_t/2 = 0.0$					$x/x_t = 1.064$				
	x/x_t					$y/w_t/2$				
	1.383	1.489	1.596	1.702	1.809	0.250	0.500	0.750	0.875	0.950
2.004	.485	.487	.489	.490	.489	.430	.445	.417	.404	.400
2.520	.383	.385	.387	.389	.388	.286	.292	.262	.220	.207
3.037	.315	.315	.318	.321	.321	.211	.199	.195	.200	.205
3.533	.124	.214	.235	.258	.283	.211	.200	.196	.201	.205
4.050	.108	.117	.122	.189	.246	.211	.201	.197	.201	.205
4.546	.108	.117	.122	.127	.138	.210	.200	.196	.200	.205
5.055	.108	.117	.122	.127	.128	.210	.200	.196	.200	.205
5.552	.108	.117	.122	.127	.127	.210	.200	.196	.200	.205

$p_{t,j}/p_\infty$	$x/x_t = 1.489$					$x/x_t = 1.809$				
	$y/w_t/2$					$y/w_t/2$				
	0.250	0.500	0.750	0.875	0.950	0.250	0.500	0.750	0.875	0.950
2.004	.487	.485	.475	.480	.482	.489	.489	.495	.495	.492
2.520	.385	.381	.370	.380	.382	.388	.388	.394	.393	.391
3.037	.314	.311	.295	.312	.315	.322	.320	.324	.325	.323
3.533	.208	.182	.245	.277	.277	.250	.281	.281	.280	.278
4.050	.118	.176	.209	.247	.243	.201	.244	.249	.244	.244
4.546	.116	.157	.158	.222	.217	.181	.179	.229	.217	.217
5.055	.116	.126	.157	.196	.195	.163	.176	.207	.197	.195
5.552	.116	.114	.154	.178	.178	.139	.171	.190	.180	.179

TABLE VII.- RATIO OF INTERNAL STATIC PRESSURE TO JET TOTAL PRESSURE FOR NOZZLE CONFIGURATION A4V20

(a) $p/p_{t,j}$ for upper flap

$p_{t,j}/p_\infty$	$y/w_t/2 = 0.0$								
	x/x_t								
	0.638	0.745	0.851	0.957	1.000	1.064	1.117	1.170	1.277
2.012	.844	.801	.746	.582	.615	.629	.623	.611	.579
2.518	.843	.800	.744	.578	.609	.624	.615	.601	.563
3.044	.843	.800	.744	.578	.609	.624	.616	.602	.563
3.527	.844	.801	.745	.579	.609	.625	.616	.602	.564
4.044	.845	.802	.745	.579	.610	.626	.616	.603	.564
4.534	.844	.803	.745	.579	.610	.626	.617	.603	.564
5.064	.845	.804	.746	.579	.610	.626	.617	.603	.565
5.564	.845	.805	.746	.578	.610	.627	.617	.603	.565

$p_{t,j}/p_\infty$	$y/w_t/2 = 0.0$					$x/x_t = 1.064$				
	x/x_t					$y/w_t/2$				
	1.383	1.489	1.596	1.702	1.809	0.250	0.500	0.750	0.875	0.950
2.012	.543	.505	.500	.491	.484	.627	.623	.624	.618	.615
2.518	.509	.460	.415	.362	.316	.620	.617	.620	.614	.611
3.044	.509	.460	.414	.362	.315	.620	.617	.619	.615	.611
3.527	.510	.460	.415	.362	.315	.620	.617	.620	.615	.611
4.044	.510	.460	.415	.362	.315	.620	.618	.620	.615	.612
4.534	.510	.461	.415	.362	.315	.620	.618	.620	.615	.612
5.064	.511	.461	.415	.362	.315	.621	.619	.621	.616	.613
5.564	.512	.461	.415	.361	.315	.621	.620	.622	.617	.613

$p_{t,j}/p_\infty$	$x/x_t = 1.489$					$x/x_t = 1.809$				
	$y/w_t/2$					$y/w_t/2$				
	0.250	0.500	0.750	0.875	0.950	0.250	0.500	0.750	0.875	0.950
2.012	.504	.497	.501	.500	.499	.486	.497	.503	.508	.500
2.518	.455	.427	.401	.399	.399	.312	.314	.345	.376	.387
3.044	.454	.424	.354	.332	.334	.305	.280	.283	.306	.323
3.527	.454	.424	.341	.291	.290	.305	.267	.248	.258	.277
4.044	.454	.424	.339	.263	.254	.305	.265	.225	.222	.236
4.534	.455	.424	.339	.248	.228	.305	.264	.206	.200	.205
5.064	.455	.424	.339	.242	.207	.305	.264	.198	.183	.181
5.564	.455	.424	.339	.241	.194	.305	.264	.197	.169	.167

TABLE VII.- Concluded

(b) $p/p_{t,j}$ for lower flap

$p_{t,j}/p_\infty$	$y/w_t/2 = 0.0$								
	x/x_t								
	0.638	0.745	0.851	0.957	1.000	1.064	1.117	1.170	1.277
2.012	.838	.798	.732	.475	.351	.457	.479	.483	.486
2.518	.837	.798	.731	.473	.345	.220	.313	.313	.311
3.044	.838	.798	.732	.472	.345	.201	.163	.203	.202
3.527	.839	.799	.733	.472	.343	.201	.122	.079	.088
4.044	.839	.799	.733	.471	.343	.201	.120	.079	.089
4.534	.840	.800	.733	.471	.344	.201	.119	.079	.090
5.064	.841	.800	.734	.471	.344	.201	.118	.080	.091
5.564	.841	.800	.734	.470	.344	.201	.117	.080	.091

$p_{t,j}/p_\infty$	$y/w_t/2 = 0.0$					$x/x_t = 1.064$				
	x/x_t					$y/w_t/2$				
	1.383	1.489	1.596	1.702	1.809	0.250	0.500	0.750	0.875	0.950
2.012	.487	.488	.490	.490	.490	.432	.449	.429	.388	.392
2.518	.323	.340	.365	.384	.395	.214	.199	.193	.196	.200
3.044	.225	.252	.280	.310	.334	.210	.198	.194	.197	.199
3.527	.164	.215	.247	.280	.303	.210	.199	.196	.198	.200
4.044	.106	.115	.196	.238	.259	.210	.200	.196	.198	.200
4.534	.106	.115	.118	.129	.227	.209	.200	.196	.198	.199
5.064	.106	.114	.118	.121	.129	.209	.199	.196	.198	.200
5.564	.106	.114	.118	.121	.119	.209	.199	.196	.198	.200

$p_{t,j}/p_\infty$	$x/x_t = 1.489$					$x/x_t = 1.809$				
	$y/w_t/2$					$y/w_t/2$				
	0.250	0.500	0.750	0.875	0.950	0.250	0.500	0.750	0.875	0.950
2.012	.488	.488	.483	.483	.482	.489	.488	.495	.493	.491
2.518	.333	.303	.385	.390	.390	.375	.382	.393	.394	.391
3.044	.254	.195	.322	.323	.324	.293	.335	.329	.326	.323
3.527	.216	.175	.284	.279	.279	.229	.292	.282	.280	.279
4.044	.159	.177	.247	.244	.243	.218	.248	.243	.245	.243
4.534	.115	.165	.190	.218	.216	.184	.195	.217	.218	.217
5.064	.113	.157	.146	.195	.194	.170	.153	.196	.195	.195
5.564	.113	.115	.136	.185	.176	.139	.158	.184	.176	.177

TABLE VIII.- RATIO OF INTERNAL STATIC PRESSURE TO JET TOTAL PRESSURE FOR NOZZLE CONFIGURATIONS D11V5 AND D12V5

(a) Configuration D11V5

Upper flap

$p_{t,j}/p_\infty$	$y/w_t/2 = 0.0$					$y/w_t/2 = 0.875$				
	x/x_t					x/x_t				
	0.791	1.011	1.286	1.560	1.890	0.791	1.011	1.286	1.560	1.890
2.002	.783	.411	.399	.468	.483	.801	.418	.400	.456	.476
2.550	.781	.414	.400	.248	.375	.803	.420	.400	.252	.370
2.998	.779	.412	.399	.249	.313	.801	.419	.399	.253	.305
3.517	.776	.413	.399	.250	.149	.802	.419	.399	.252	.163
4.106	.776	.412	.399	.250	.149	.805	.419	.399	.252	.163
5.391	.775	.411	.398	.249	.150	.803	.418	.399	.252	.162
5.940	.774	.411	.398	.249	.150	.801	.418	.398	.252	.162
6.557	.774	.412	.398	.249	.150	.802	.417	.398	.252	.162
7.344	.773	.412	.398	.248	.150	.800	.416	.398	.251	.160
8.426	.772	.411	.397	.247	.148	.799	.415	.397	.250	.160
10.034	.772	.411	.398	.248	.148	.799	.416	.398	.251	.159

Lower flap

$p_{t,j}/p_\infty$	$y/w_t/2 = 0.0$					$y/w_t/2 = 0.875$			
	x/x_t					x/x_t			
	0.791	1.011	1.286	1.560	1.890	1.011	1.286	1.560	1.890
2.002	.781	.379	.271	.274	.524	.383	.282	.265	.506
2.550	.785	.379	.272	.263	.345	.384	.283	.264	.325
2.998	.786	.377	.273	.261	.215	.384	.283	.262	.212
3.517	.784	.376	.273	.262	.217	.383	.283	.263	.213
4.106	.787	.375	.273	.261	.217	.383	.283	.262	.213
5.391	.787	.374	.272	.259	.216	.381	.282	.262	.214
5.940	.788	.373	.271	.258	.216	.382	.281	.261	.214
6.557	.787	.373	.271	.257	.216	.381	.281	.261	.214
7.344	.788	.372	.270	.256	.215	.381	.280	.260	.213
8.426	.785	.370	.269	.253	.214	.380	.279	.260	.212
10.034	.787	.370	.269	.253	.214	.381	.279	.259	.212

TABLE VIII.- Concluded

(b) Configuration D12V5

Upper flap

$p_{t,j}/p_\infty$	$y/w_t/2 = 0.0$					$y/w_t/2 = 0.875$				
	x/x_t					x/x_t				
	0.791	1.011	1.286	1.560	1.890	0.791	1.011	1.286	1.560	1.890
1.976	.784	.414	.398	.424	.478	.804	.419	.426	.483	.511
2.550	.782	.416	.400	.249	.374	.807	.422	.395	.359	.394
3.047	.781	.415	.399	.250	.307	.804	.420	.393	.286	.320
3.572	.777	.415	.399	.250	.148	.805	.420	.393	.233	.259
4.091	.777	.414	.398	.250	.149	.805	.419	.392	.191	.218
5.416	.775	.413	.398	.249	.150	.804	.418	.393	.140	.155
5.894	.774	.414	.398	.248	.150	.802	.418	.393	.139	.140
6.464	.775	.413	.398	.248	.150	.802	.417	.392	.139	.124
7.294	.774	.412	.398	.248	.150	.800	.417	.392	.139	.101
8.342	.773	.411	.397	.247	.148	.799	.415	.392	.138	.069
9.976	.773	.411	.398	.247	.148	.799	.416	.392	.138	.067

Lower flap

$p_{t,j}/p_\infty$	$y/w_t/2 = 0.0$					$y/w_t/2 = 0.875$			
	x/x_t					x/x_t			
	0.791	1.011	1.286	1.560	1.890	1.011	1.286	1.560	1.890
1.976	.781	.380	.271	.431	.530	.383	.452	.511	.509
2.550	.785	.380	.274	.262	.292	.386	.297	.389	.397
3.047	.786	.378	.274	.261	.217	.383	.283	.329	.330
3.572	.785	.377	.273	.261	.217	.383	.282	.277	.275
4.091	.787	.376	.273	.261	.218	.383	.281	.242	.237
5.416	.787	.374	.272	.258	.216	.381	.281	.178	.172
5.694	.787	.374	.271	.259	.216	.382	.280	.159	.157
6.464	.787	.374	.271	.258	.216	.382	.280	.141	.140
7.294	.788	.373	.270	.257	.215	.382	.279	.134	.118
8.342	.786	.371	.270	.255	.214	.380	.278	.133	.098
9.976	.787	.371	.270	.254	.214	.381	.278	.133	.081

TABLE IX.- RATIO OF INTERNAL STATIC PRESSURE TO JET TOTAL PRESSURE FOR NOZZLE CONFIGURATION F5V5

Upper flap

$p_{t,j}/p_\infty$	$y/w_t/2 = 0.0$				
	x/x_t				
	0.943	1.000	1.086	1.157	1.229
2.002	.808	.405	.403	.406	.466
2.493	.807	.405	.407	.271	.385
2.991	.808	.404	.406	.271	.186
3.508	.804	.404	.405	.271	.185
4.019	.804	.402	.404	.269	.185
5.293	.804	.402	.404	.271	.188
5.826	.803	.402	.404	.271	.187
6.334	.803	.401	.404	.271	.187
7.300	.803	.400	.404	.271	.187
8.440	.804	.400	.405	.272	.187
10.601	.806	.400	.407	.273	.188
12.413	.806	.400	.408	.275	.189

Lower flap

$p_{t,j}/p_\infty$	$y/w_t/2 = 0.0$				
	x/x_t				
	0.943	1.000	1.086	1.157	1.229
2.002	.825	.382	.271	.257	.418
2.493	.828	.385	.273	.251	.238
2.991	.823	.385	.273	.255	.238
3.508	.823	.381	.273	.261	.238
4.019	.819	.381	.270	.260	.237
5.293	.822	.379	.274	.259	.237
5.826	.821	.379	.274	.258	.236
6.334	.821	.379	.274	.258	.236
7.300	.820	.378	.273	.257	.235
8.440	.818	.376	.271	.256	.234
10.601	.819	.375	.271	.255	.235
12.413	.820	.375	.274	.254	.234

TABLE X.- RATIO OF STATIC PRESSURE ON THE THRUST BLOCKER TO JET TOTAL PRESSURE FOR THRUST REVERSER CONFIGURATIONS

Configuration R1

$P_{t,j}/P_\infty$	$y/w_t/2 = 0.0$			
	z/h_b			
	0.000	0.394	0.787	1.181
1.970	1.004	.996	.993	.887
2.467	1.005	.995	.992	.873
2.465	1.005	.996	.992	.873
2.949	1.005	.995	.991	.861
3.427	1.005	.995	.990	.851
3.930	1.004	.995	.989	.850
4.405	1.003	.994	.989	.849
4.888	1.004	.995	.988	.849
5.375	1.003	.995	.988	.848
5.863	1.003	.996	.988	.849
6.345	1.003	.996	.988	.848
6.812	1.003	.996	.988	.848
6.843	1.003	.996	.988	.848
7.315	1.003	.997	.988	.848
7.802	1.003	.997	.988	.848
8.294	1.003	.998	.988	.848
9.139	1.003	.998	.988	.848

Configuration R2

$P_{t,j}/P_\infty$	$y/w_t/2 = 0.0$			
	z/h_b			
	0.000	0.512	0.984	1.378
1.985	1.003	.993	.962	.685
2.495	1.004	.992	.959	.658
3.000	1.004	.991	.958	.649
3.495	1.004	.991	.958	.649
3.475	1.003	.990	.958	.649
3.963	1.003	.990	.957	.648
4.459	1.003	.989	.957	.649
4.963	1.003	.990	.957	.648
5.445	1.003	.990	.957	.648
5.952	1.002	.990	.957	.648
6.441	1.002	.990	.957	.648
6.941	1.002	.990	.956	.648
7.477	1.002	.991	.956	.648
7.414	1.002	.990	.956	.648
7.924	1.002	.991	.957	.648
8.422	1.002	.992	.957	.648
8.403	1.002	.992	.956	.648
9.316	1.002	.992	.956	.648

Configuration R3

$P_{t,j}/P_\infty$	$y/w_t/2 = 0.0$			
	z/h_b			
	0.000	0.512	0.984	1.378
1.987	1.005	.992	.960	.669
2.477	1.005	.990	.958	.654
2.971	1.004	.990	.958	.651
3.466	1.004	.990	.957	.651
3.474	1.004	.990	.958	.650
3.971	1.004	.990	.957	.650
4.466	1.003	.989	.957	.650
4.949	1.003	.989	.957	.648
5.437	1.003	.990	.957	.648
5.933	1.002	.991	.957	.648
6.432	1.002	.990	.956	.648
6.919	1.002	.991	.956	.648
7.411	1.002	.991	.956	.648
7.903	1.002	.991	.956	.648
8.467	1.002	.992	.956	.648
8.369	1.002	.992	.956	.648
9.303	1.002	.992	.957	.648

Configuration R4

$P_{t,j}/P_\infty$	$y/w_t/2 = 0.0$			
	z/h_b			
	0.000	0.512	0.984	1.378
1.991	1.004	.993	.964	.701
2.498	1.004	.991	.960	.670
2.983	1.004	.990	.958	.655
3.474	1.004	.989	.958	.650
3.987	1.003	.990	.957	.649
4.479	1.003	.989	.957	.650
4.464	1.003	.989	.957	.649
4.975	1.003	.989	.957	.648
5.446	1.003	.989	.957	.648
5.952	1.002	.990	.957	.648
6.436	1.002	.990	.956	.648
6.981	1.002	.990	.956	.648
7.450	1.002	.990	.956	.648
7.924	1.002	.991	.956	.648
8.420	1.002	.992	.956	.648
9.314	1.002	.992	.956	.648

Configuration R5

$P_{t,j}/P_\infty$	$y/w_t/2 = 0.0$			
	z/h_b			
	0.000	0.512	0.984	1.378
1.991	1.005	.990	.962	.682
2.492	1.004	.989	.958	.656
2.972	1.004	.989	.958	.654
3.483	1.004	.988	.957	.652
3.473	1.004	.988	.957	.653
3.978	1.004	.989	.957	.652
4.470	1.004	.988	.957	.652
4.945	1.004	.989	.957	.650
5.448	1.003	.989	.956	.649
5.951	1.003	.990	.956	.649
6.444	1.003	.990	.956	.649
6.937	1.003	.990	.957	.649
7.411	1.003	.990	.956	.648
7.909	1.003	.991	.956	.648
8.405	1.003	.992	.956	.648
9.324	1.003	.992	.956	.648

Configuration R6

$P_{t,j}/P_\infty$	$y/w_t/2 = 0.0$			
	z/h_b			
	0.000	0.512	0.984	1.378
1.969	1.003	.993	.965	.698
2.477	1.004	.992	.958	.649
2.453	1.004	.991	.958	.649
2.946	1.004	.991	.958	.649
3.430	1.004	.991	.958	.648
3.926	1.003	.990	.957	.648
4.401	1.003	.990	.957	.648
4.896	1.003	.990	.957	.647
5.393	1.003	.990	.957	.647
5.864	1.002	.991	.956	.647
6.378	1.002	.990	.956	.647
6.822	1.002	.992	.956	.647
7.292	1.002	.992	.956	.647
7.331	1.002	.992	.956	.648
7.800	1.003	.992	.956	.648
8.298	1.002	.992	.956	.648
8.288	1.002	.993	.956	.648
9.195	1.003	.993	.956	.648

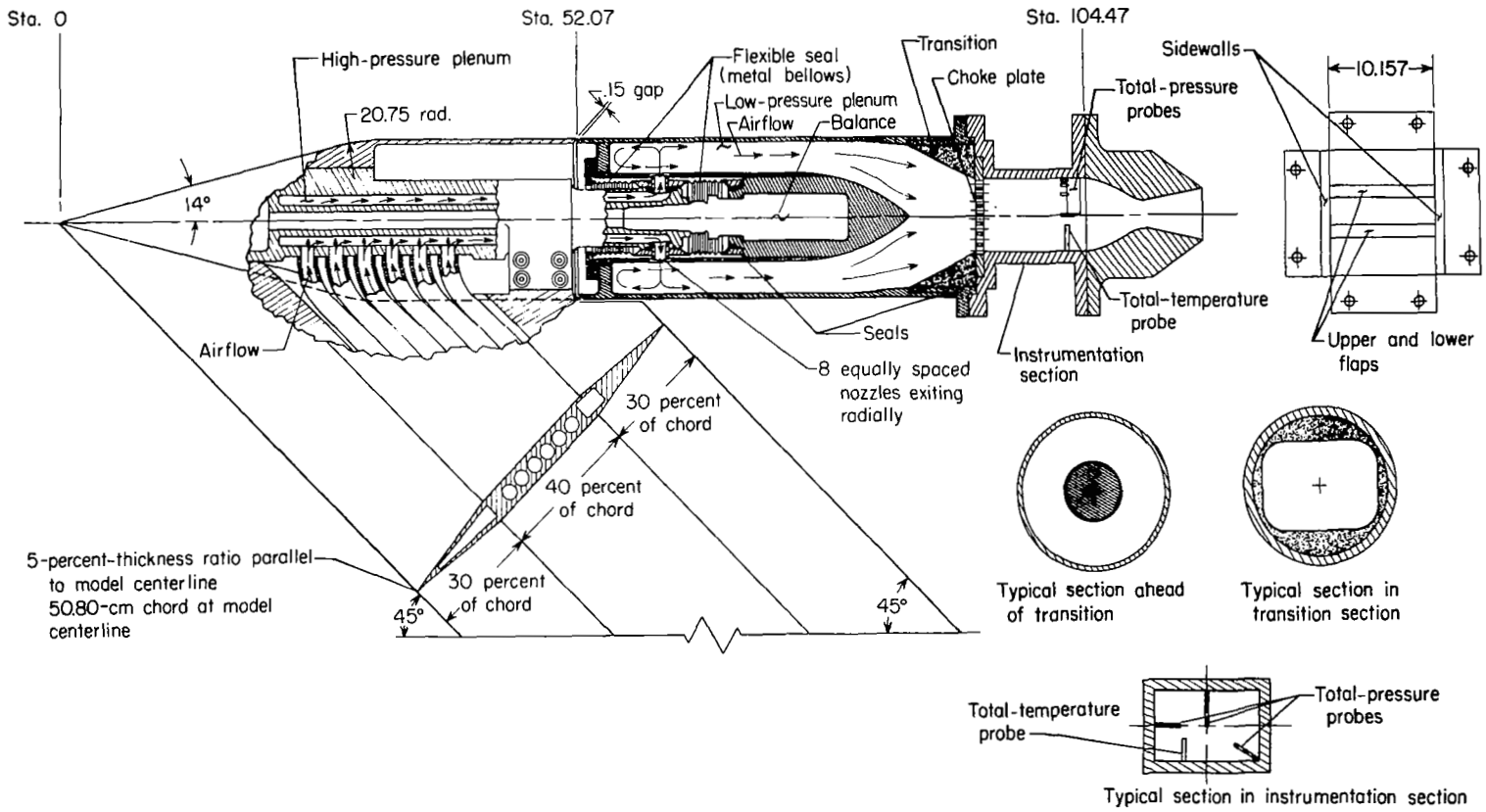

(a) Air-powered nacelle test apparatus.

Figure 1.- Sketch of air-powered nacelle model with typical nozzle configuration installed. All dimensions are in centimeters unless otherwise noted.

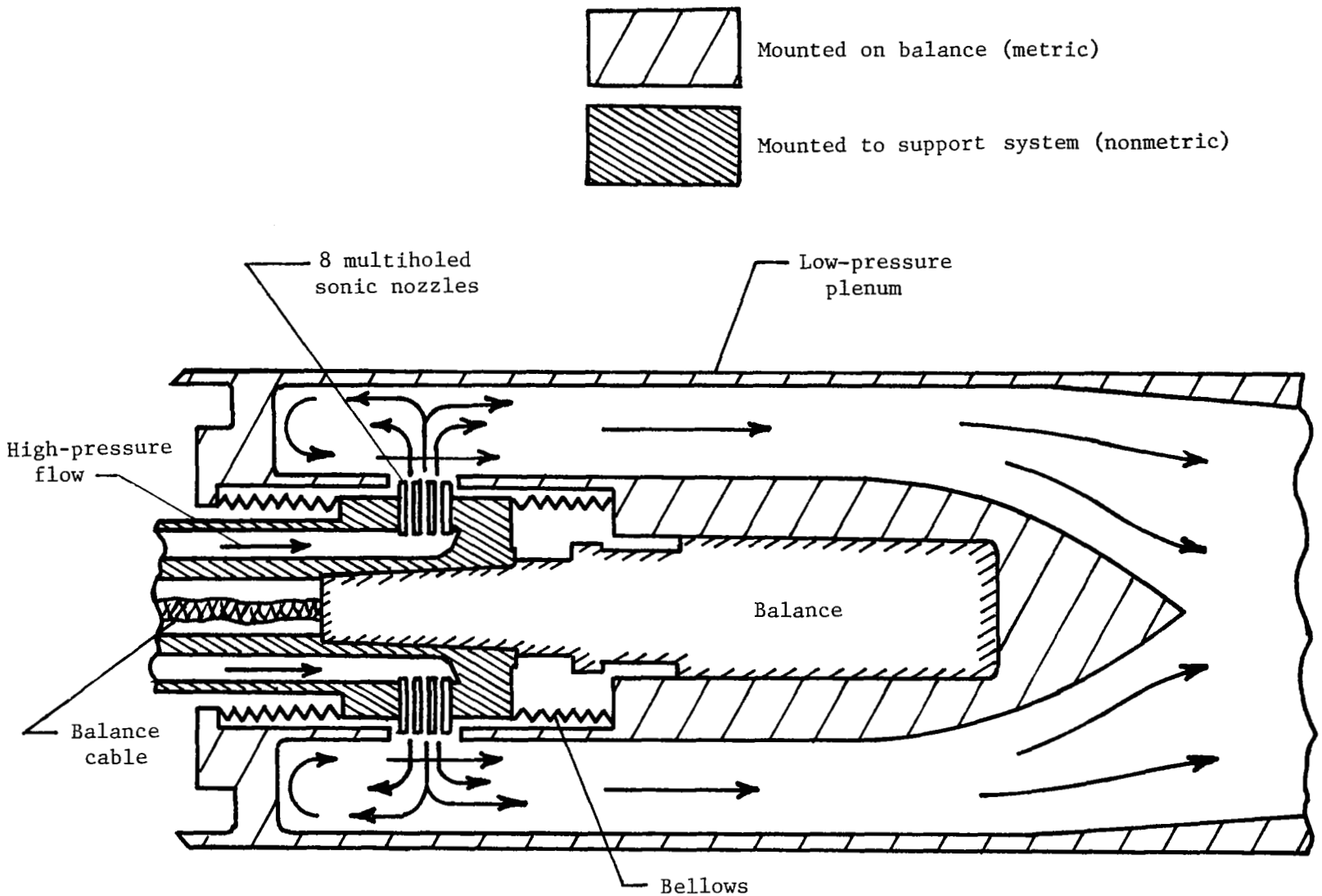

(b) Schematic cross section of flow transfer system.

Figure 1.- Concluded.

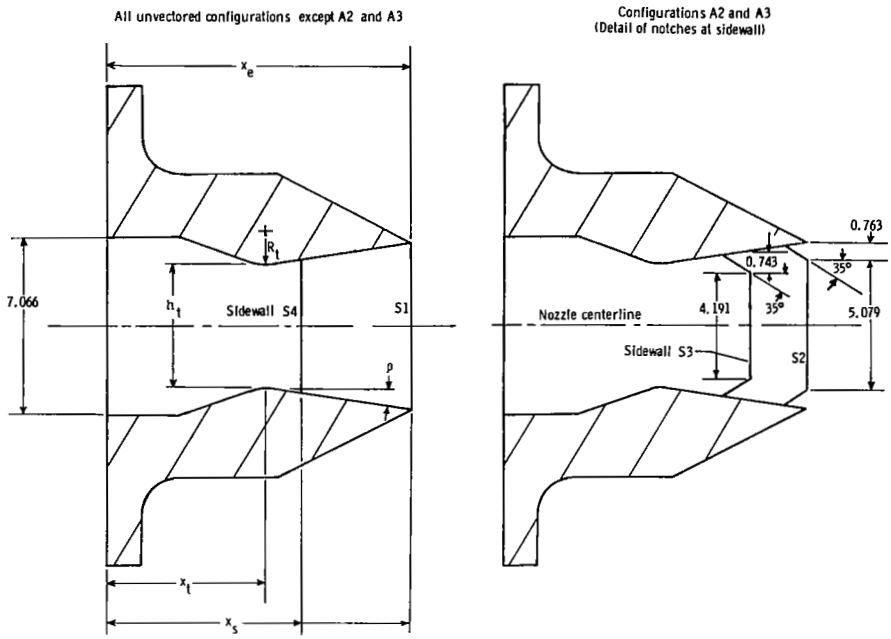

Configuration	Design $P_{t,j}/P_\infty$	AR	A_e/A_t	ρ, deg	$\frac{x_e - x_t}{h_t}$	$\frac{x_s - x_t}{x_e - x_t}$	R_t, cm	A_t, cm^2	x_t, cm	x_e, cm	x_s, cm	Pressure Data Table	Internal Performance Figure
A1	4.65	2.012	1.300	8.00	1.100	1.0	1.588	51.305	5.969	11.557	11.557	I(a)	10
A2	↓	↓	↓	↓	↓	↓	↓	↓	↓	↓	↓	—	↓
A3	↓	↓	↓	↓	↓	.614	↓	↓	↓	↓	9.398	I(b)	↓
A4	↓	↓	↓	↓	↓	.227	↓	↓	↓	↓	7.239	I(c)	↓
B1	3.72	3.106	1.183	2.50	2.097	1.0	0	33.232	4.699	↓	11.557	—	11
B2	8.79	3.696	1.797	5.88	3.857	↓	↓	27.911	5.989	16.637	16.637	—	12
D1	2.94	↓	1.086	5.50	.477	↓	1.588	↓	8.776	10.089	10.089	I(d)	13
D2	2.97	↓	1.089	1.28	2.100	↓	↓	↓	5.779	11.557	11.557	I(e)	14
D3	4.25	↓	1.250	10.67	.707	↓	↓	↓	8.143	10.089	10.089	I(f)	15
D4	5.43	↓	1.400	10.83	1.099	↓	↓	↓	8.534	11.557	11.557	I(g)	16
D5	7.07	↓	1.600	↓	1.621	↓	↓	↓	7.097	↓	↓	I(h)	17
D6	8.79	↓	1.797	10.92	2.100	↓	↓	↓	5.779	↓	↓	I(i)	18
D7	2.97	↓	1.089	1.21	↓	↓	.683	↓	↓	↓	↓	Ref. 9	19
D8	↓	↓	↓	1.17	↓	↓	2.738	↓	↓	↓	↓	↓	20
D9	8.79	↓	1.797	10.92	↓	↓	.683	↓	↓	↓	↓	↓	21
D10	↓	↓	↓	11.25	↓	↓	2.738	↓	↓	↓	↓	↓	22
E1	2.97	5.806	1.089	1.25	2.032	↓	.952	17.787	8.001	↓	↓	I(j)	23(a)
E2	↓	↓	↓	↓	↓	.587	↓	↓	↓	↓	10.089	—	23(b)
E3	8.79	↓	1.797	11.08	↓	1.0	↓	↓	↓	↓	11.557	I(j)	24(a)
E4	↓	↓	↓	↓	↓	.587	↓	↓	↓	↓	10.089	—	24(b)
F1	2.79	7.612	1.089	1.33	1.998	1.0	.734	13.561	8.890	↓	11.557	I(j)	25(a)
F2	↓	↓	↓	↓	↓	.450	↓	↓	↓	↓	10.089	—	25(b)
F3	8.79	↓	1.797	11.00	↓	1.0	↓	↓	↓	↓	11.557	I(k)	26(a)
F4	↓	↓	↓	↓	↓	.450	↓	↓	↓	↓	10.089	—	26(b)

Figure 2.- Unvectored-nozzle geometry. All dimensions are in centimeters unless otherwise indicated.

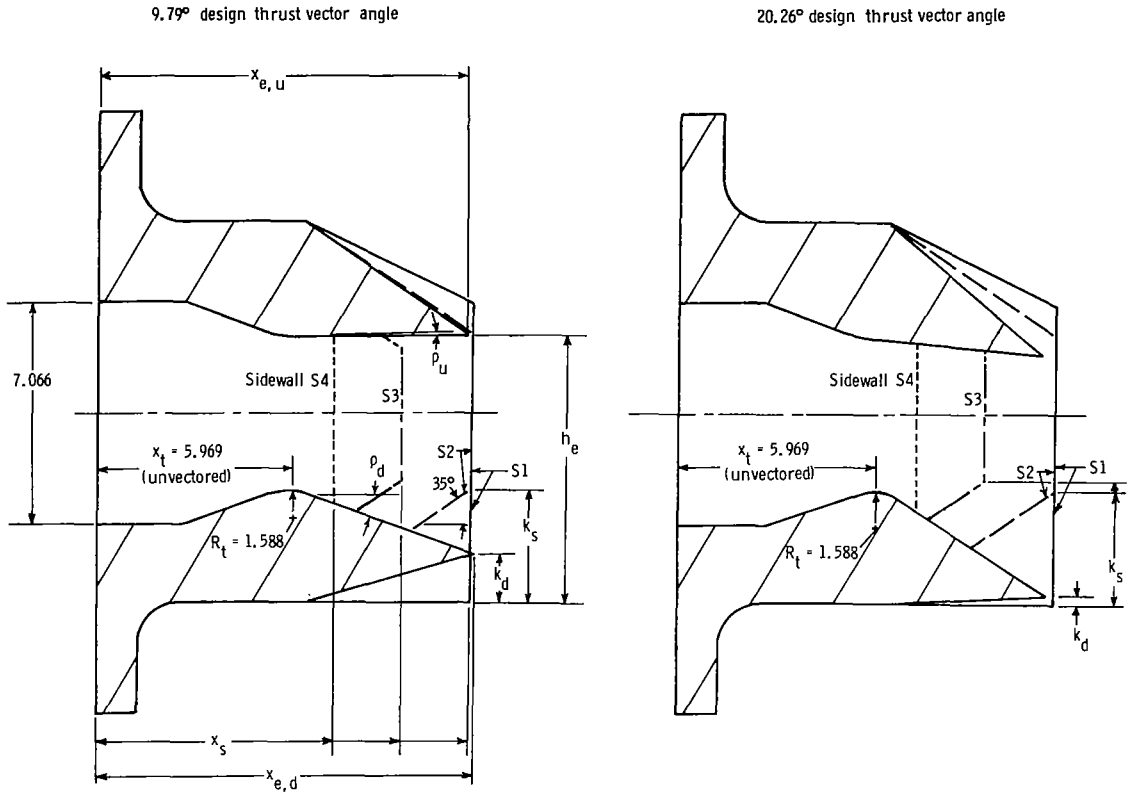

Configuration	Unvectored A_e/A_t	δ_v, deg	Sidewall	Sidewall Length Unvectored $\frac{x_s - x_t}{x_e - x_t}$	x_s, cm	k_s, cm	$x_{e,u}$, cm	$x_{e,d}$, cm	k_d, cm	h_e, cm	ρ_u, deg	ρ_d, deg	Pressure Data Table	Internal Performance Figure
A1V10	1.300	9.79	S1	1.000	11.557	—	11.405	11.608	1.600	8.547	-.08	19.50	II	27
A2V10	↓	↓	S2	↓	↓	3.493	↓	↓	↓	↓	↓	↓	—	↓
A3V10	↓	↓	S3	.614	9.398	3.937	↓	↓	↓	↓	↓	↓	—	↓
A4V10	↓	↓	S4	.227	7.239	—	↓	↓	↓	↓	↓	↓	—	↓
A1V13	1.166	13.22	S1	1.000	11.557	—	11.176	↓	↓	7.912	-6.93	↓	III	28
A2V13	↓	↓	S2	↓	↓	3.493	↓	↓	↓	↓	↓	↓	—	↓
A3V13	↓	↓	S3	.614	9.398	3.937	↓	↓	↓	↓	↓	↓	—	↓
A4V13	↓	↓	S4	.227	7.239	—	↓	↓	↓	↓	↓	↓	—	↓
A1V20	1.300	20.26	S1	1.000	11.557	—	↓	11.328	.274	↓	↓	33.58	IV	29
A2V20	↓	↓	S2	↓	↓	3.493	↓	↓	↓	↓	↓	↓	V	↓
A3V20	↓	↓	S3	.614	9.398	3.937	↓	↓	↓	↓	↓	↓	VI	↓
A4V20	↓	↓	S4	.227	7.239	—	↓	↓	↓	↓	↓	↓	VII	↓

(a) AR = 2.012. (Unvectored versions of these configurations are A1 through A4.)

Figure 3.- Vectored-nozzle geometry. All dimensions are in centimeters unless otherwise indicated.

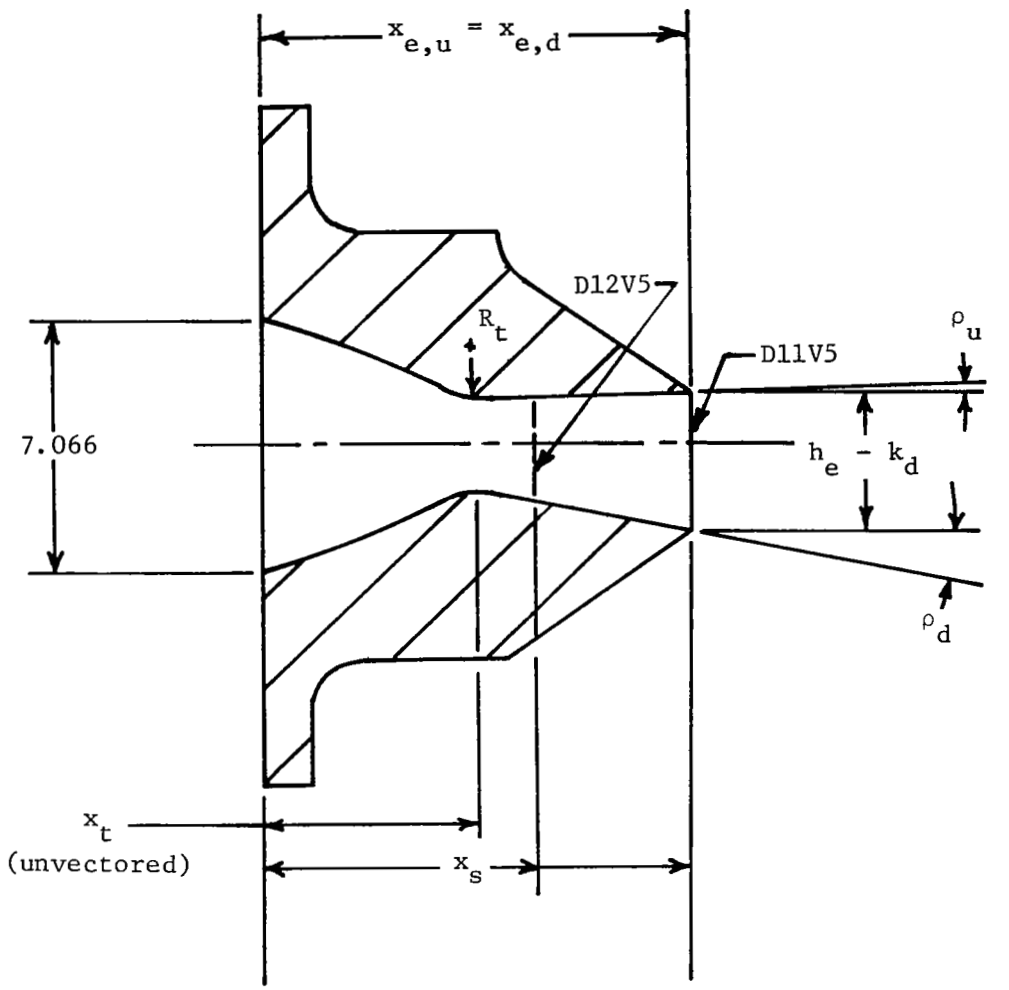

Configuration	AR	Unvectored A_e/A_t	δ_v, deg	Sidewall Length Unvectored $\frac{x_s - x_t}{x_e - x_t}$	x_t, cm	x_s, cm	$x_{e,u}$ and $x_{e,d}$, cm	$h_e - k_d$, cm	ρ_u, deg	ρ_d, deg	Pressure Data Table
D11V5	3.696	1.443	4.82	1.000	5.779	11.557	11.557	3.967	1.28	10.92	VIII (a)
D12V5	↓	↓	↓	.253	↓	7.239	↓	↓	↓	↓	VIII (b)
F5V5	7.612	↓	4.84	1.000	8.890	11.557	↓	1.926	1.33	11.00	IX

(b) AR = 3.696 and 7.612.

Figure 3.- Concluded.

Configuration D6

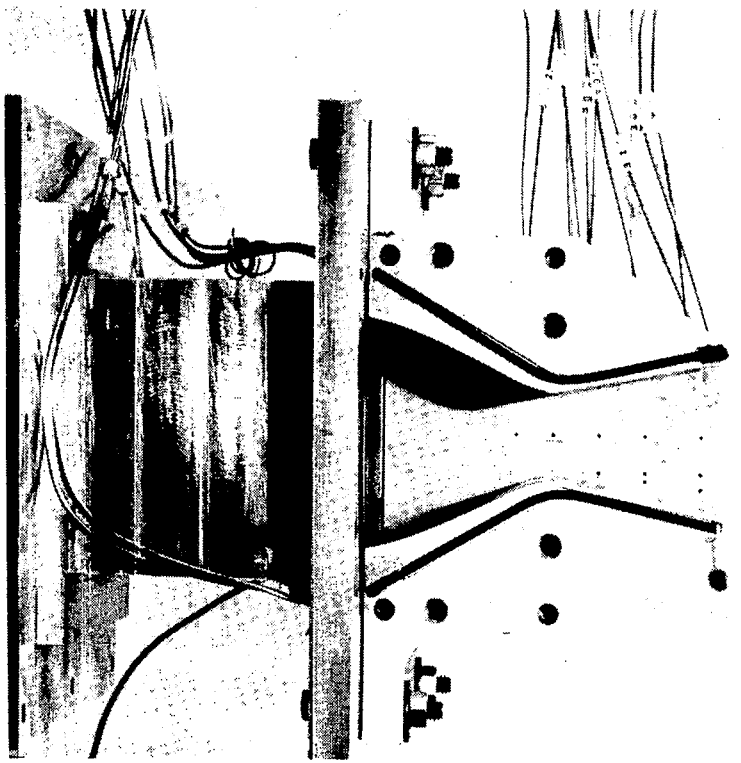

L-77-6571

Configuration F3

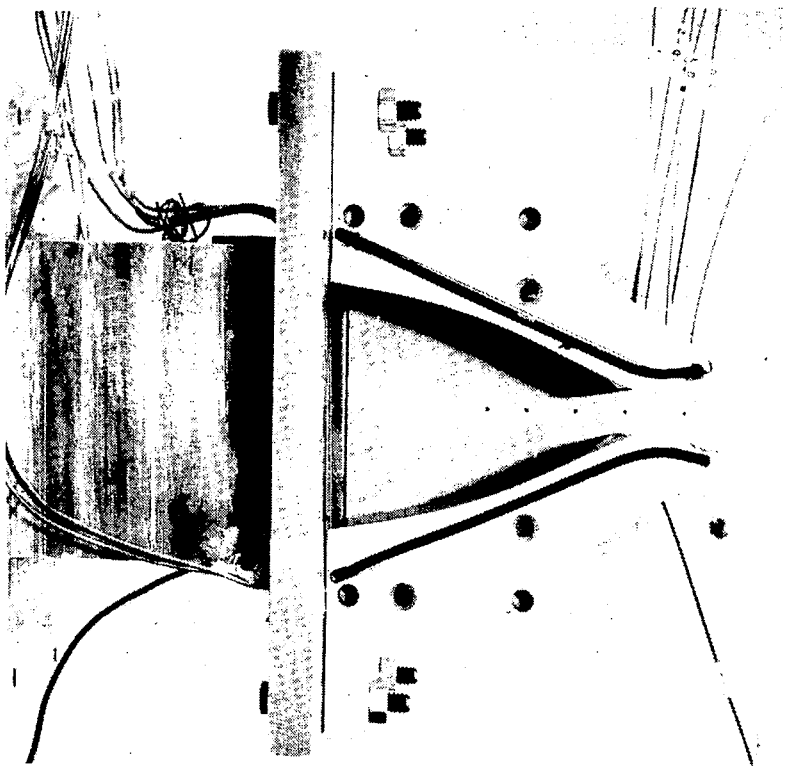

L-77-6558

Figure 4.- Photographs of configurations D6 and F3 with one sidewall removed.

Configuration A1

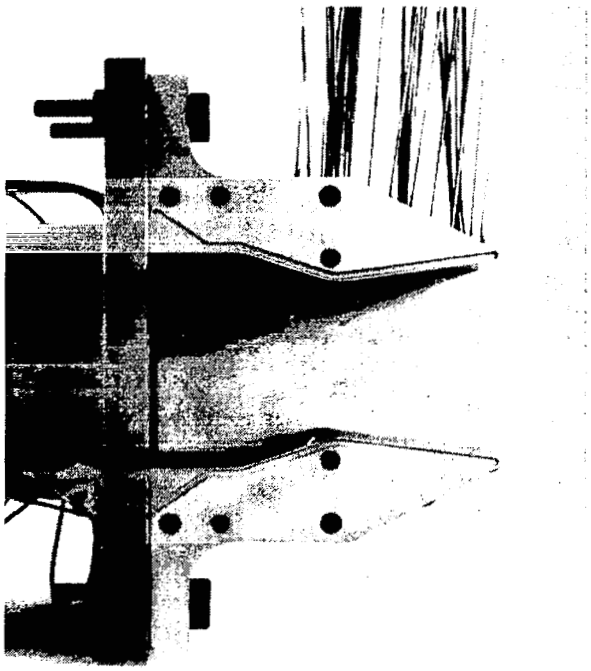

L-82-495

Configuration A3

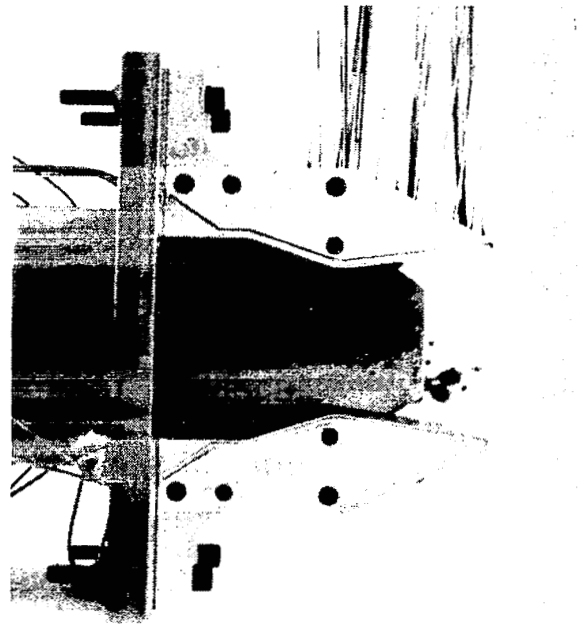

L-82-506

Configuration A4

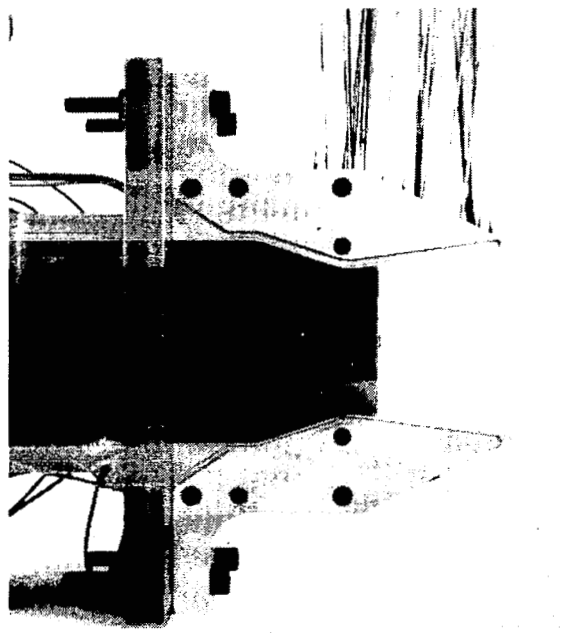

L-82-491

Figure 5.- Photographs of configurations A1, A3, and A4 with one sidewall removed.

Configuration A1

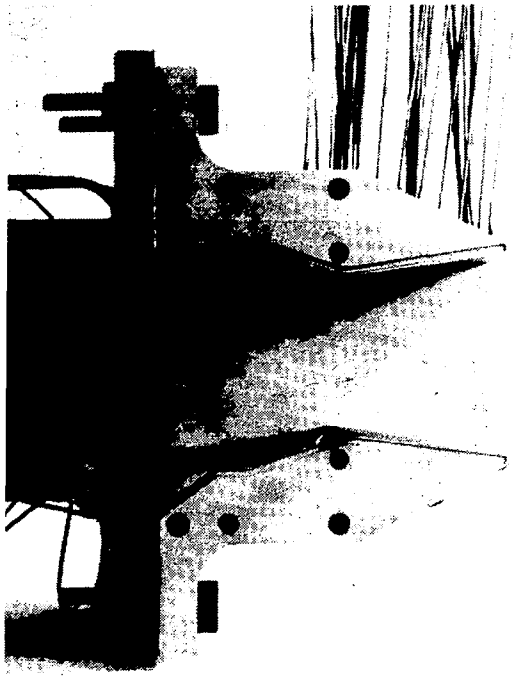

L-82-495

Configuration A1V10

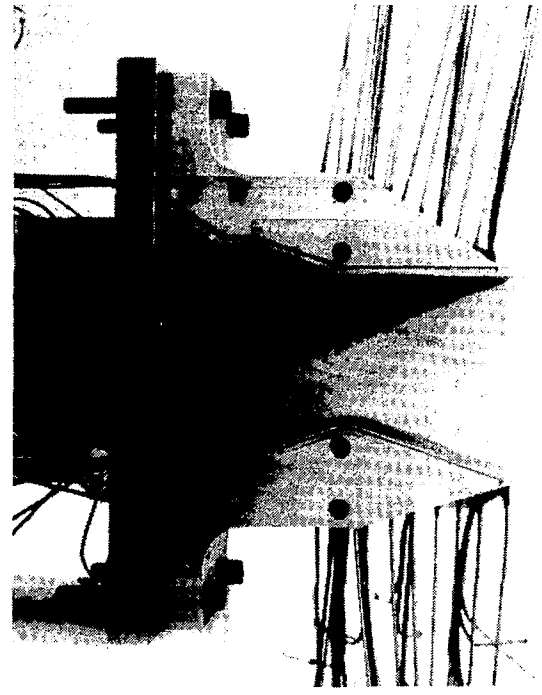

L-82-519

Configuration A1V13

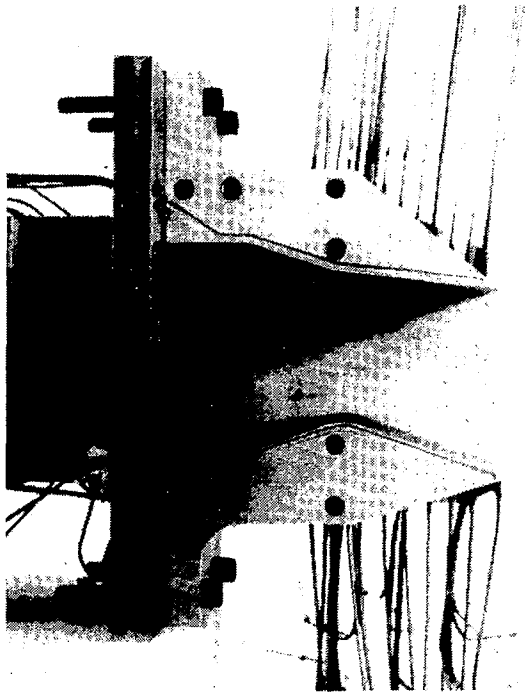

L-82-504

Configuration A1V20

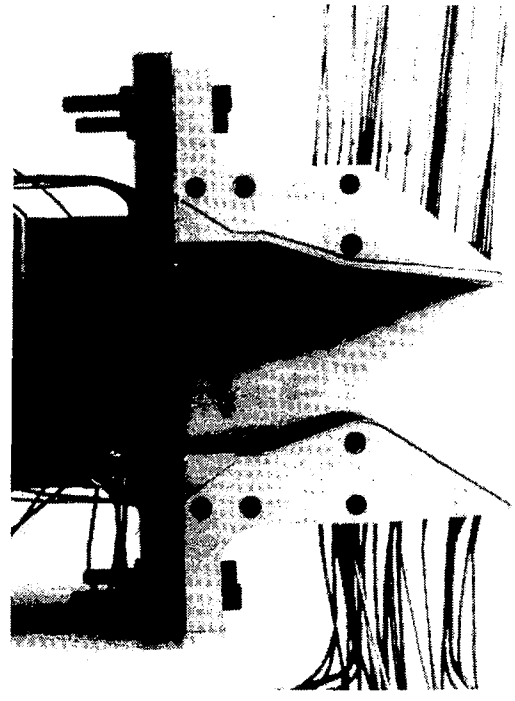

L-82-517

(a) Configurations A1, A1V10, A1V13, and A1V20.

Figure 6.- Photographs of AR = 2.012 configurations with one sidewall removed.

Configuration A1V20

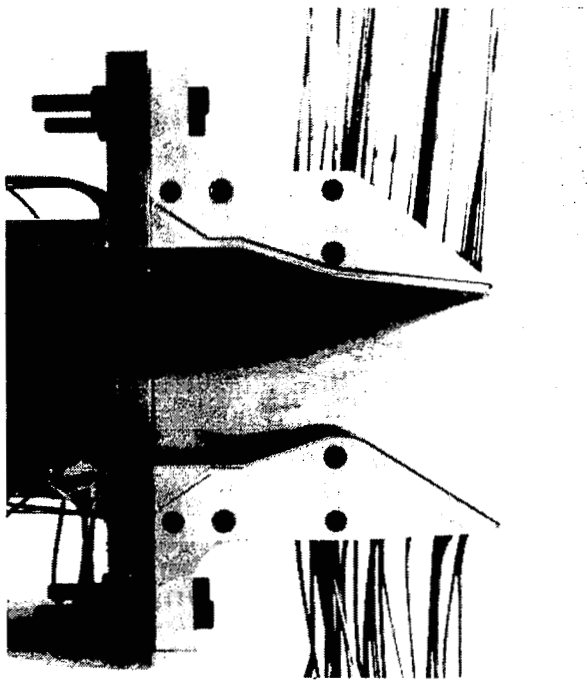

L-82-517

Configuration A2V20

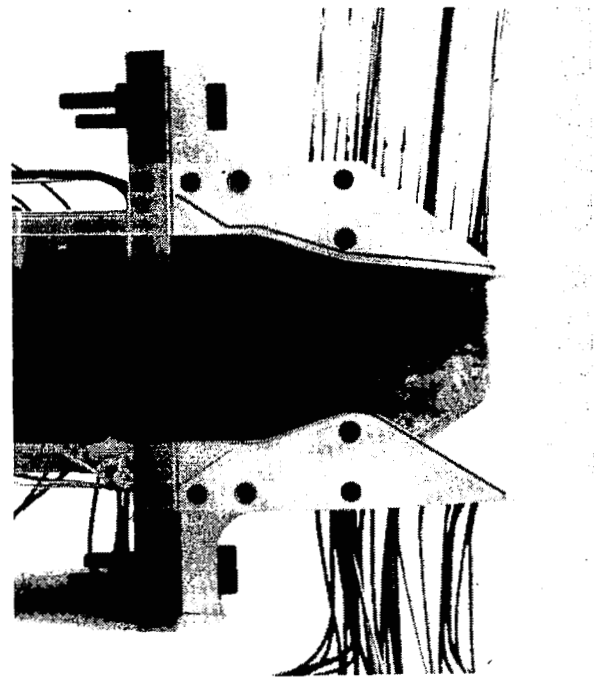

L-82-511

Configuration A3V20

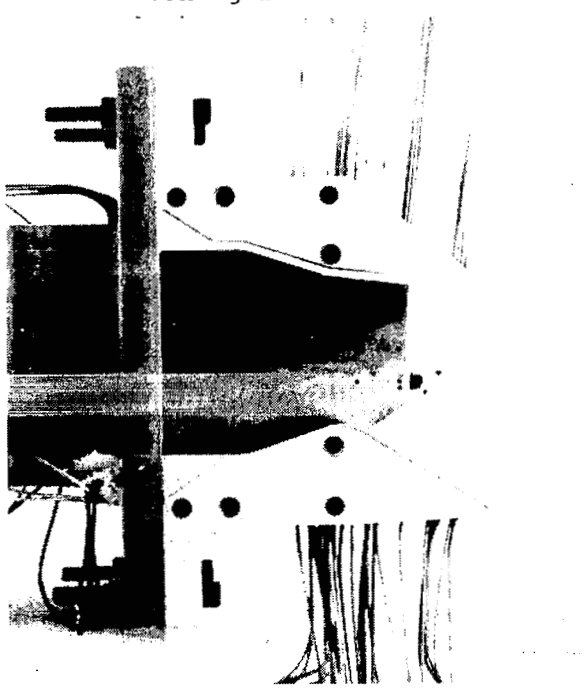

L-82-498

Configuration A4V20

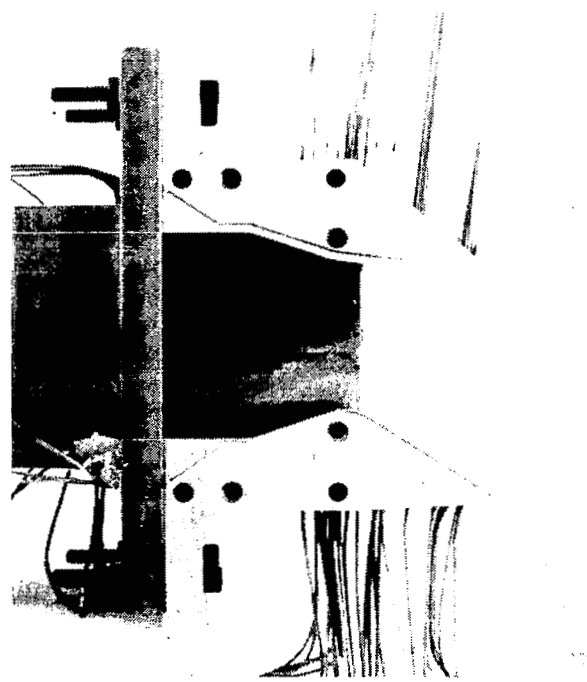

L-82-503

(b) Configurations A1V20, A2V20, A3V20, and A4V20.

Figure 6.- Concluded.

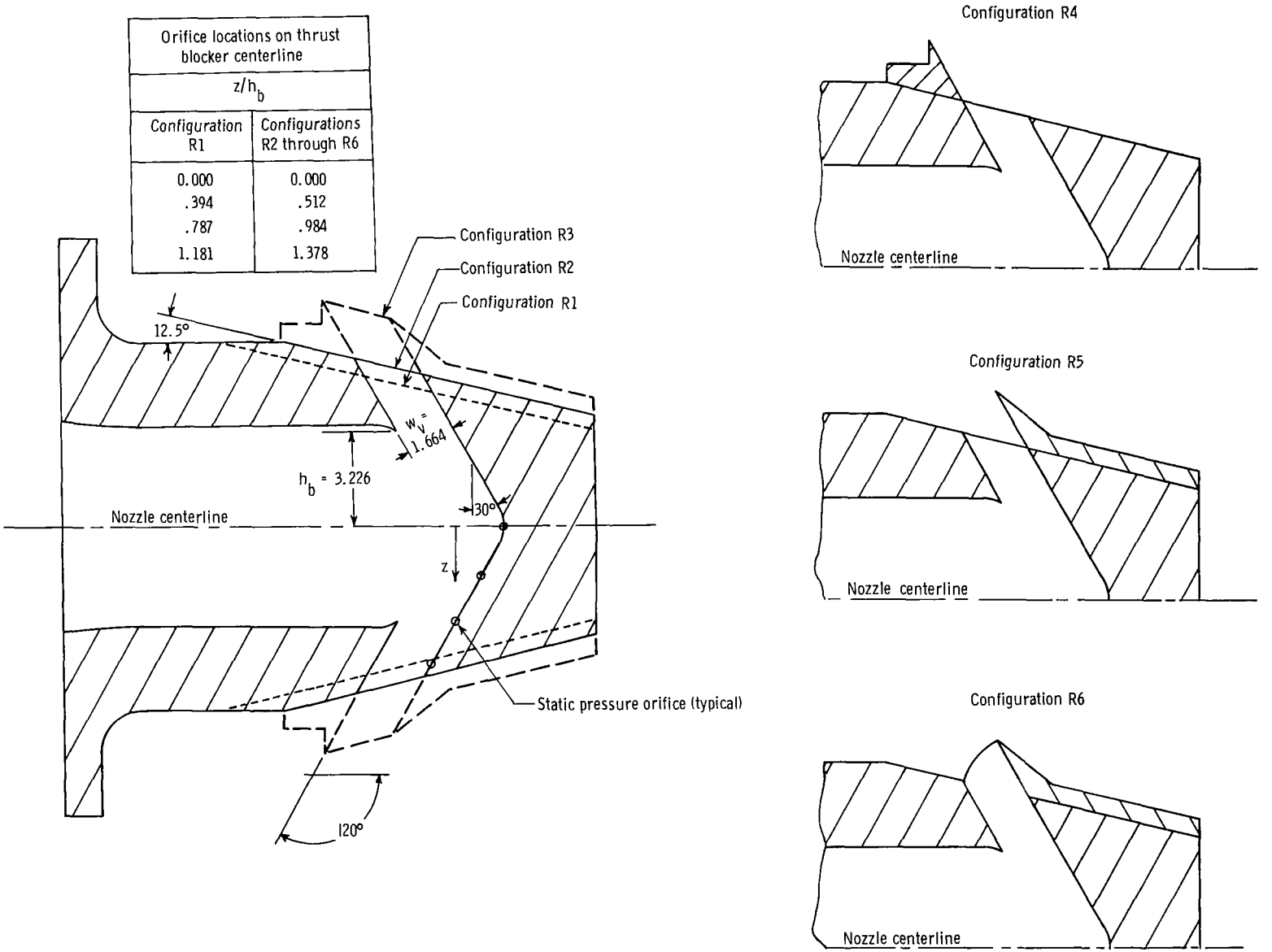

(a) Sketches of thrust-reverser configurations.

Figure 7.- Thrust-reverser configurations. All dimensions are in centimeters unless otherwise indicated.

Configuration	Port passage length	Uncontained port passage length		Internal performance	Pressure data
	$\frac{v}{w_v}$	$\frac{s}{w_v}$	Location of $\frac{s}{w_v}$	Figure	Table
R1	0.197	0.945	forward	31(a)	X
R2	.600	.951	↓	(b)	↓
R3	1.952	.979	↓	(c)	↓
R4	.600	2.331	↓	(d)	↓
R5	1.551	.401	aft	(e)	↓
R6	↓	↓	↓	(f)	↓

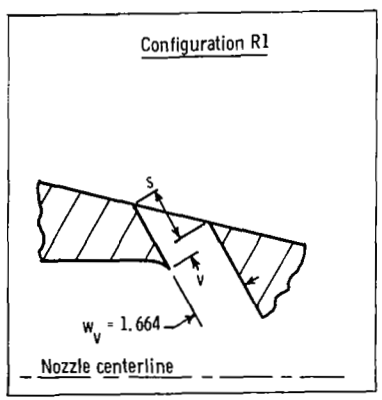

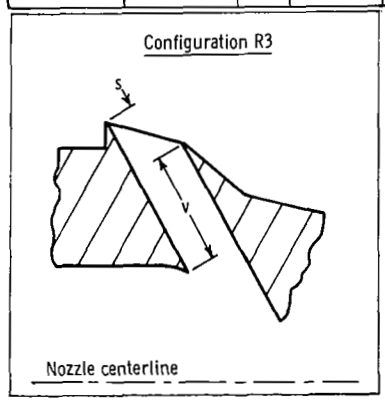

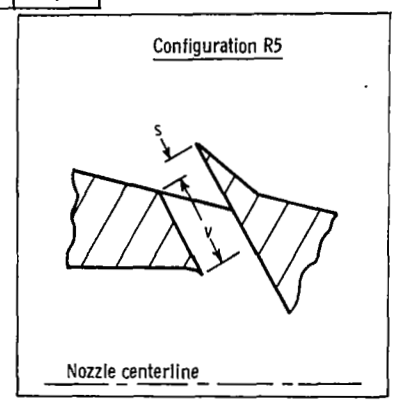

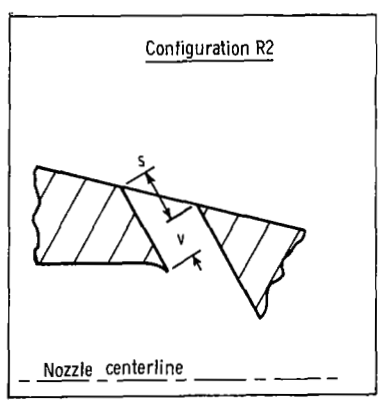

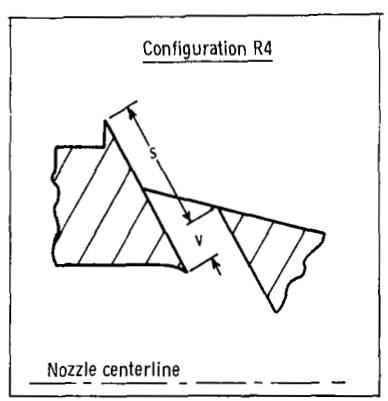

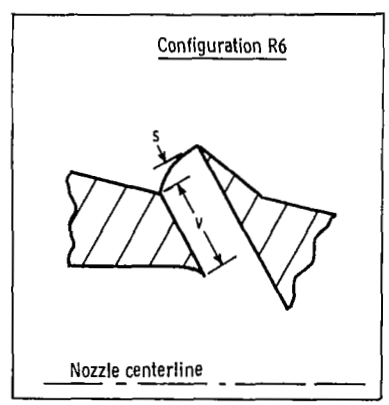

(b) Thrust-reverser port geometry details.

Figure 7.- Concluded.

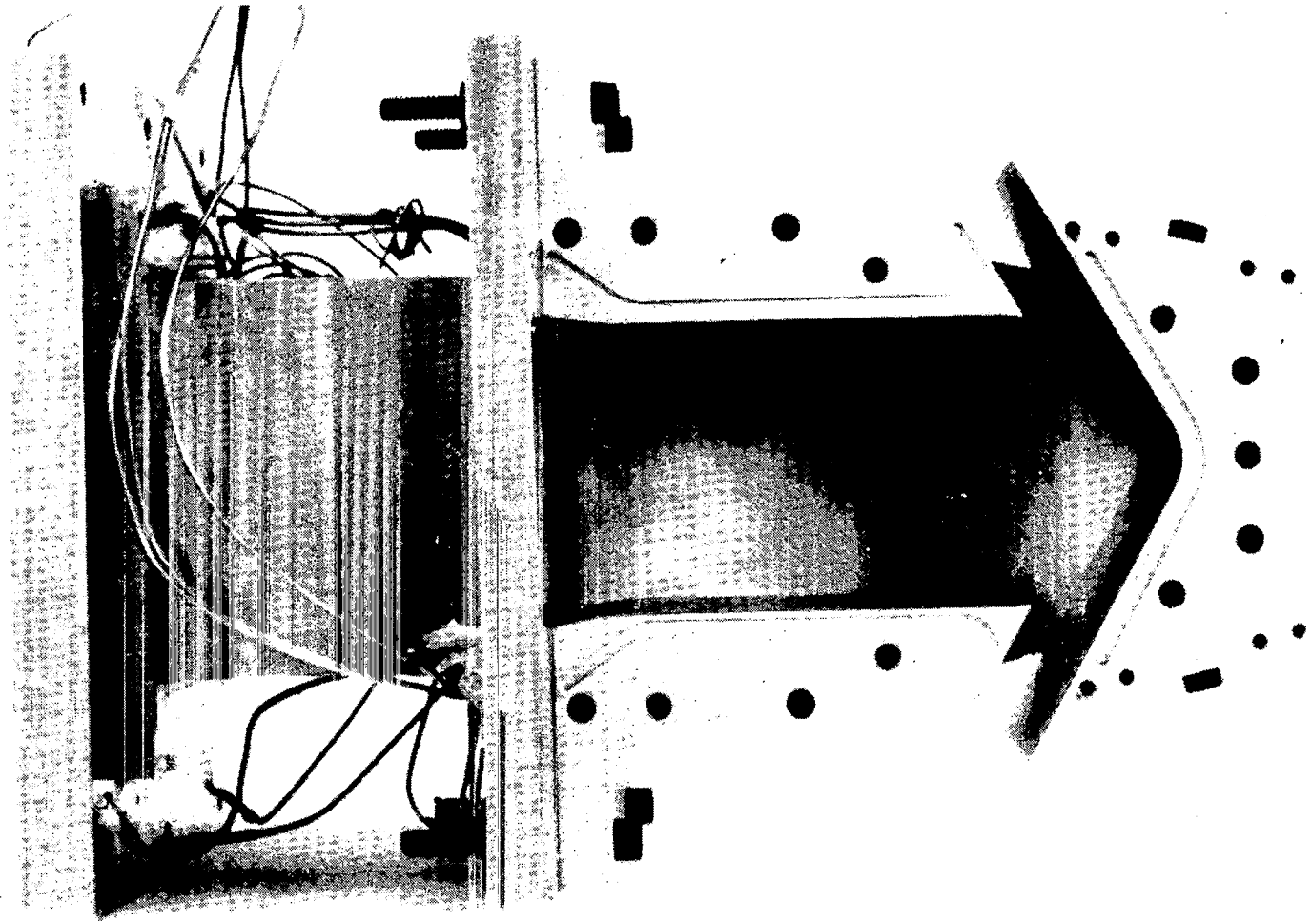

L-82-501

Figure 8.- Photograph of thrust-reverser configuration R5 with one sidewall removed.

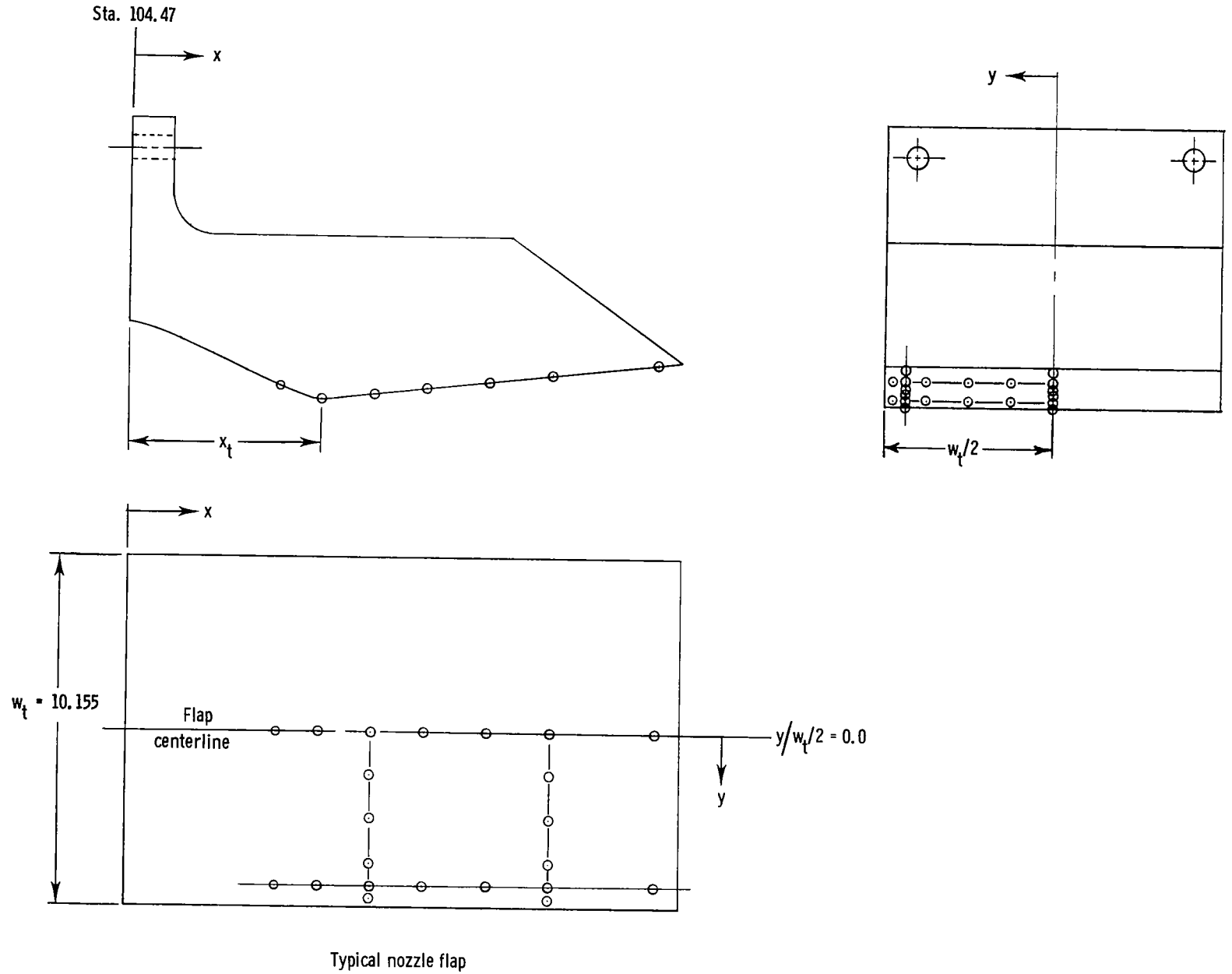

Figure 9.- Sketch of typical nozzle flap internal static-pressure instrumentation. All dimensions are in centimeters unless otherwise indicated.

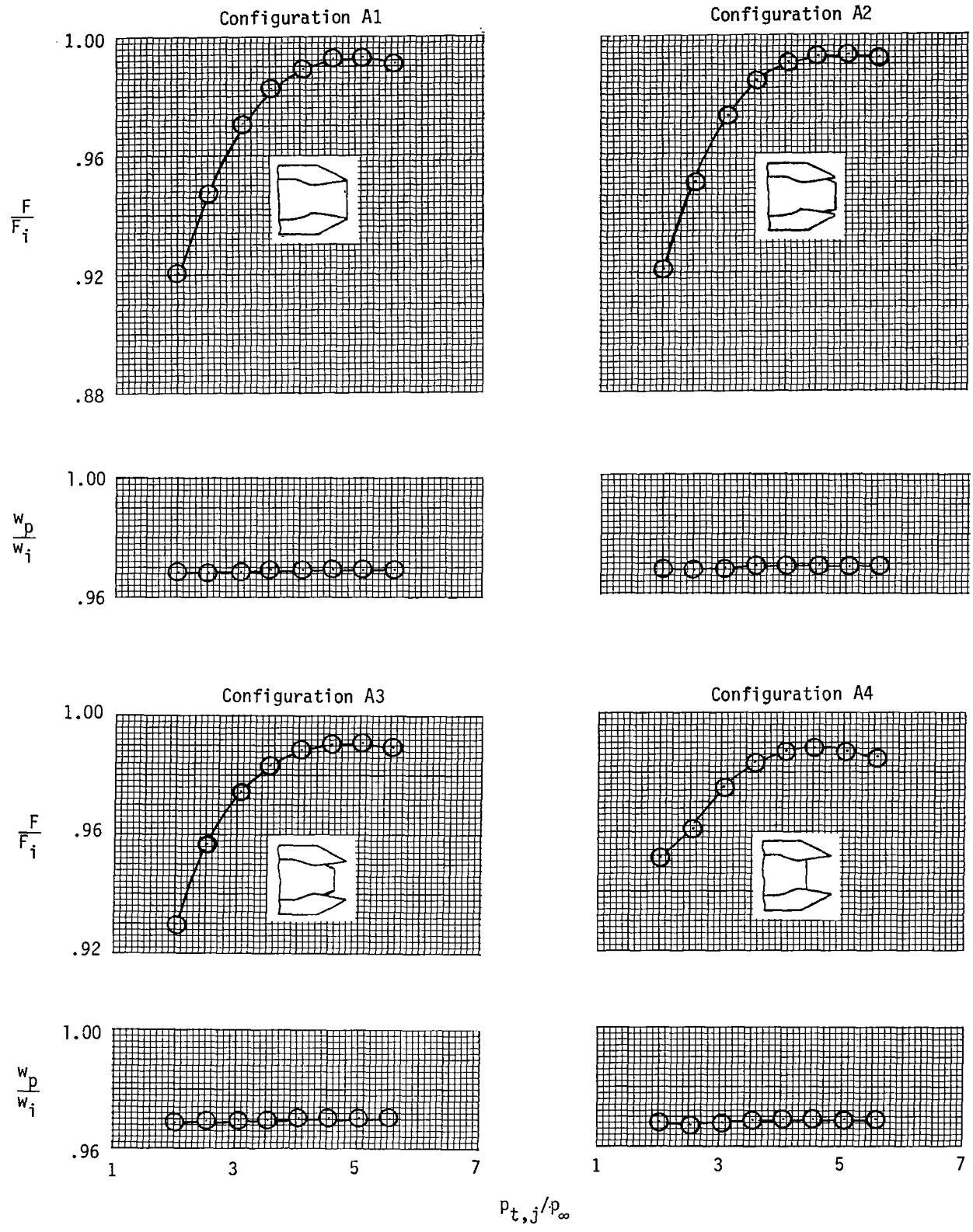

Figure 10.- Variation of nozzle thrust ratio and discharge coefficient with nozzle pressure ratio for unvectored AR = 2.012 nozzle with four sidewall configurations. A_e/A_t = 1.300.

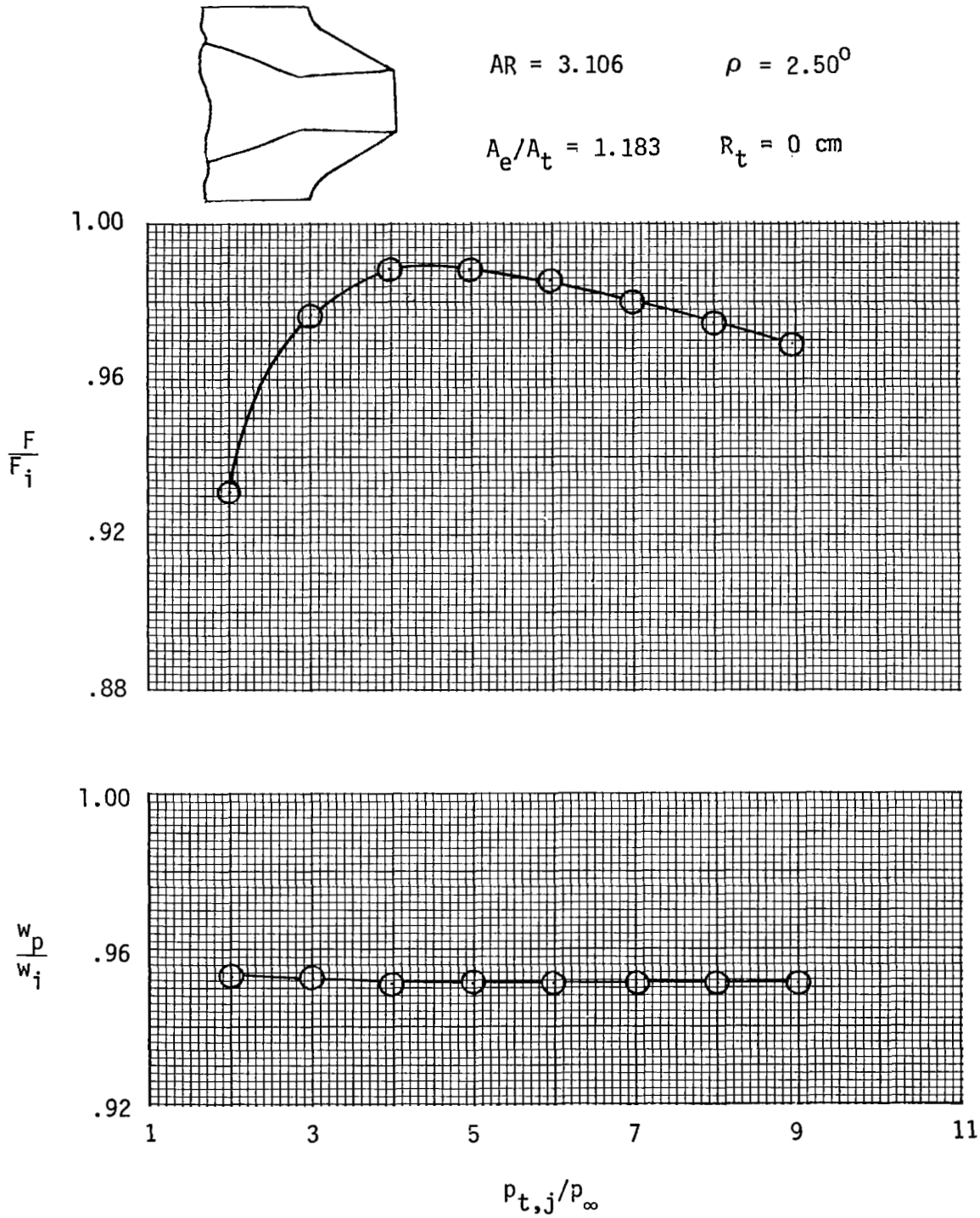

Figure 11.- Variation of nozzle thrust ratio and discharge coefficient with nozzle pressure ratio for configuration B1.

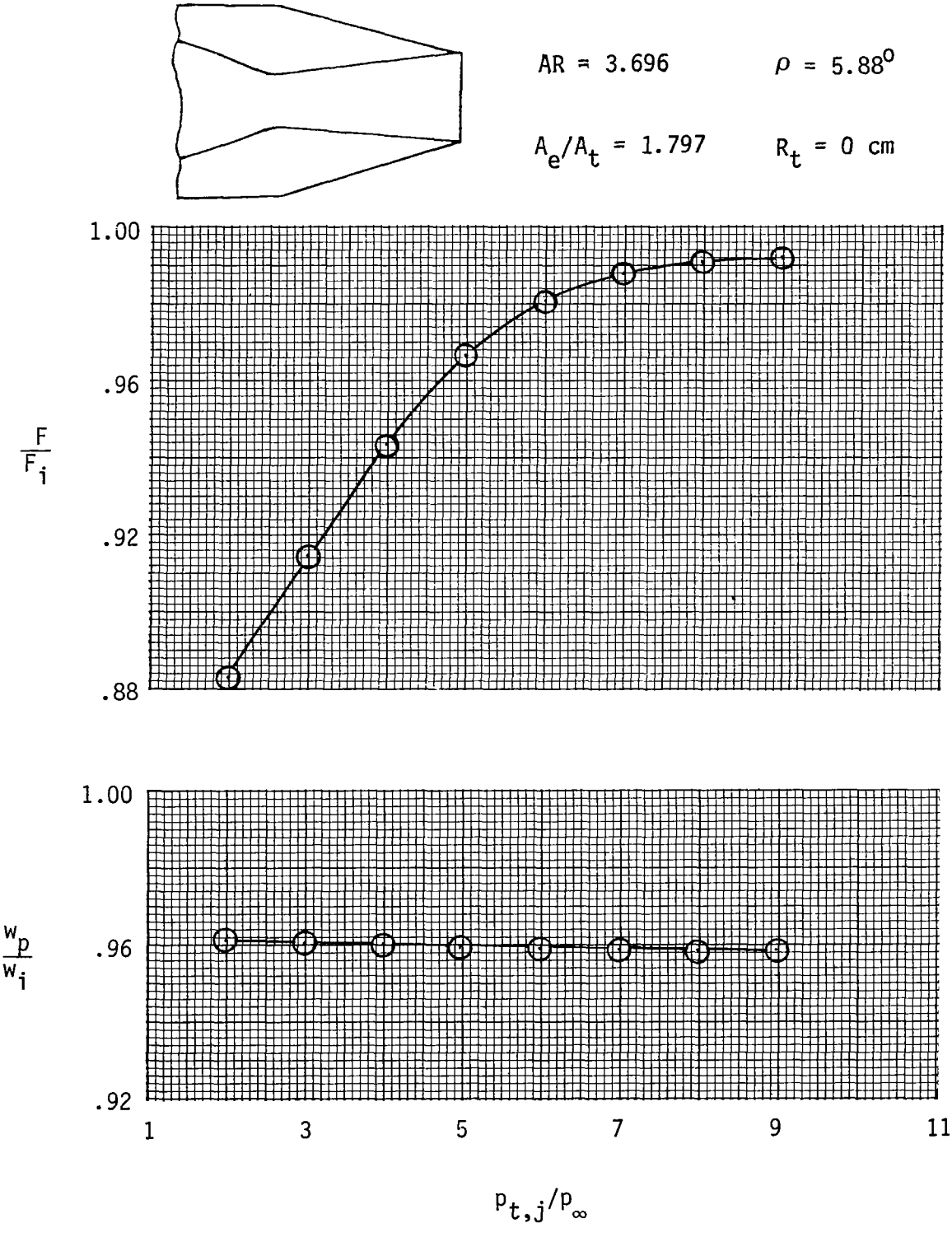

Figure 12.- Variation of nozzle thrust ratio and discharge coefficient with nozzle pressure ratio for configuration B2.

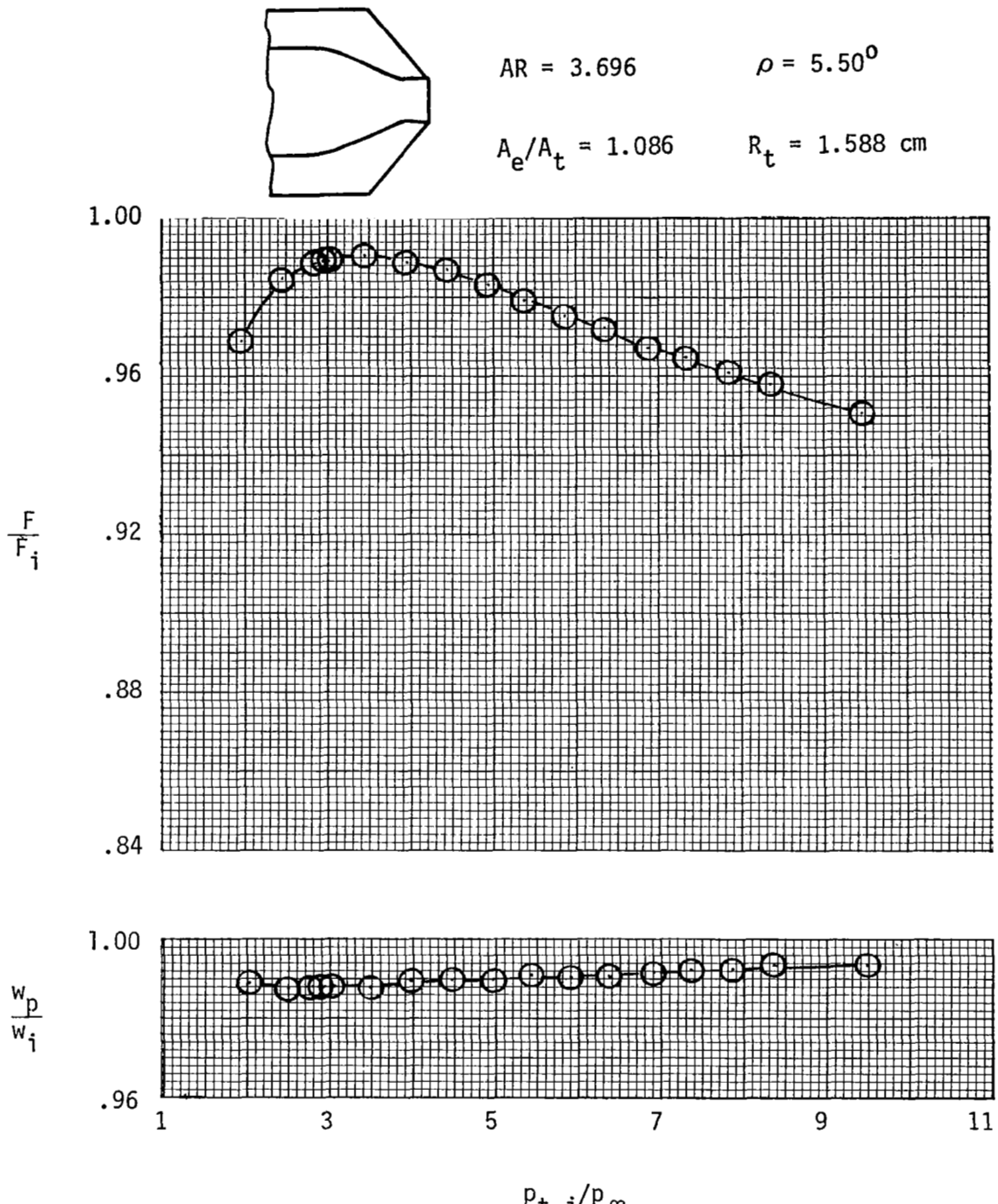

Figure 13.- Variation of nozzle thrust ratio and discharge coefficient with nozzle pressure ratio for configuration D1.

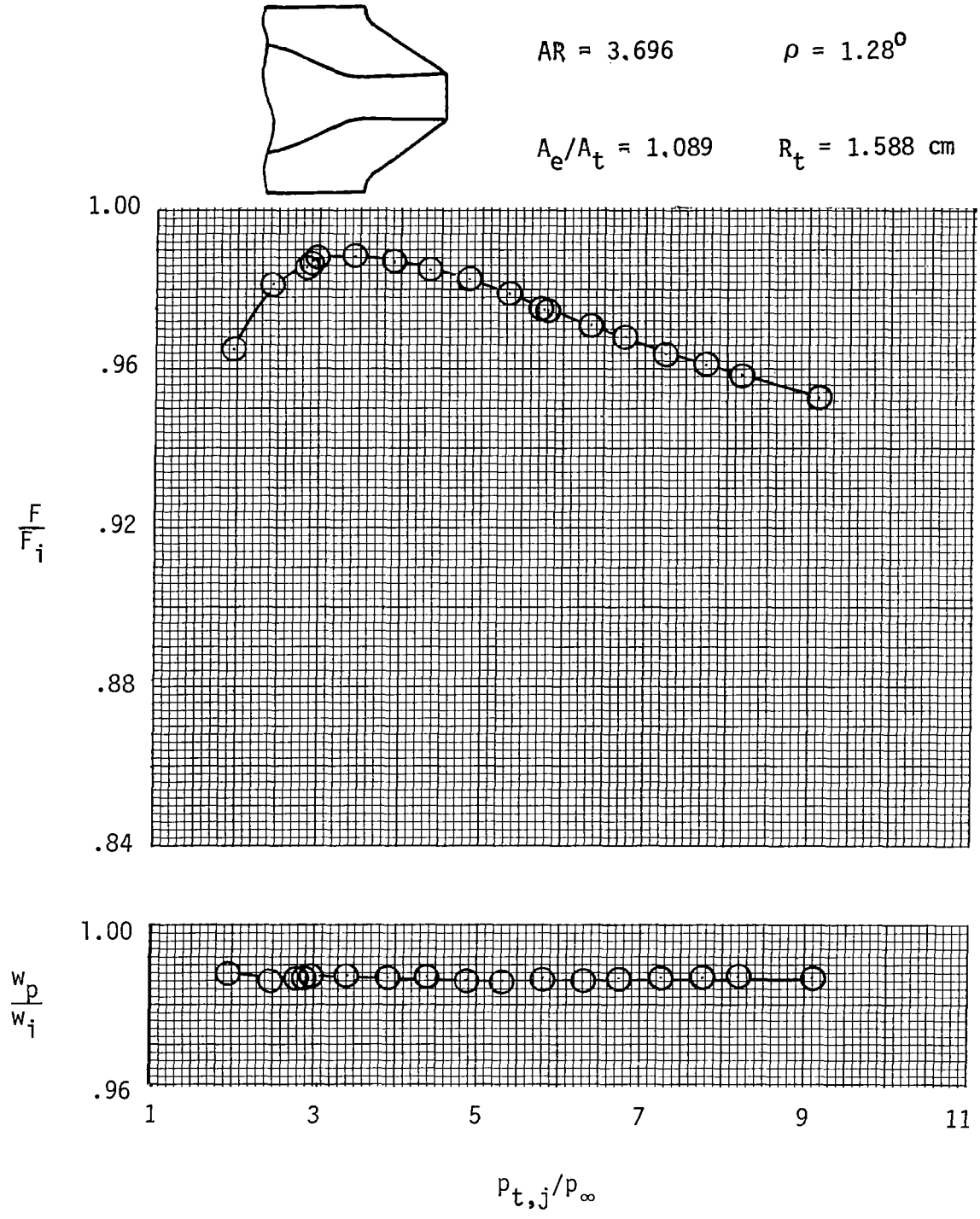

Figure 14.- Variation of nozzle thrust ratio and discharge coefficient with nozzle pressure ratio for configuration D2.

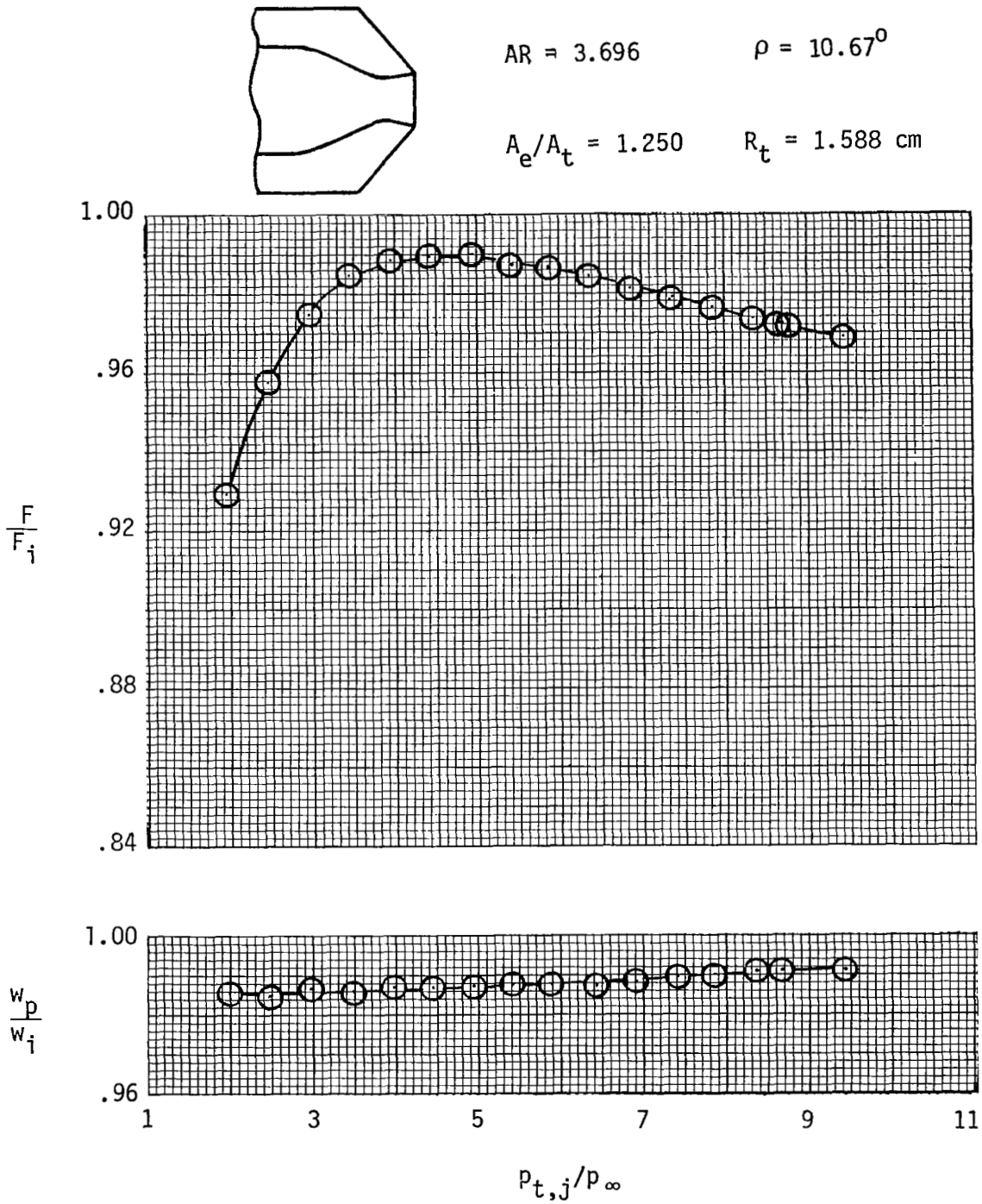

Figure 15.- Variation of nozzle thrust ratio and discharge coefficient with nozzle pressure ratio for configuration D3.

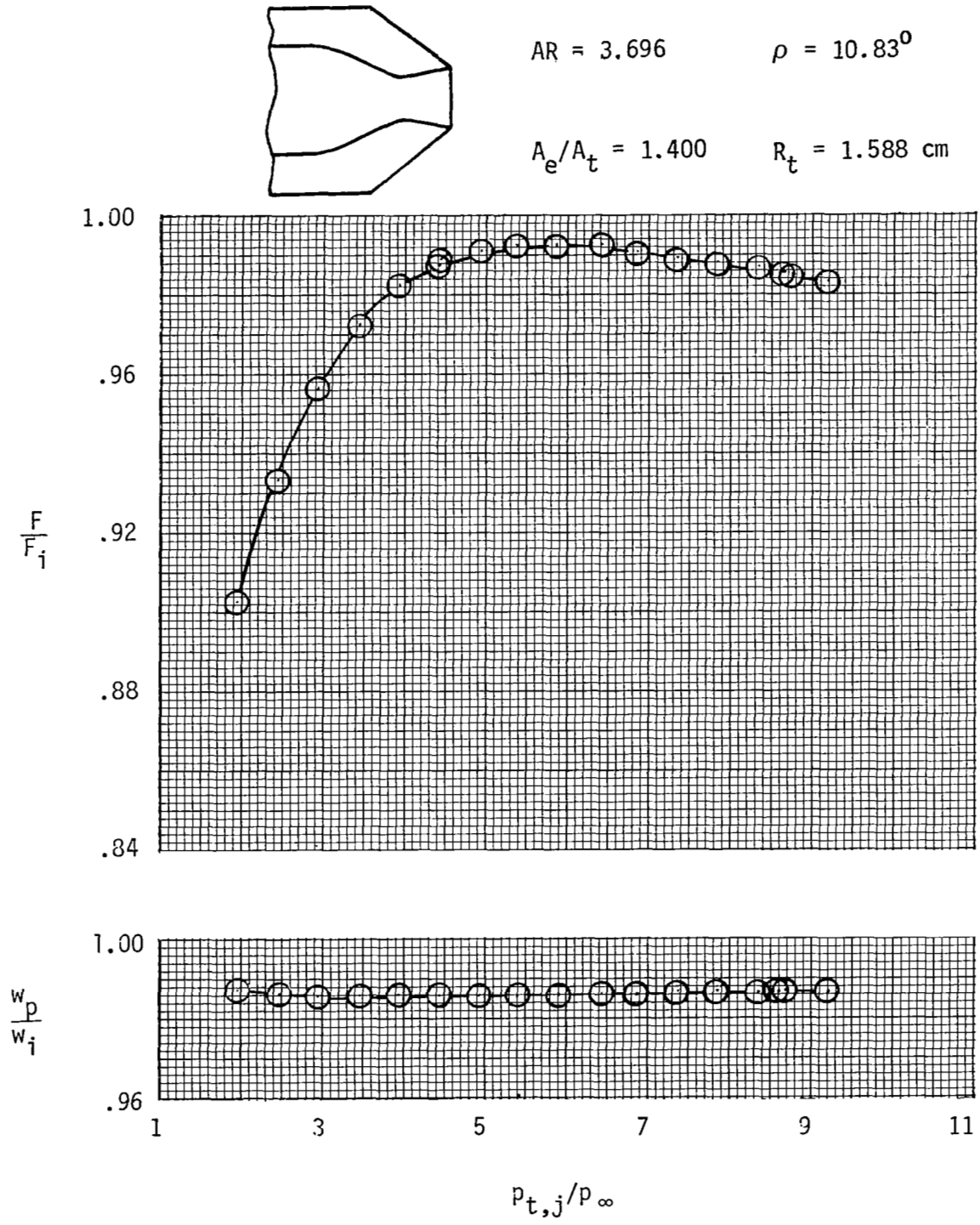

Figure 16.- Variation of nozzle thrust ratio and discharge coefficient with nozzle pressure ratio for configuration D4.

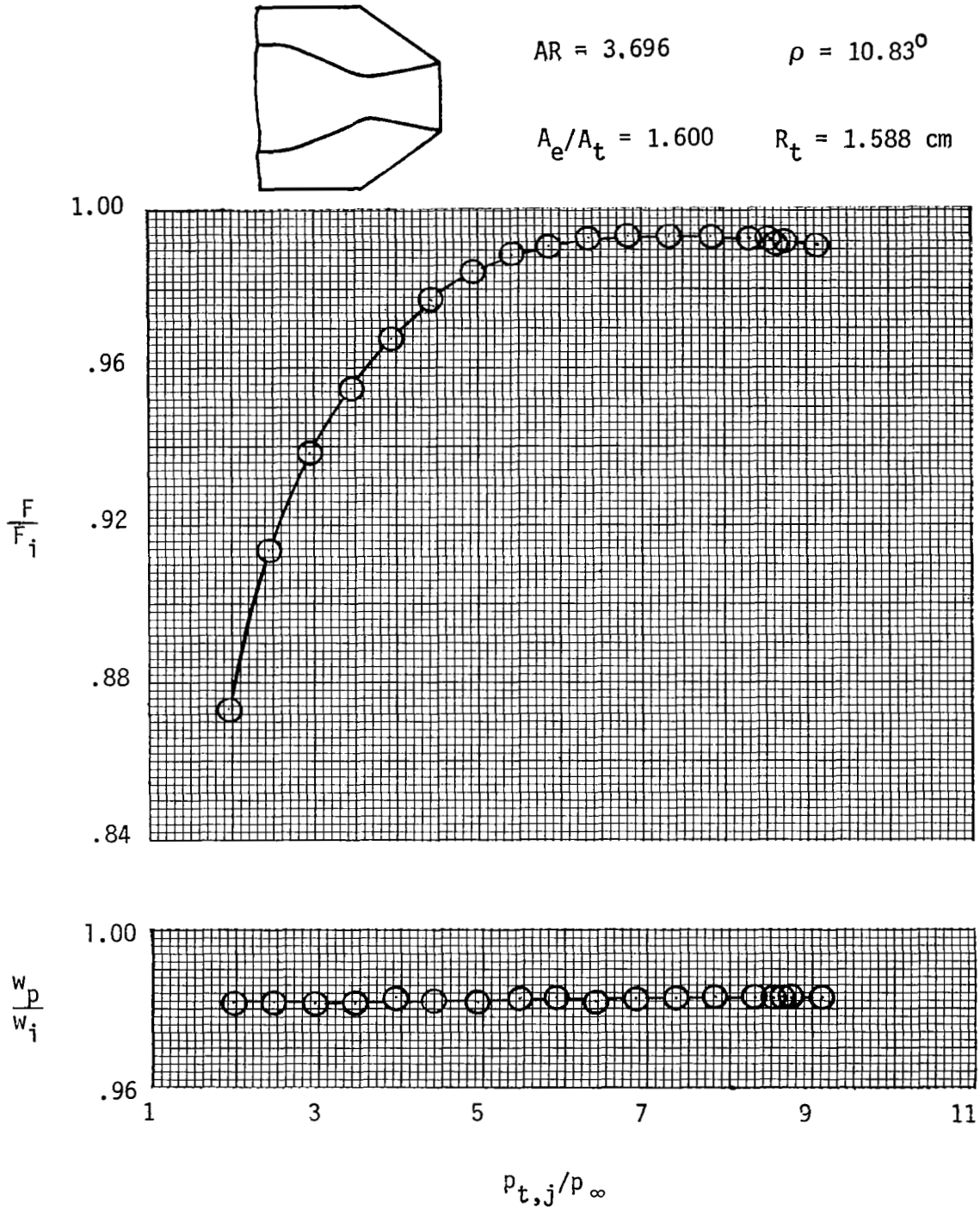

Figure 17.- Variation of nozzle thrust ratio and discharge coefficient with nozzle pressure ratio for configuration D5.

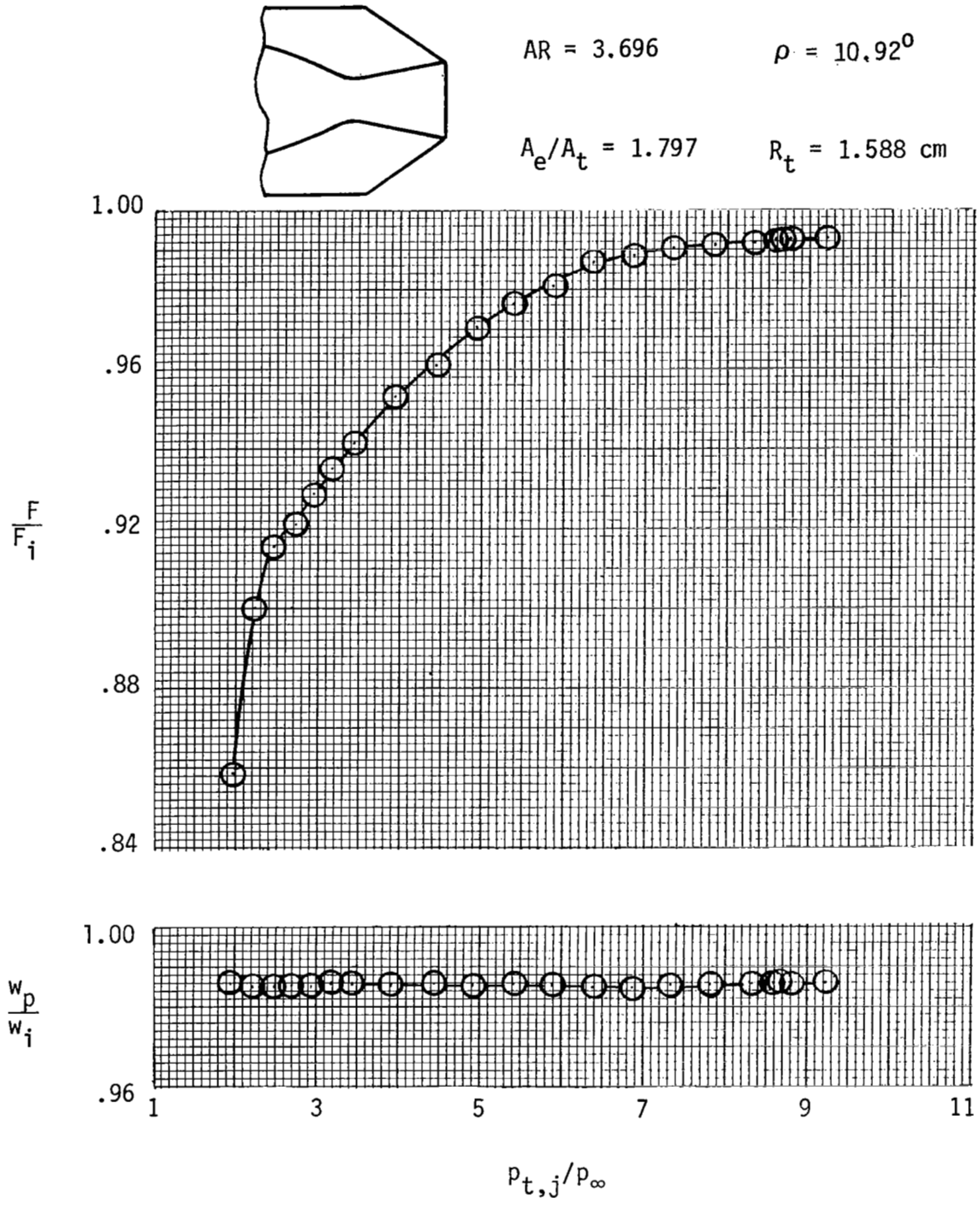

Figure 18.- Variation of nozzle thrust ratio and discharge coefficient with nozzle pressure ratio for configuration D6.

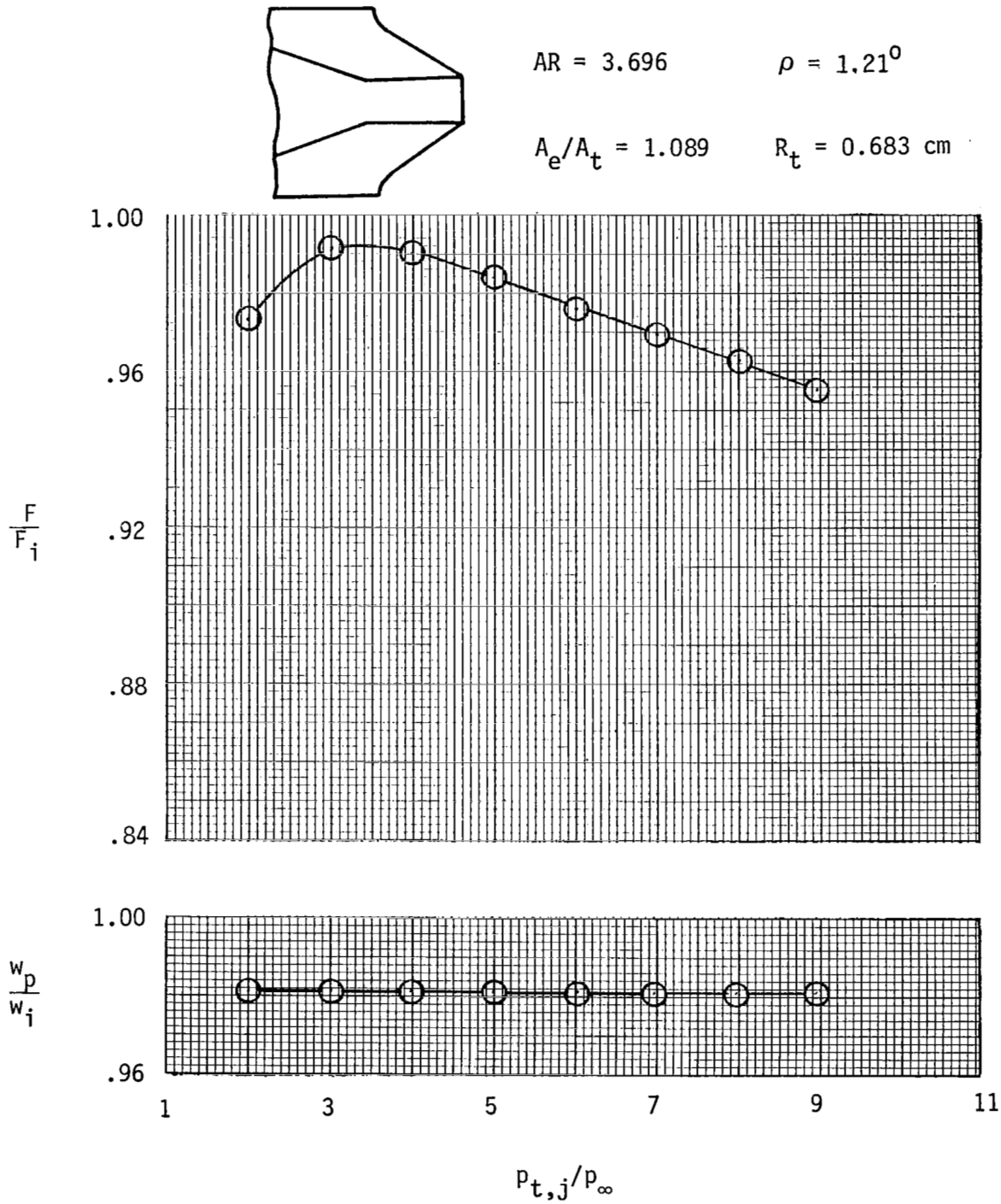

Figure 19.- Variation of nozzle thrust ratio and discharge coefficient with nozzle pressure ratio for configuration D7.

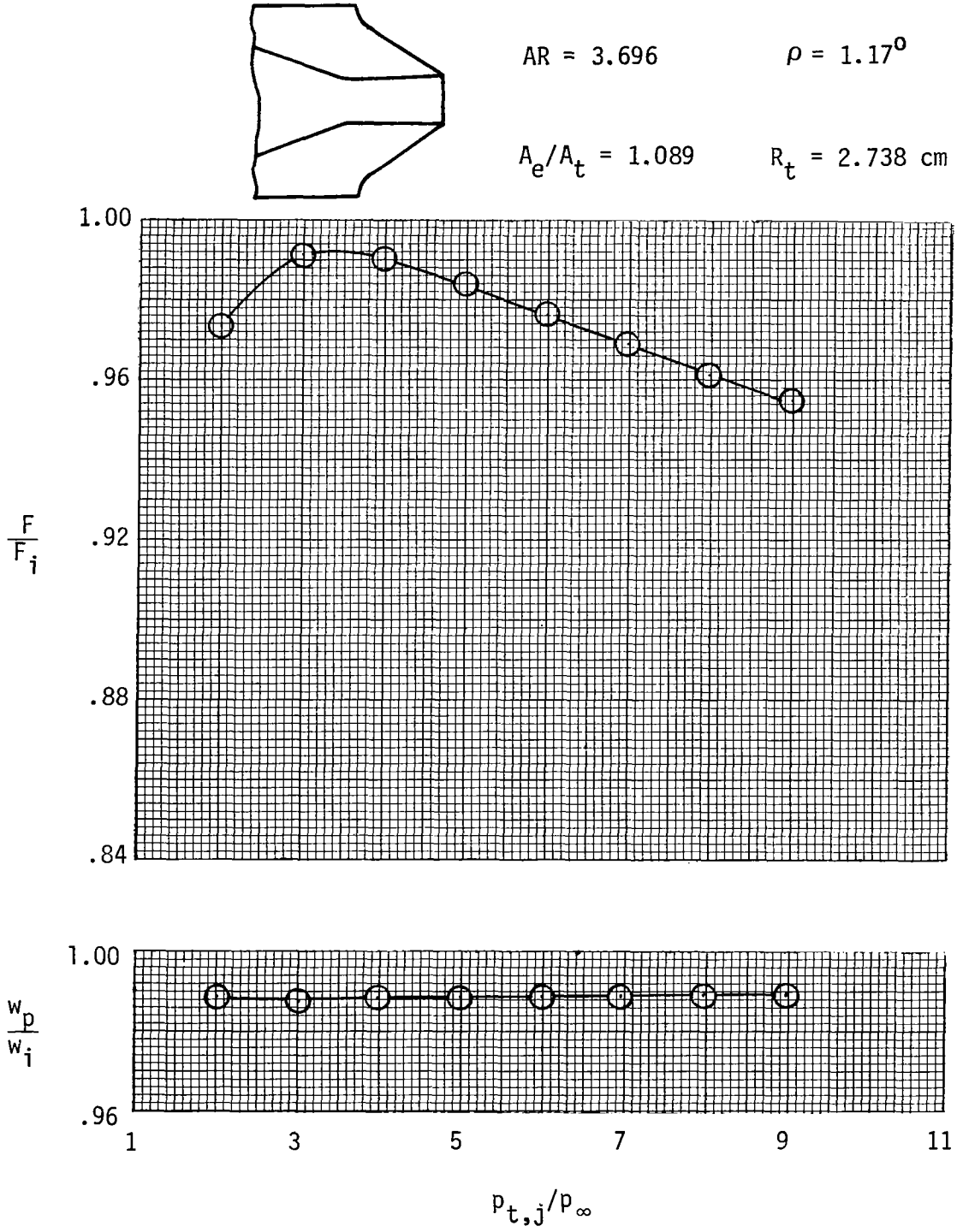

Figure 20.- Variation of nozzle thrust ratio and discharge coefficient with nozzle pressure ratio for configuration D8.

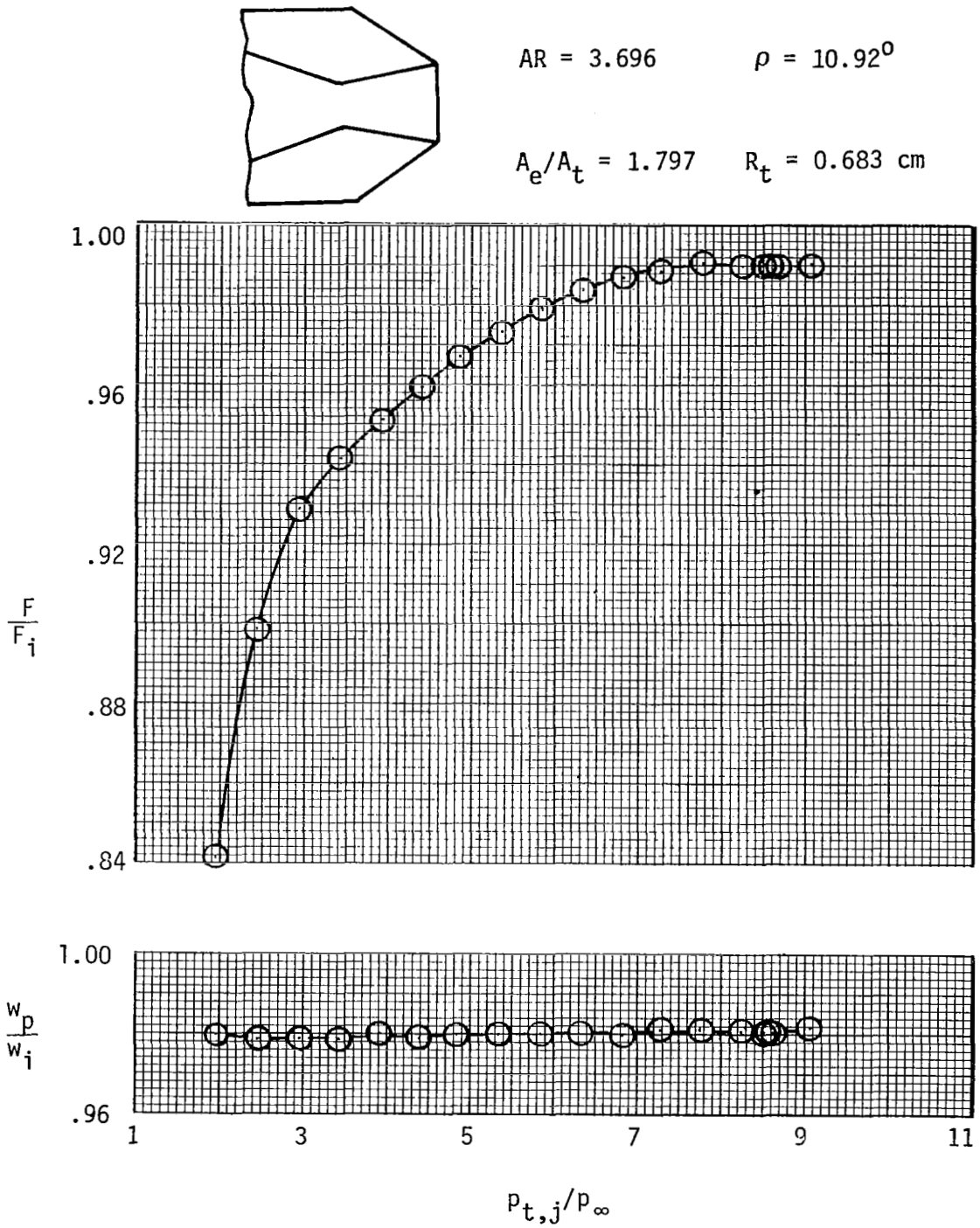

Figure 21.- Variation of nozzle thrust ratio and discharge coefficient with nozzle pressure ratio for configuration D9.

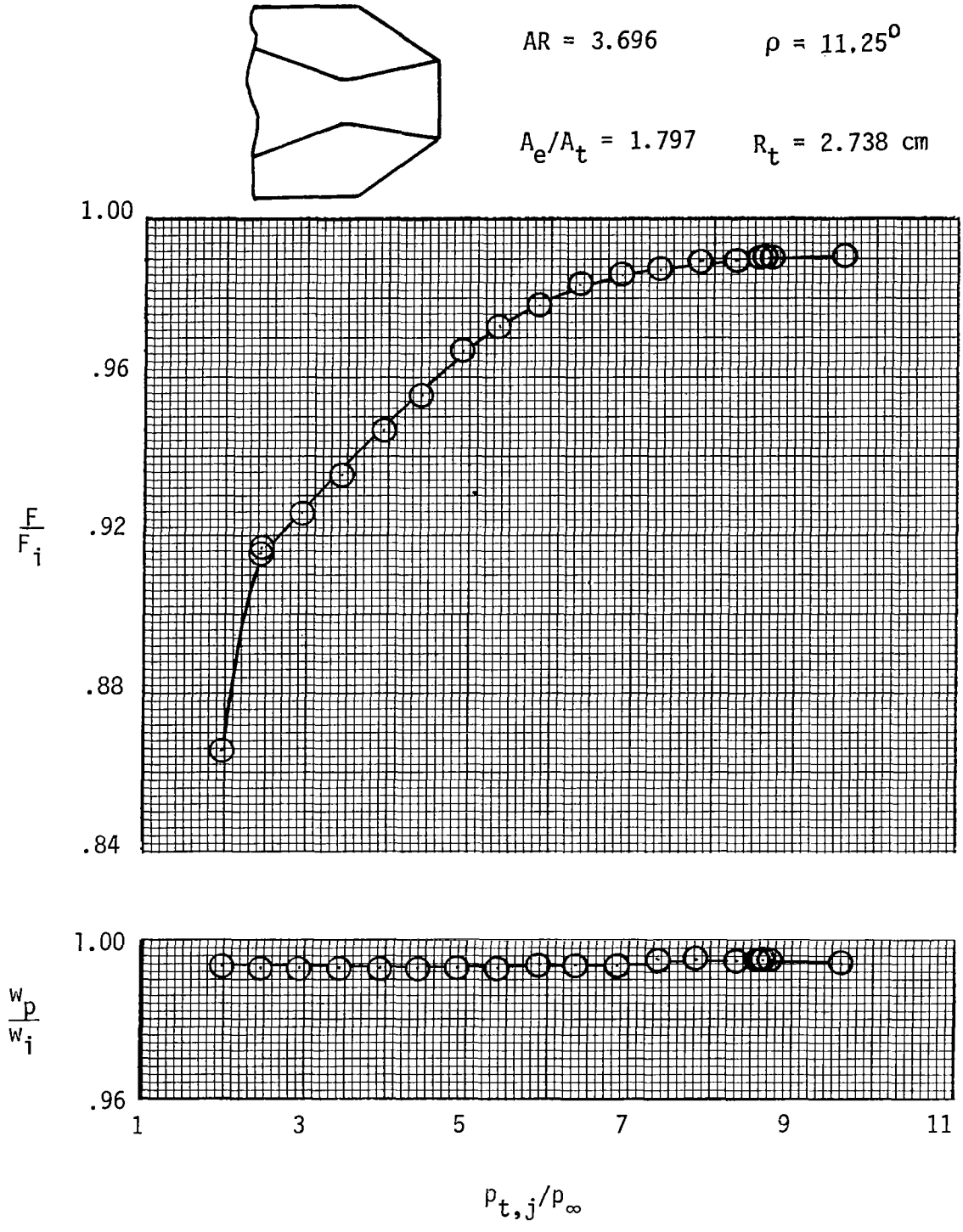

Figure 22.- Variation of nozzle thrust ratio and discharge coefficient with nozzle pressure ratio for configuration D10.

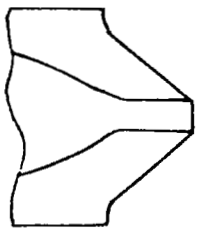

$\frac{x_s - x_t}{x_e - x_t} = 1.000$ $\rho = 1.25^o$

$R_t = 0.952$ cm

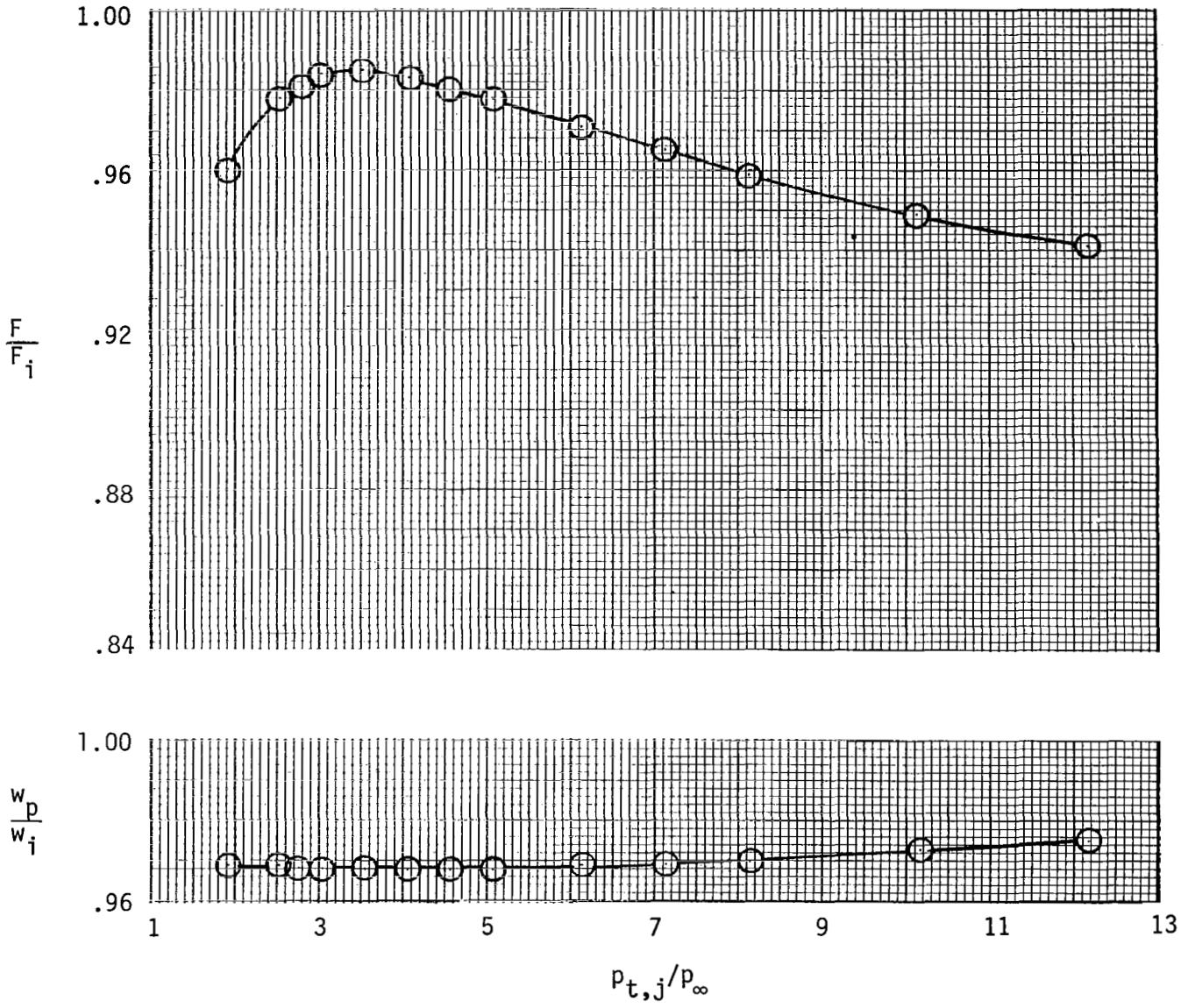

(a) Configuration E1.

Figure 23.- Variation of nozzle thrust ratio and discharge coefficient with nozzle pressure ratio for AR = 5.806 nozzle with $A_e/A_t = 1.089$ and two sidewall configurations.

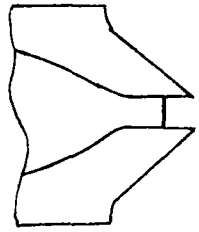

$\frac{x_s - x_t}{x_e - x_t} = 0.587$ $\rho = 1.25^o$

$R_t = 0.952$ cm

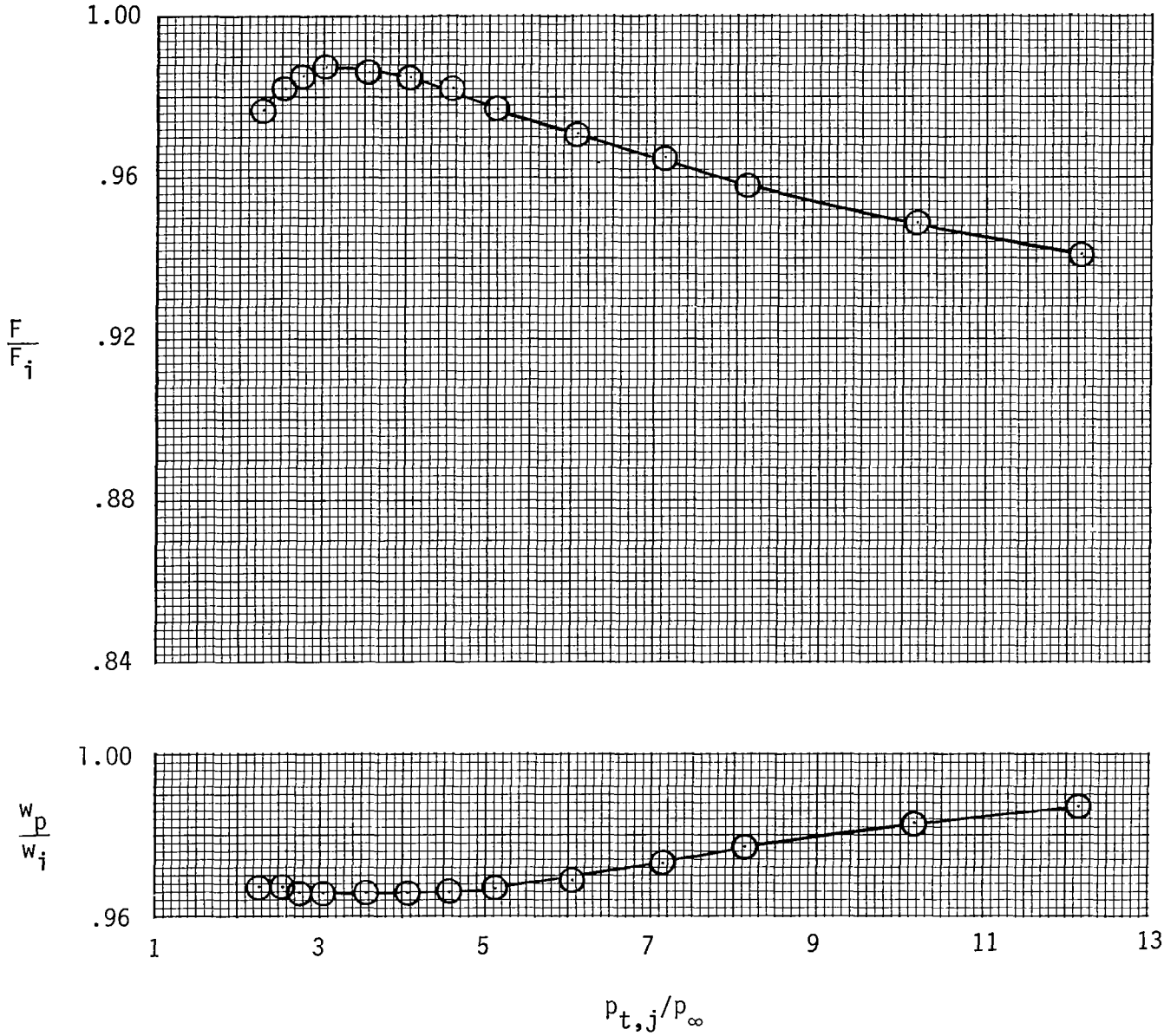

(b) Configuration E2.

Figure 23.- Concluded.

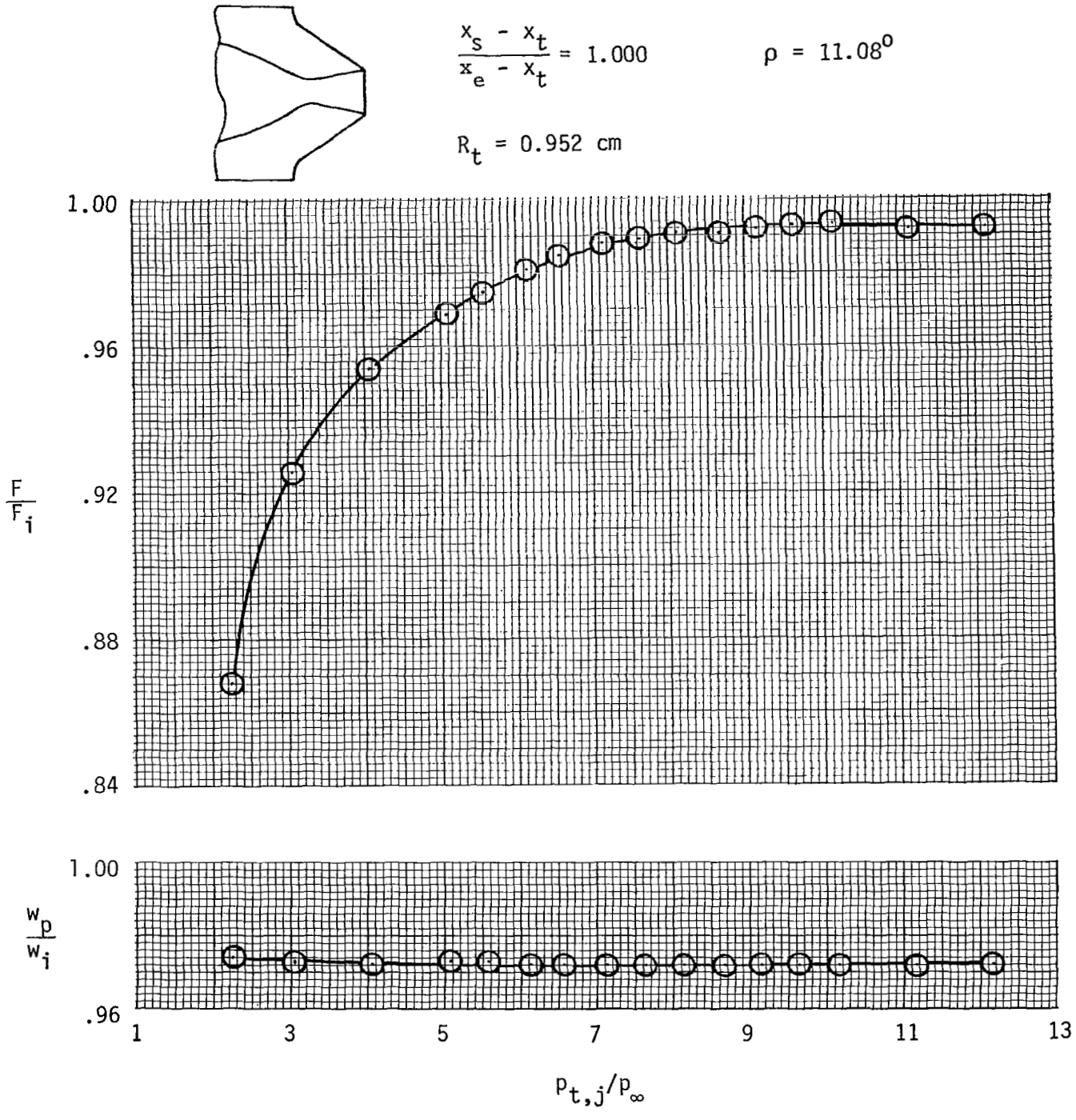

(a) Configuration E3.

Figure 24.- Variation of nozzle thrust ratio and discharge coefficient with nozzle pressure ratio for AR = 5.806 nozzle with $A_e/A_t = 1.797$ and two sidewall configurations.

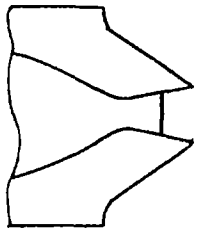

$\frac{x_s - x_t}{x_e - x_t} = 0.587$ $\rho = 11.08^0$

$R_t = 0.952$ cm

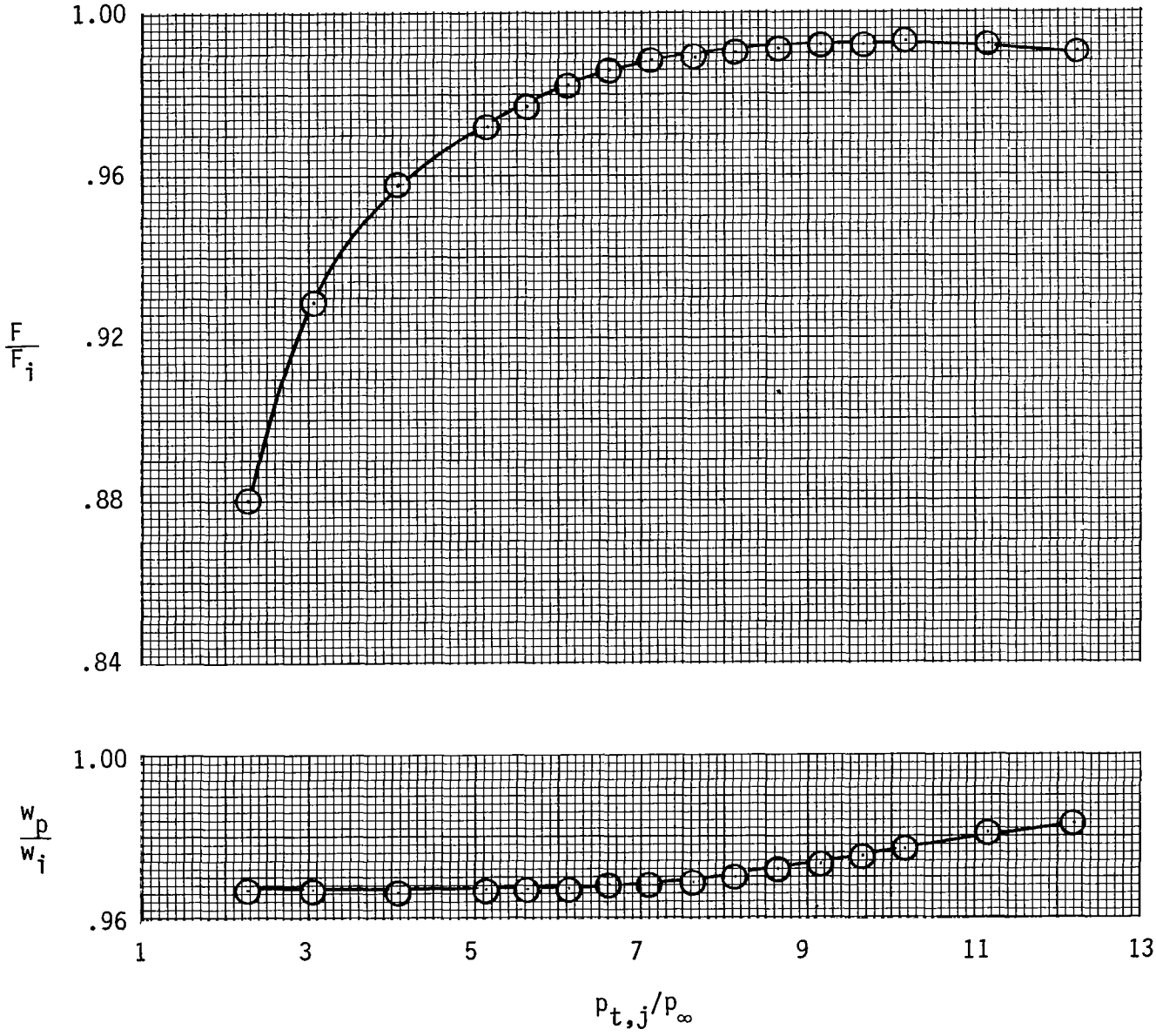

(b) Configuration E4.

Figure 24.- Concluded.

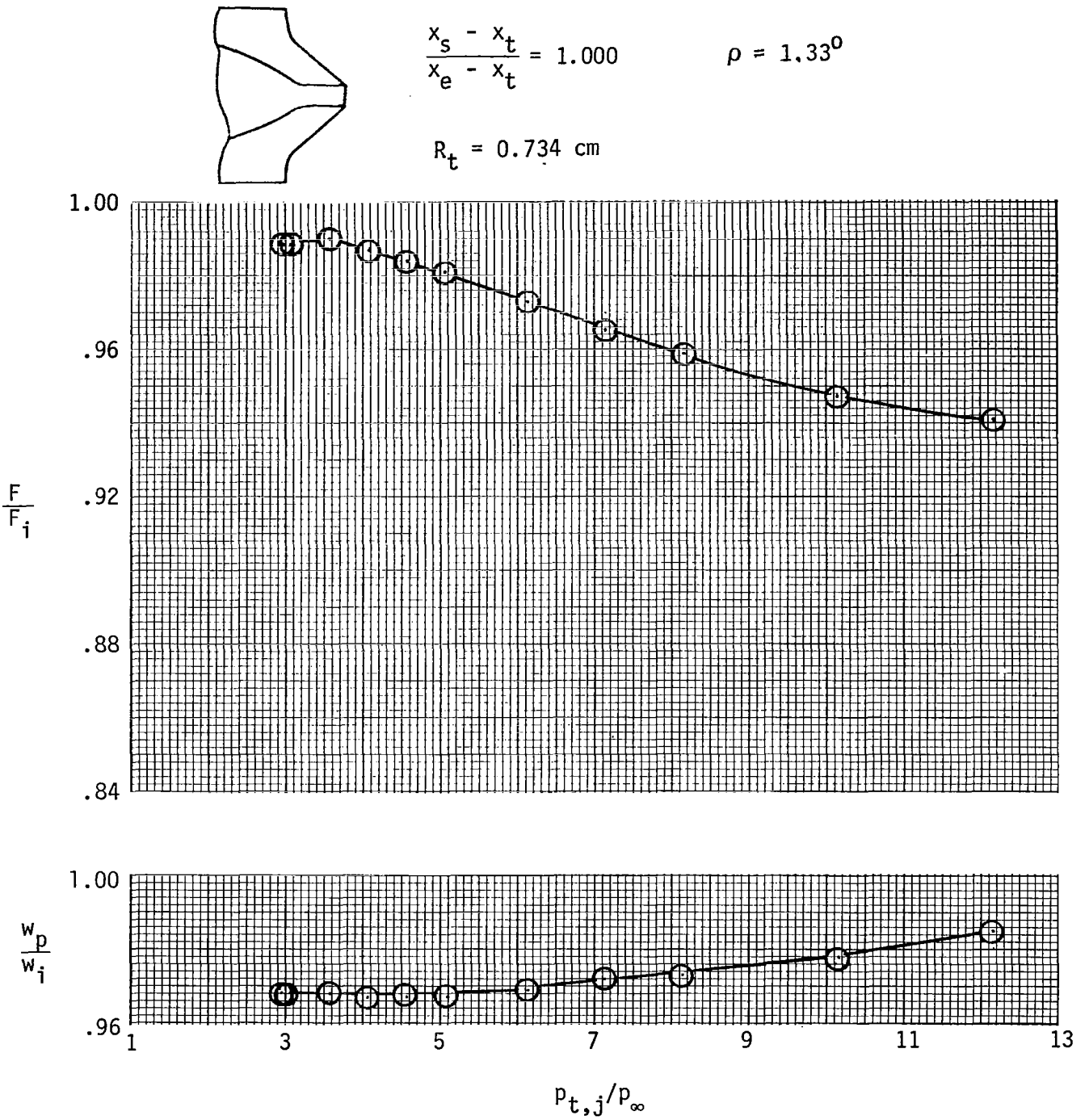

(a) Configuration F1.

Figure 25.- Variation of nozzle thrust ratio and discharge coefficient with nozzle pressure ratio for AR = 7.612 nozzle with A_e/A_t = 1.089 and two sidewall configurations.

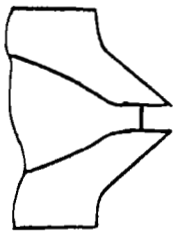

$\frac{x_s - x_t}{x_e - x_t} = 0.450$ $\rho = 1.33^o$

$R_t = 0.734$ cm

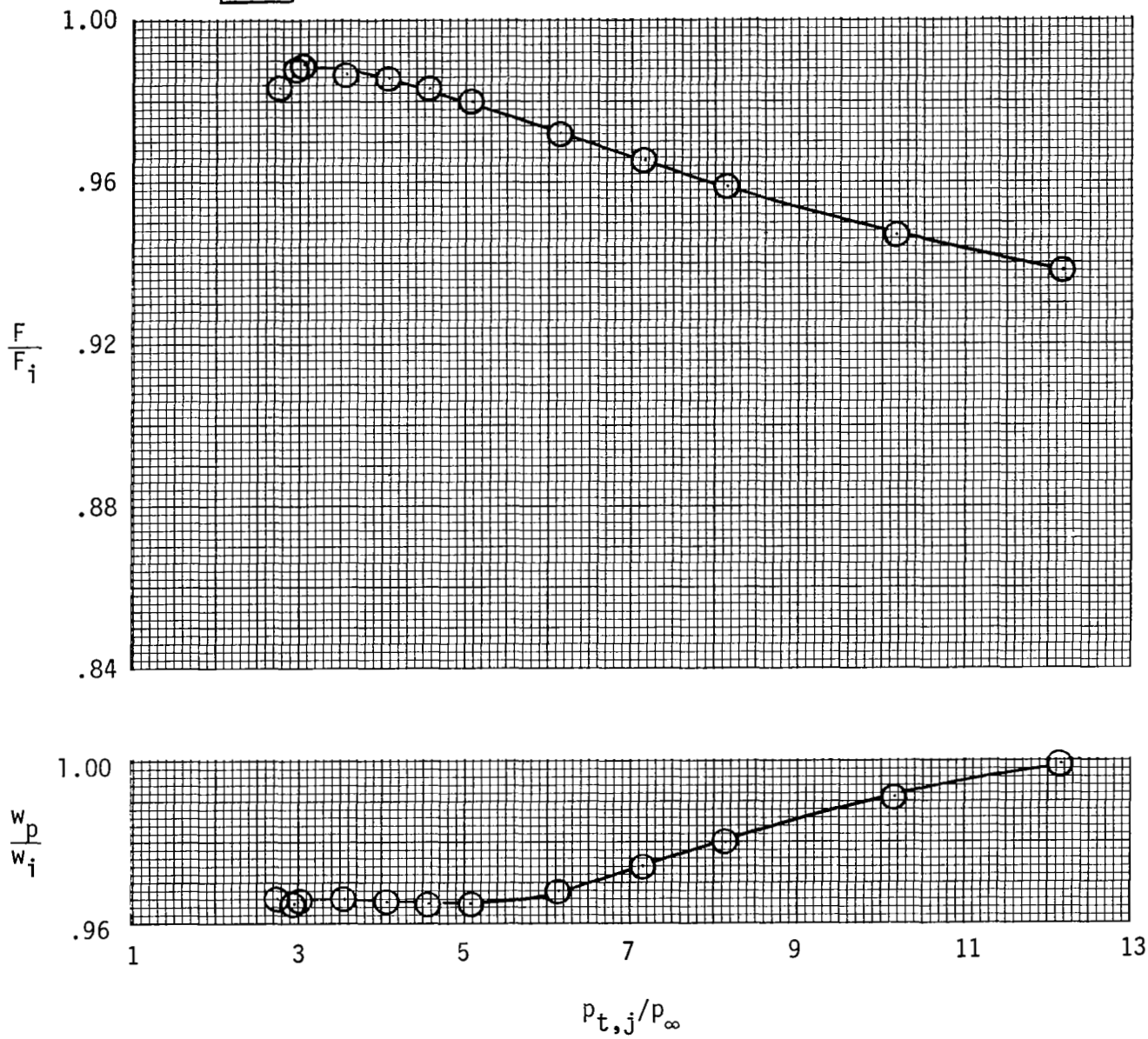

(b) Configuration F2.

Figure 25.- Concluded.

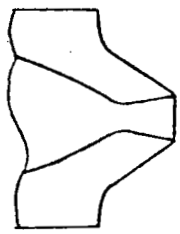

$\frac{x_s - x_t}{x_e - x_t} = 1.000$ $\rho = 11.00^o$

$R_t = 0.734$ cm

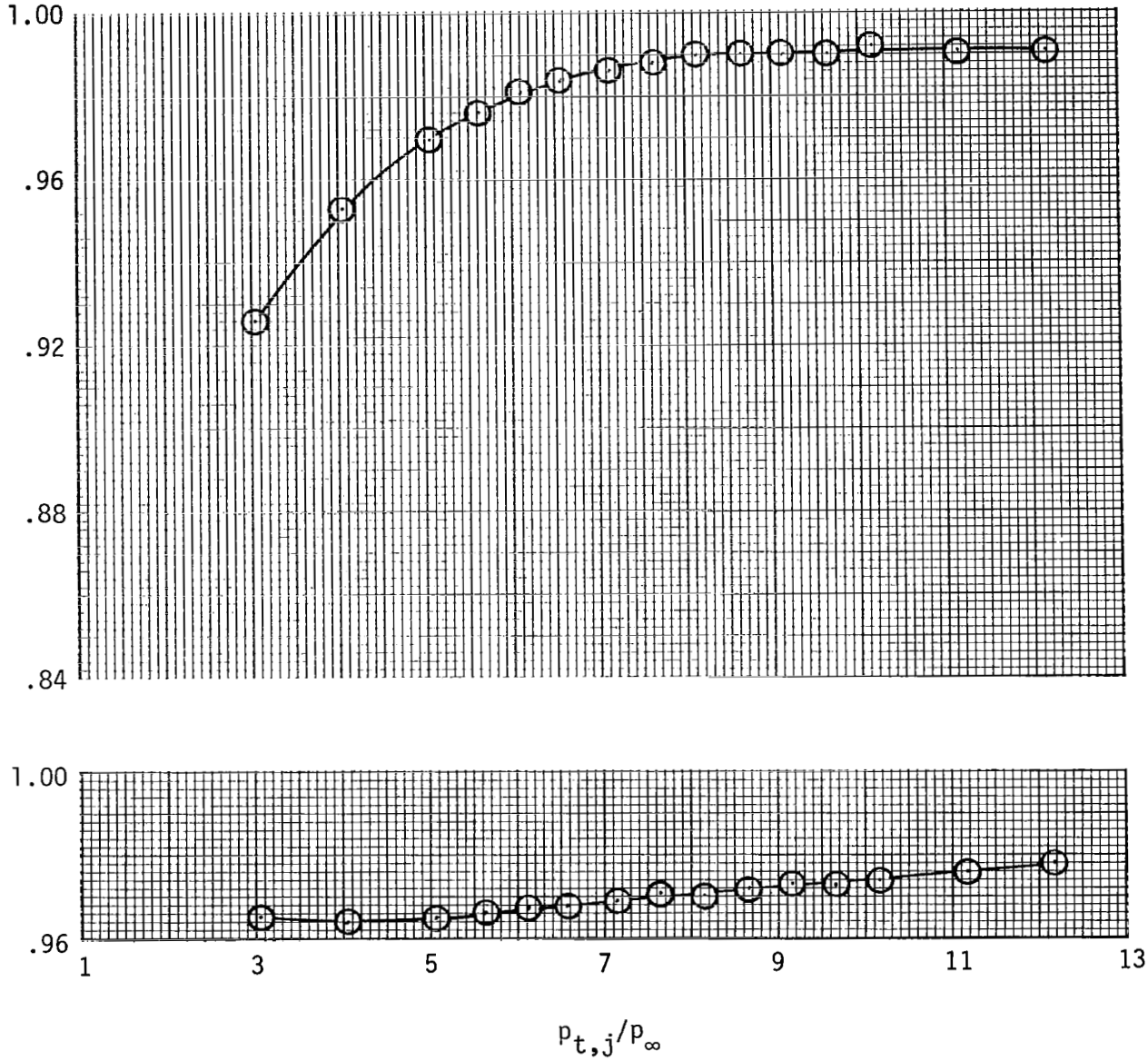

(a) Configuration F3.

Figure 26.- Variation of nozzle thrust ratio and discharge coefficient with nozzle pressure ratio for AR = 7.612 nozzle with $A_e/A_t = 1.797$ and two sidewall configurations.

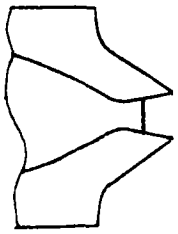

$\frac{x_s - x_t}{x_e - x_t} = 0.450$ $\rho = 11.00^o$

$R_t = 0.734$ cm

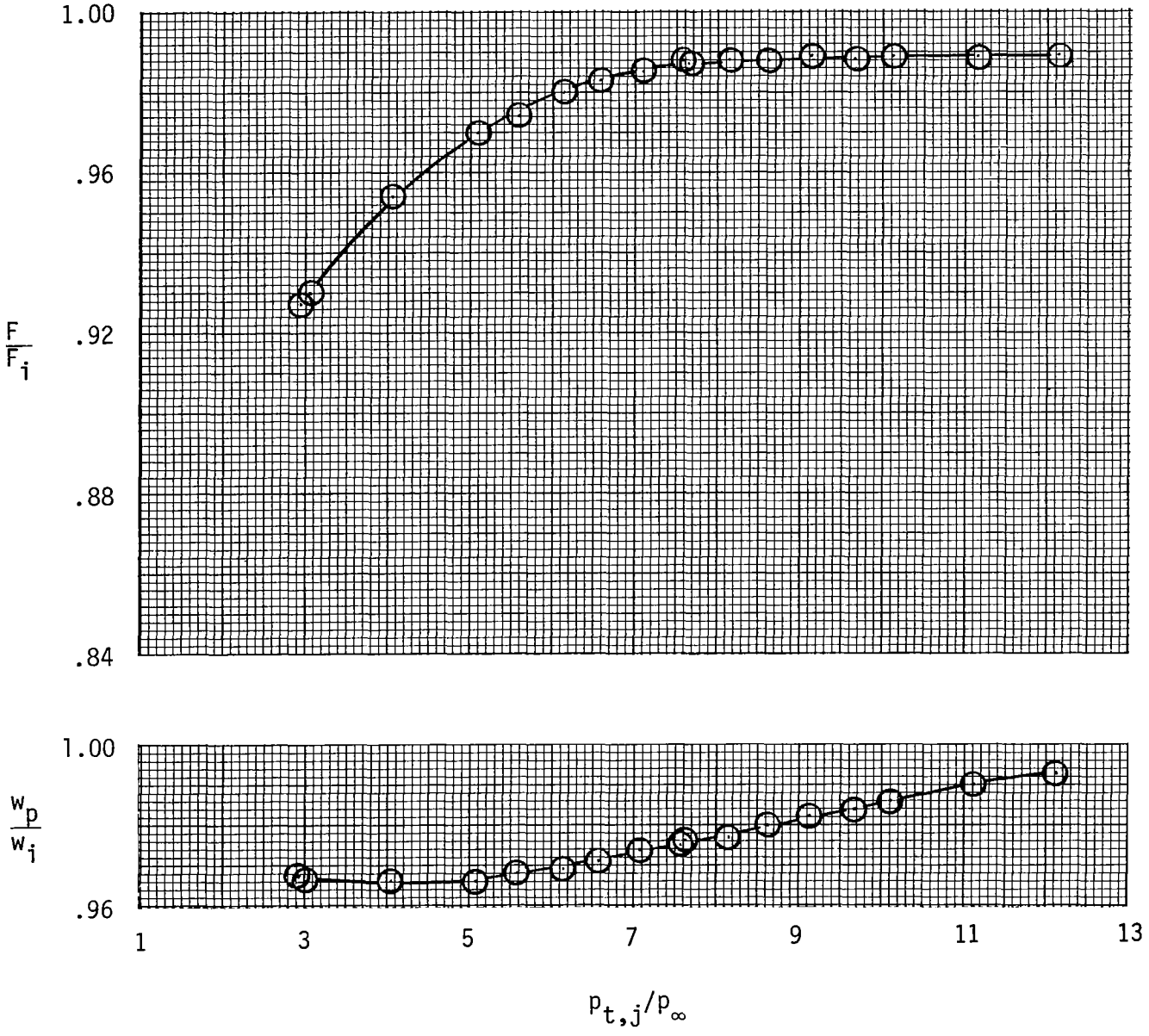

(b) Configuration F4.

Figure 26.- Concluded.

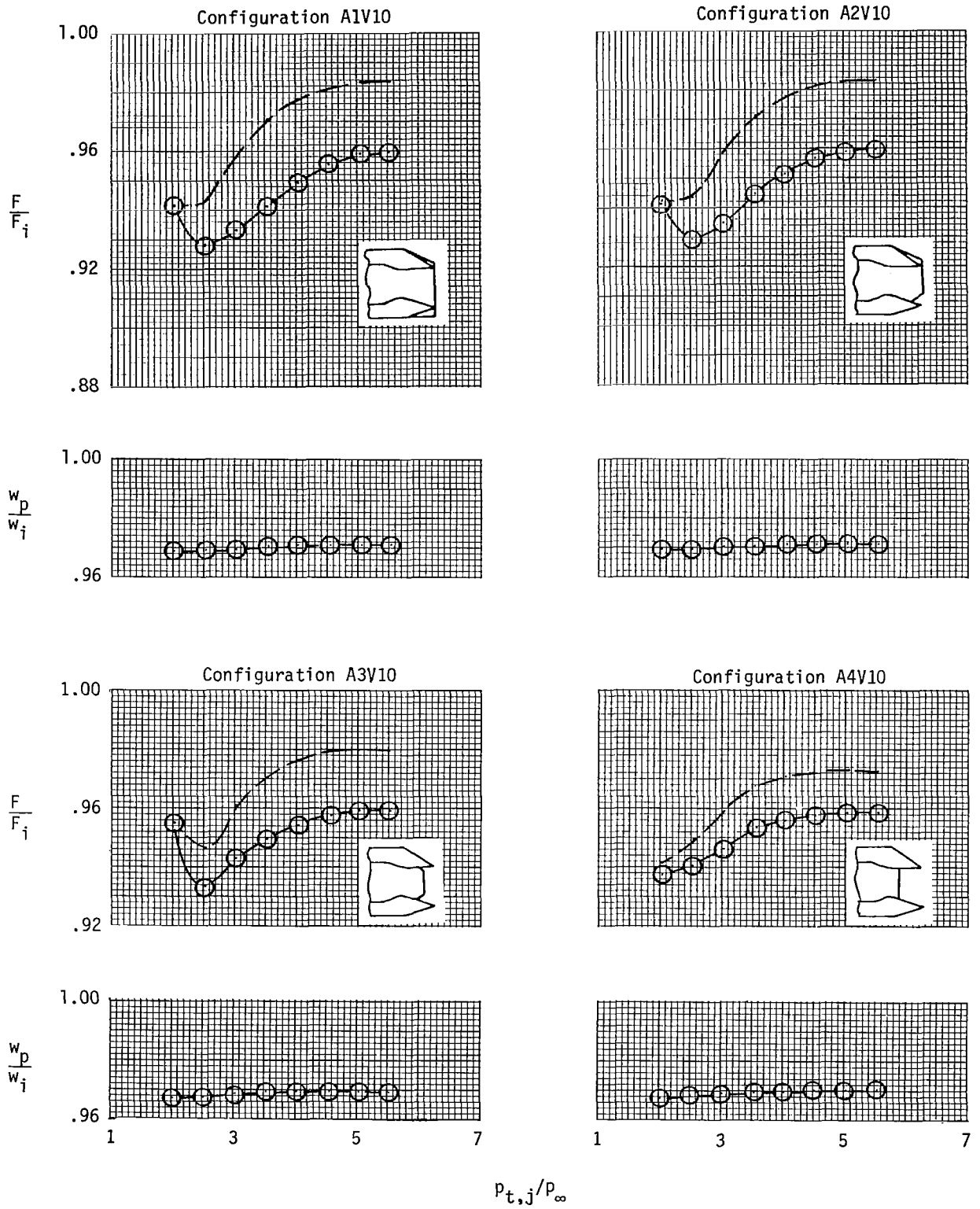

Figure 27.- Variation of nozzle thrust ratio and discharge coefficient with nozzle pressure ratio for AR = 2.012 nozzle vectored 9.79° with four sidewalls. Dashed lines indicate values of resultant thrust ratio F_r/F_i. A_e/A_t = 1.300.

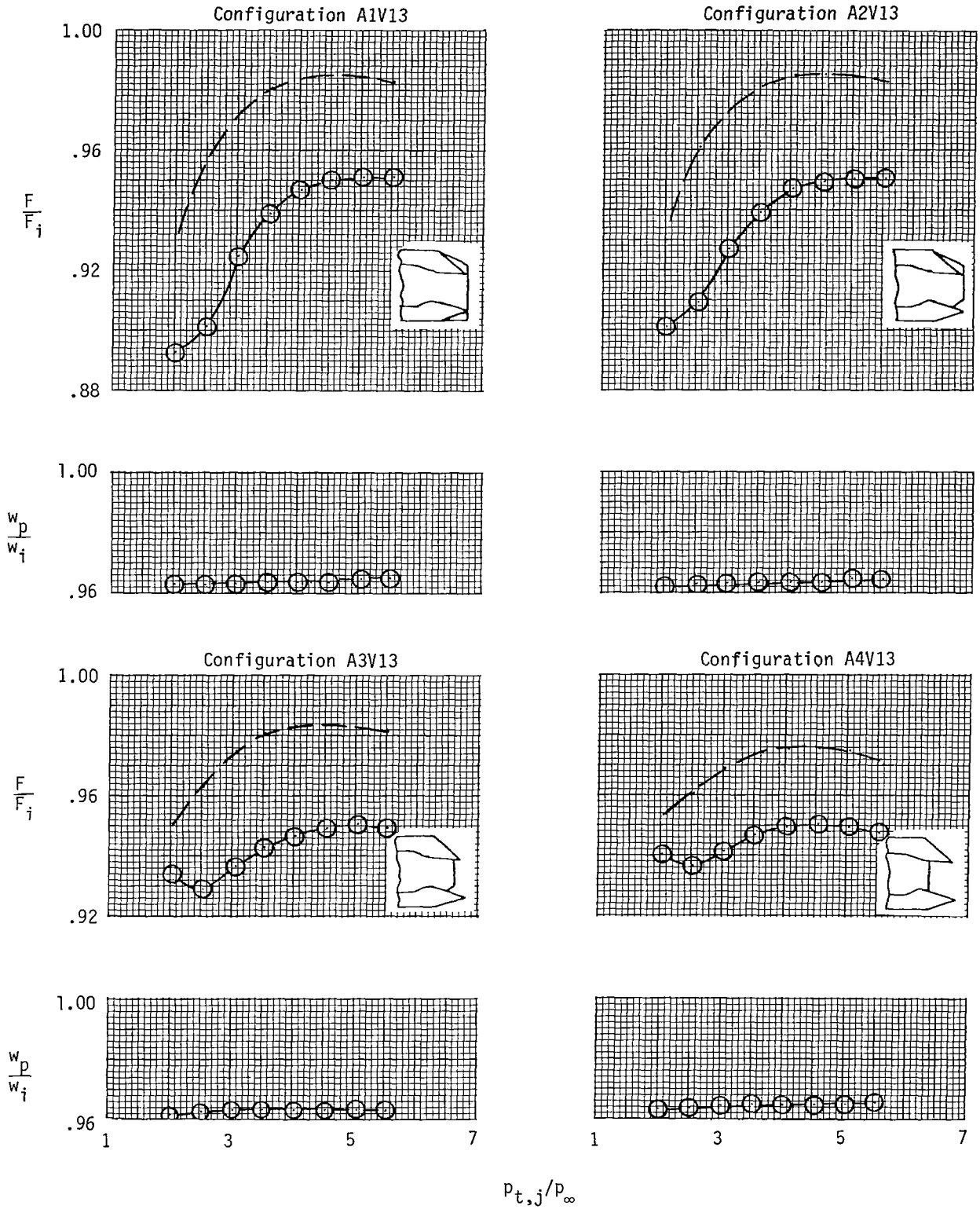

Figure 28.- Variation of nozzle thrust ratio and discharge coefficient with nozzle pressure ratio for AR = 2.012 nozzle vectored 13.22° with four sidewalls. Dashed lines indicate values of resultant thrust ratio F_r/F_i. A_e/A_t = 1.166.

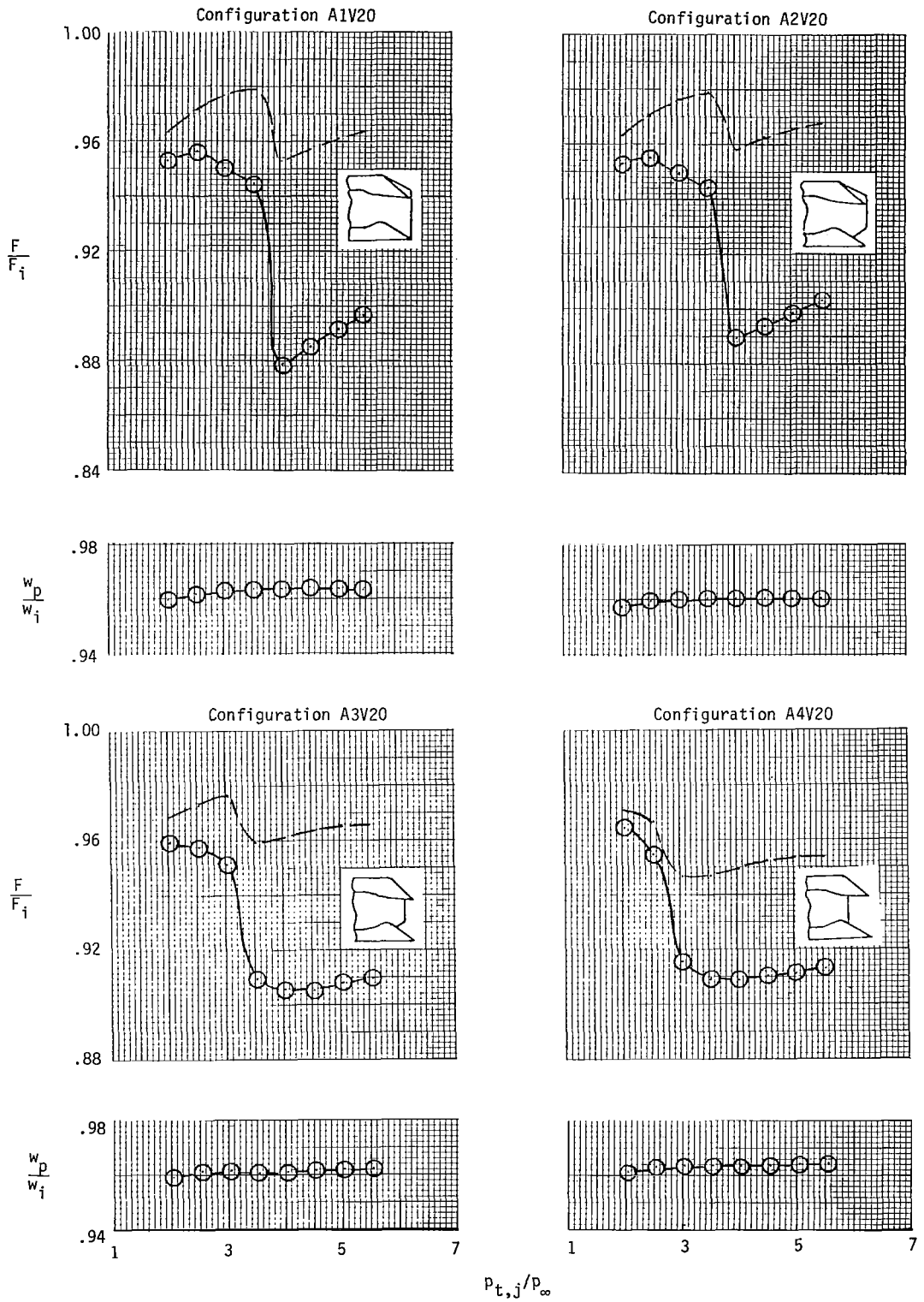

Figure 29.- Variation of nozzle thrust ratio and discharge coefficient with nozzle pressure ratio for AR = 2.012 nozzle vectored 20.26° with four sidewalls. Dashed lines indicate values of resultant thrust ratio F_r/F_i. A_e/A_t = 1.300.

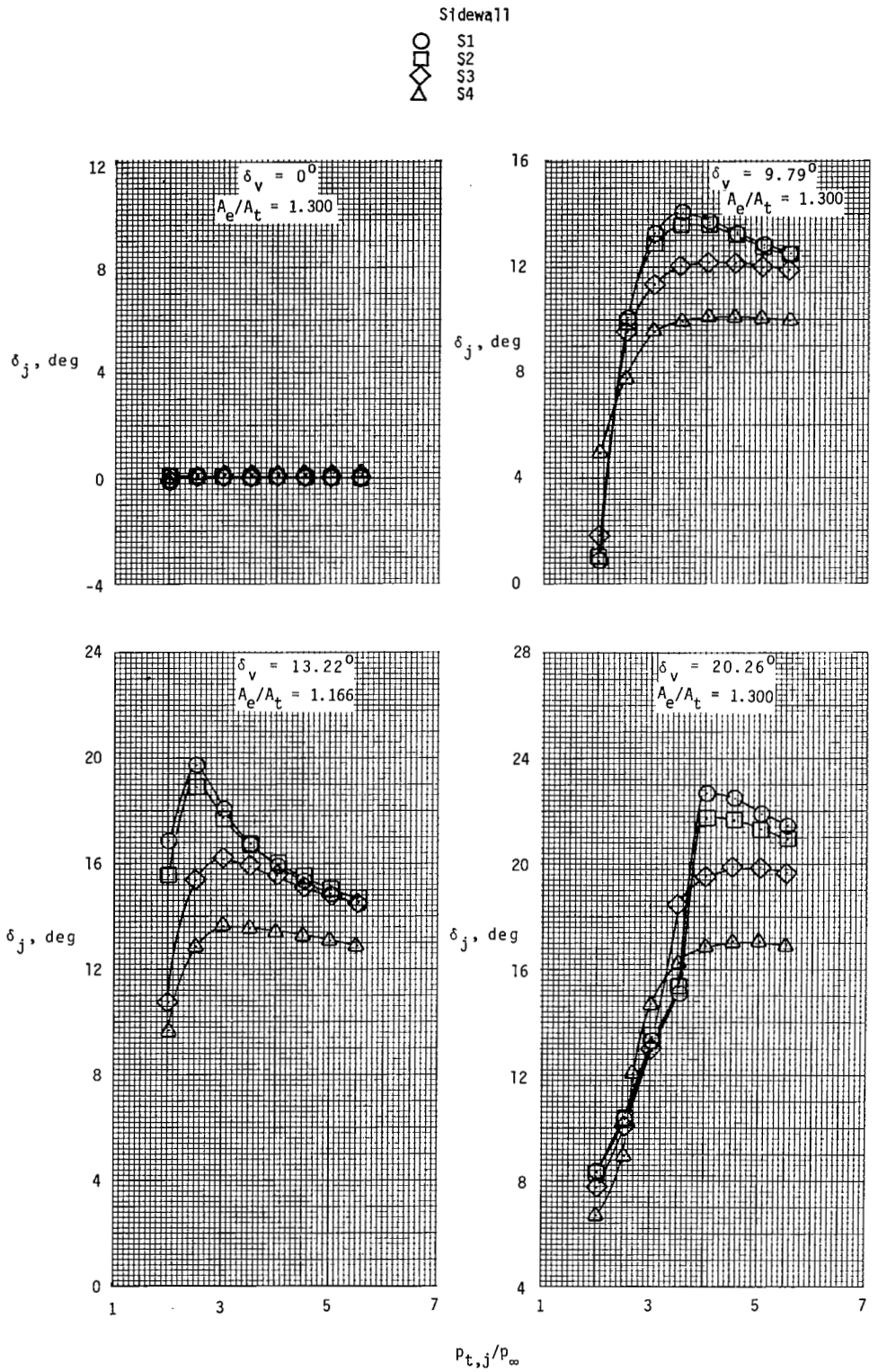

(a) Thrust vector angle.

Figure 30.- Effect of sidewall configuration on variation of thrust vector angle and pitching-moment ratio with nozzle pressure ratio for AR = 2.012 nozzles.

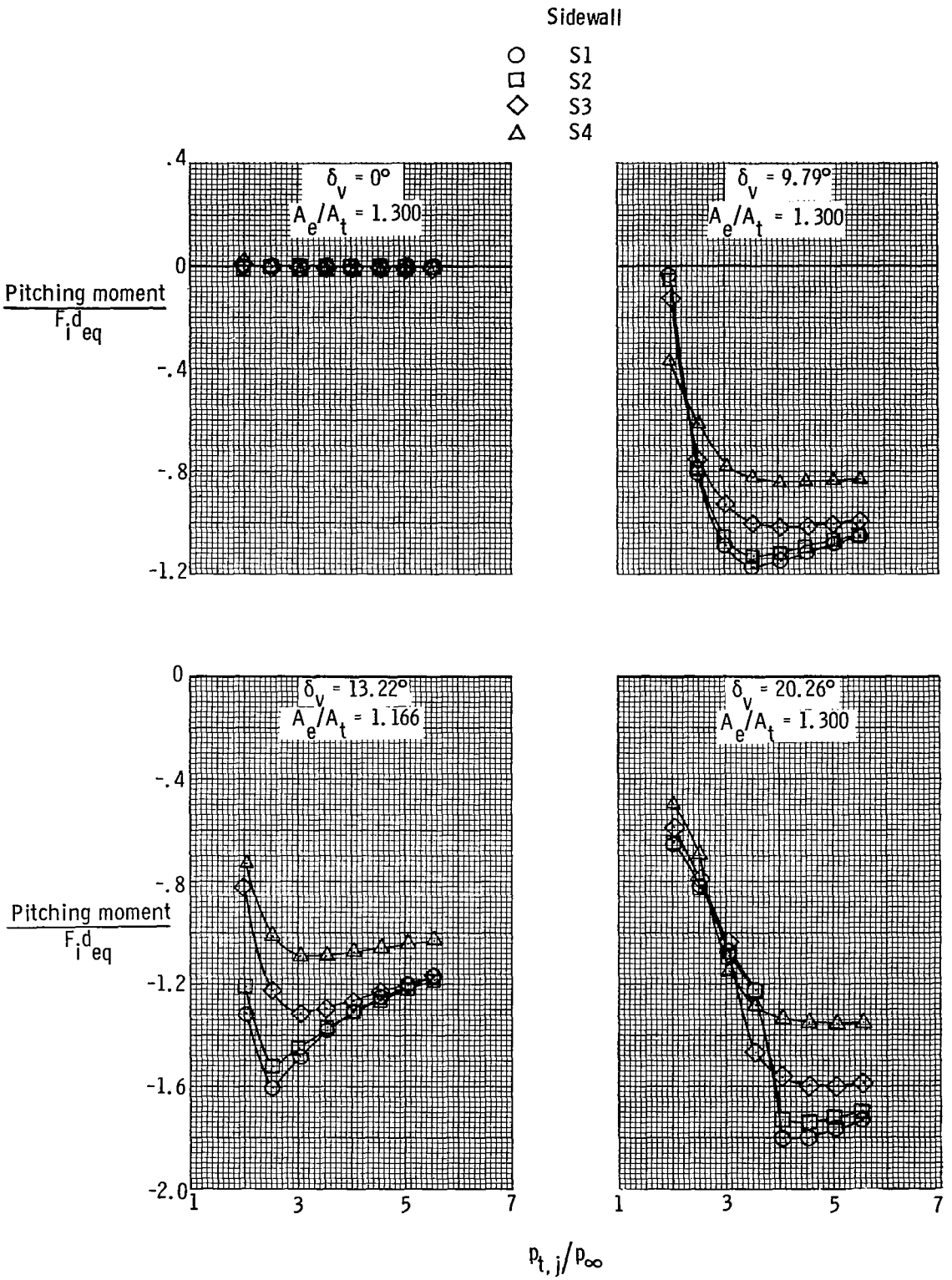

(b) Pitching-moment ratio.

Figure 30.- Concluded.

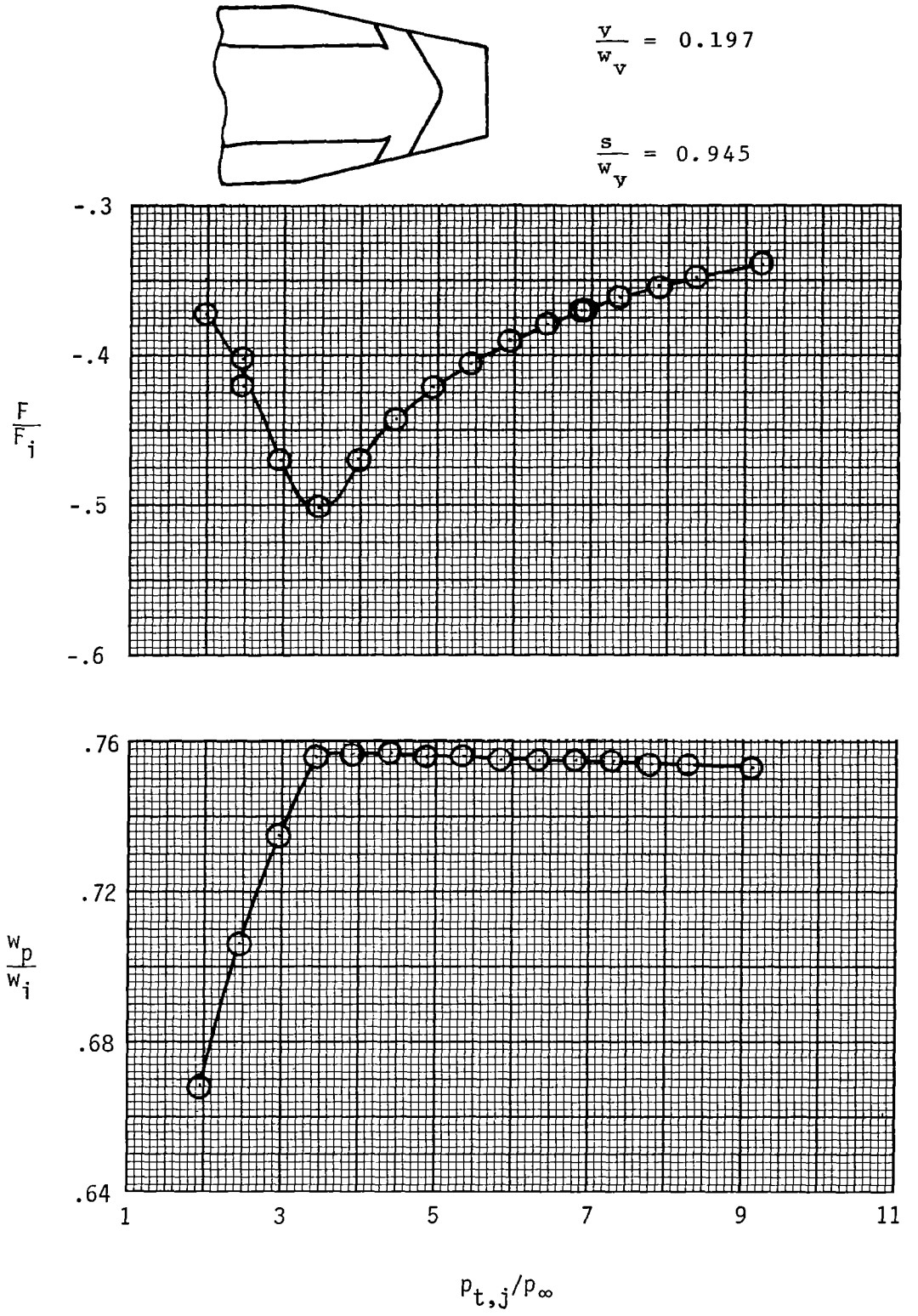

(a) Configuration R1.

Figure 31.- Variation of nozzle thrust ratio and discharge coefficient with nozzle pressure ratio for six thrust-reverser configurations.

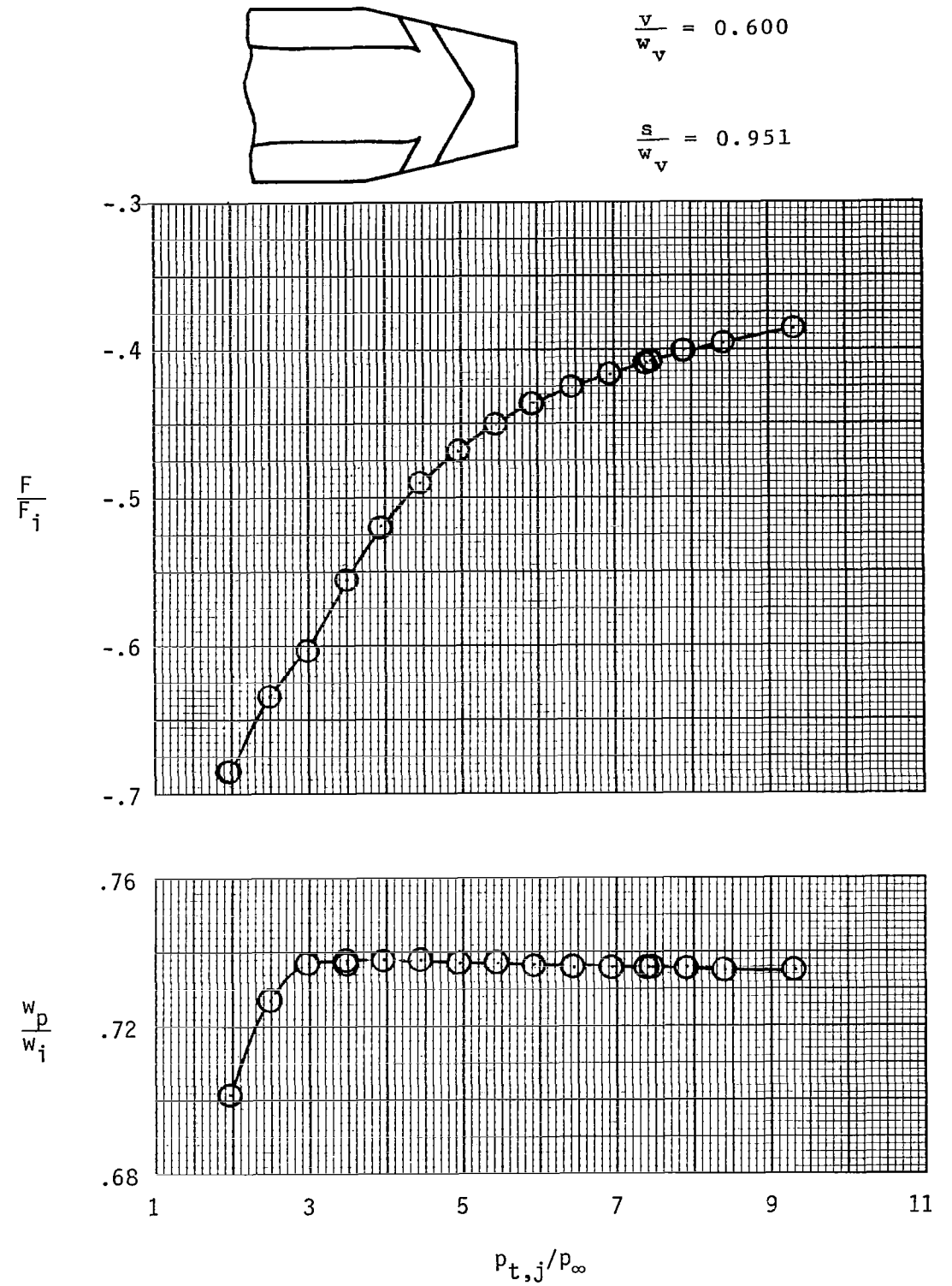

(b) Configuration R2.

Figure 31.- Continued.

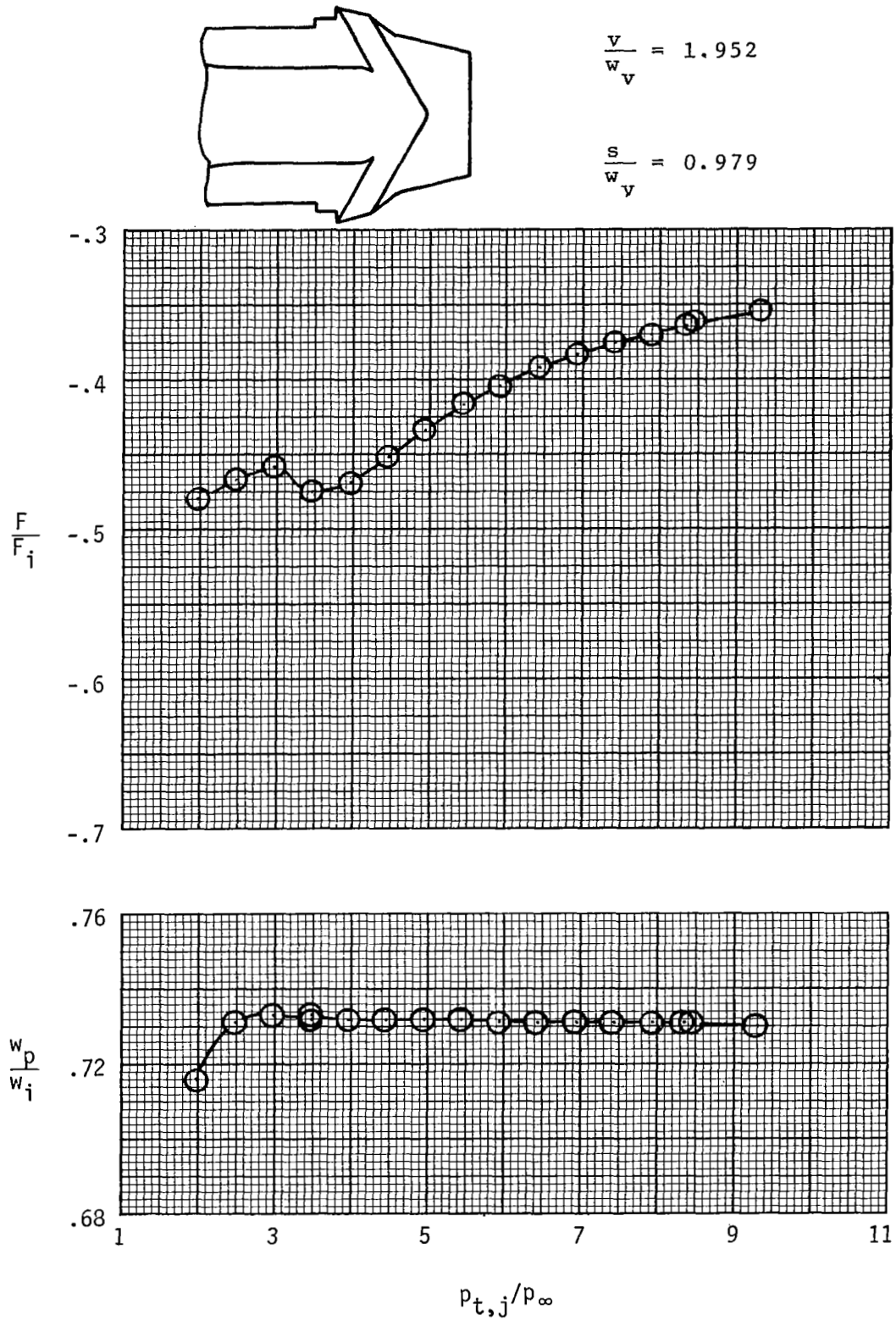

(c) Configuration R3.

Figure 31.- Continued.

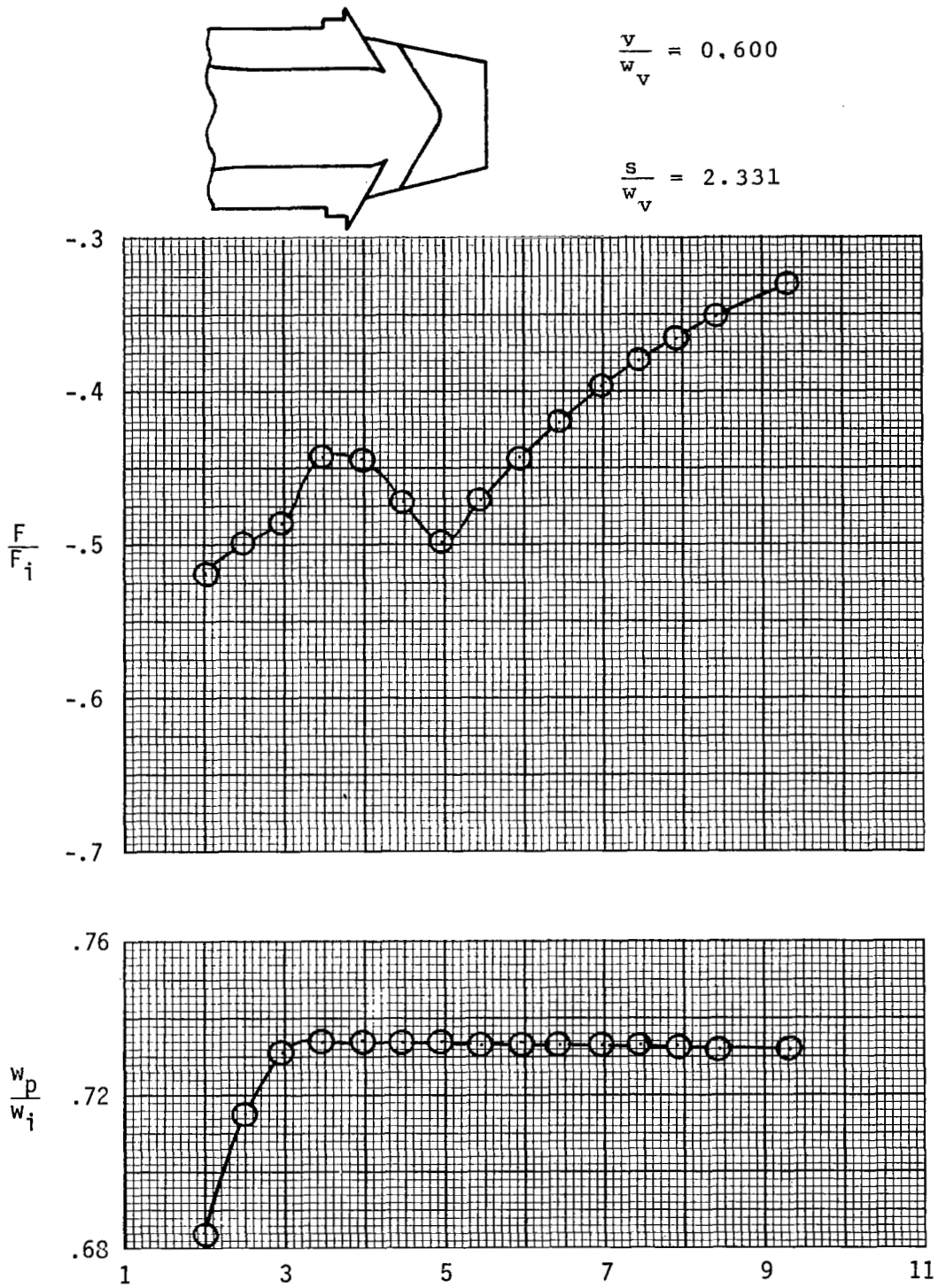

(d) Configuration R4.

Figure 31.- Continued.

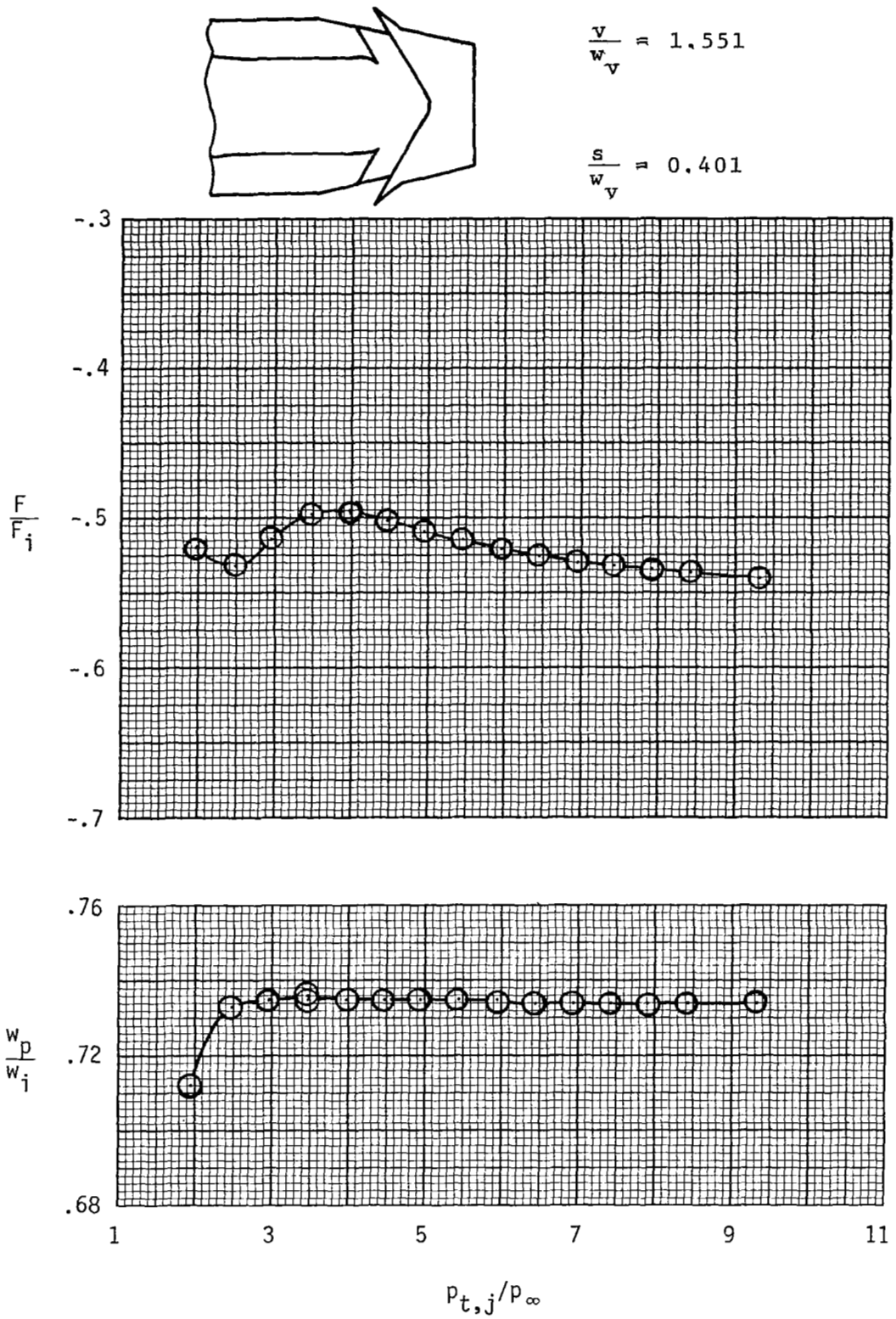

(e) Configuration R5.

Figure 31.- Continued.

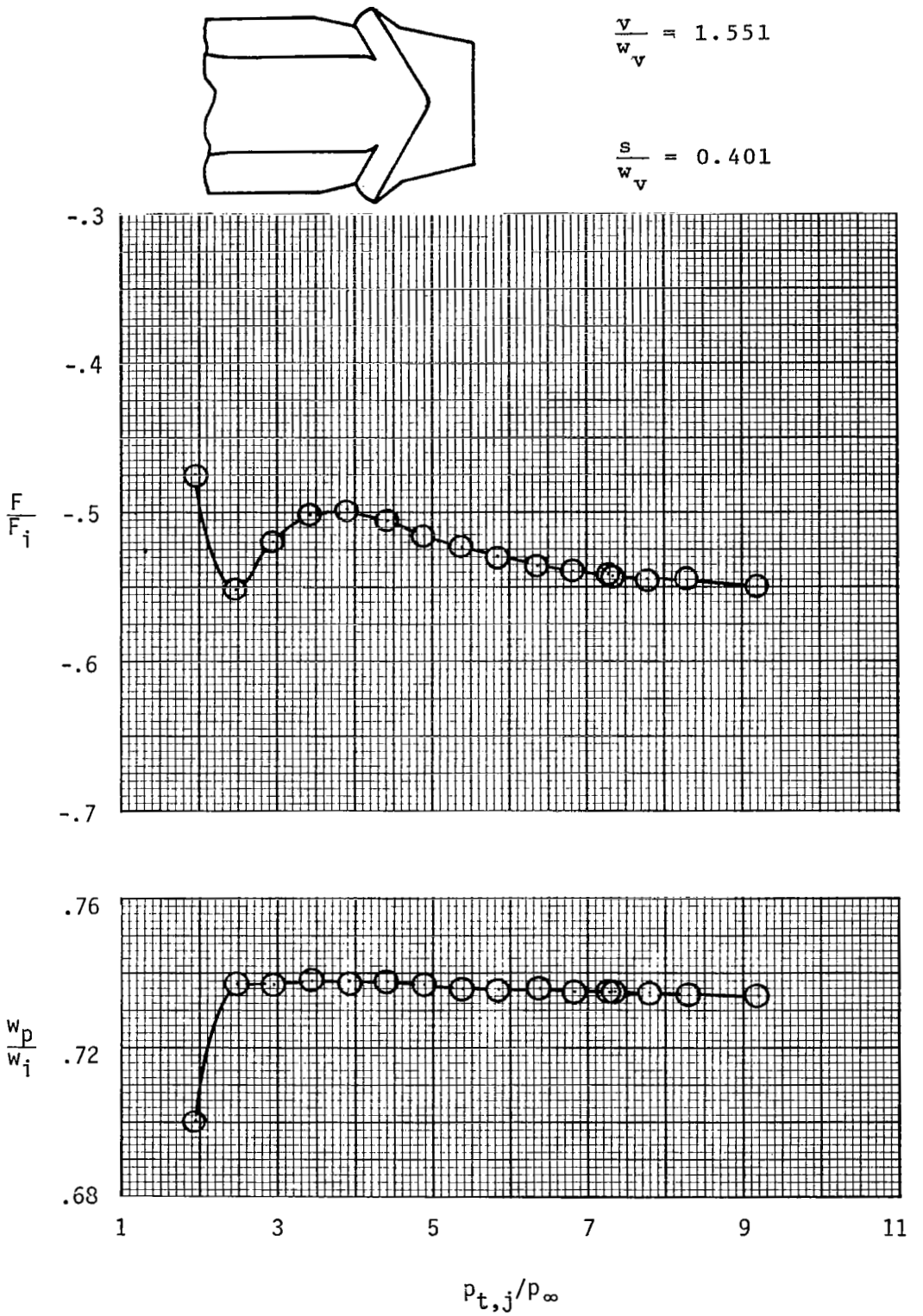

(f) Configuration R6.

Figure 31.- Concluded.

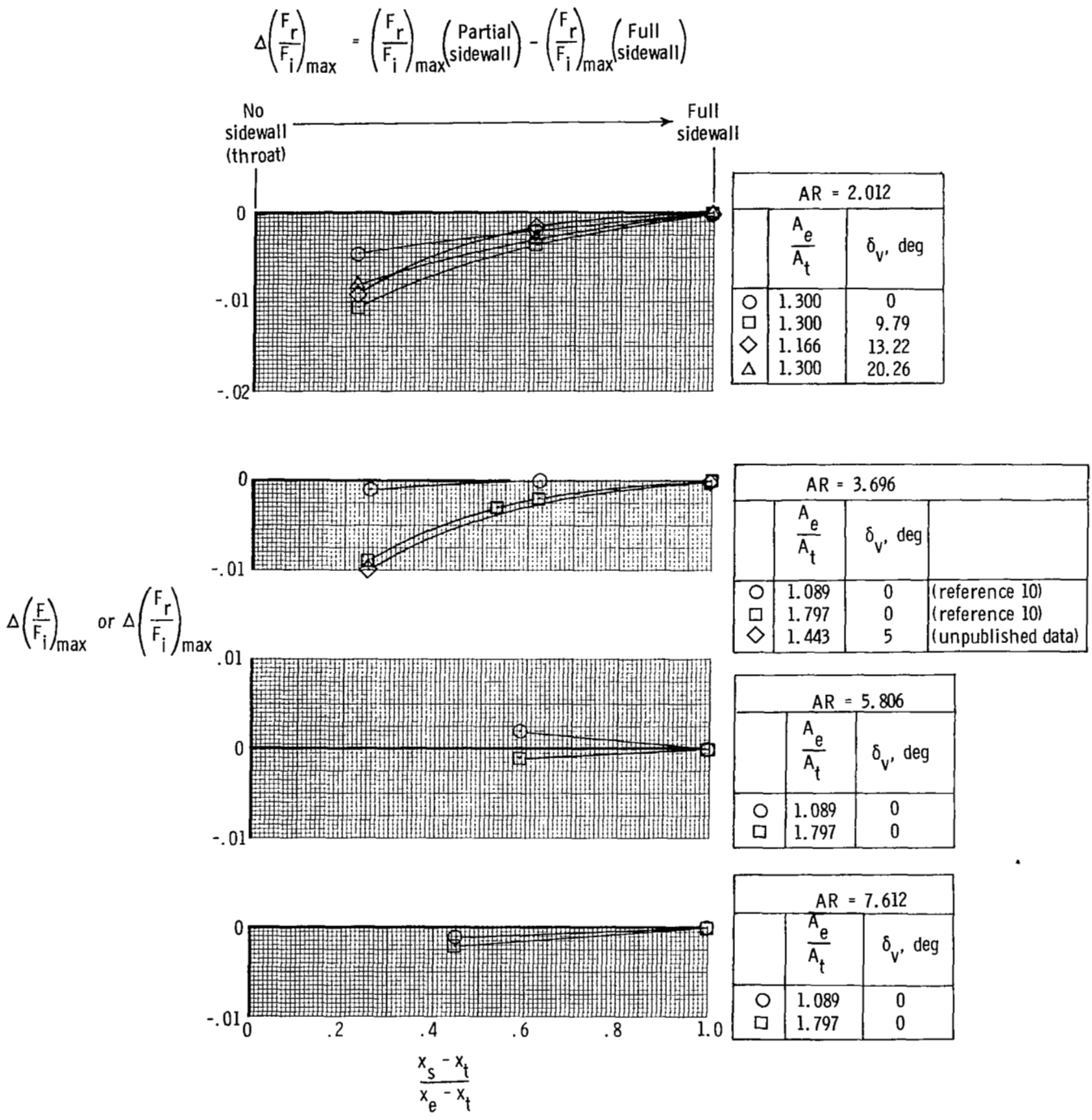

Figure 32.- Incremental effect of reduction in nozzle sidewall length (cutback) on maximum thrust ratio (or maximum resultant thrust ratio for vectored nozzles) for nozzles of various throat aspect ratios and expansion ratios.

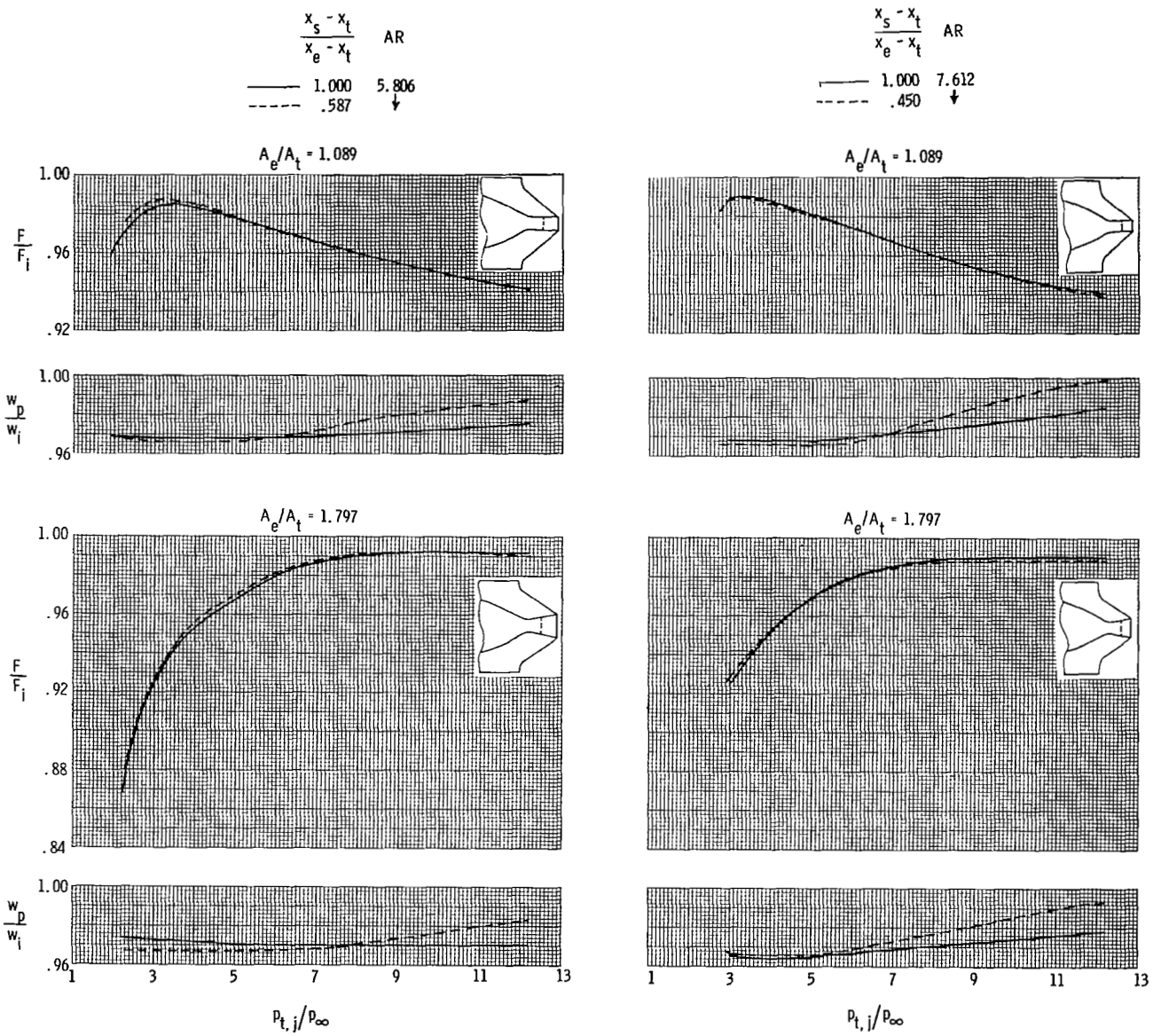

Figure 33.- Effect of sidewall length (cutback) on variation of nozzle thrust ratio and discharge coefficient with nozzle pressure ratio for AR = 5.806 and AR = 7.612 nozzles.

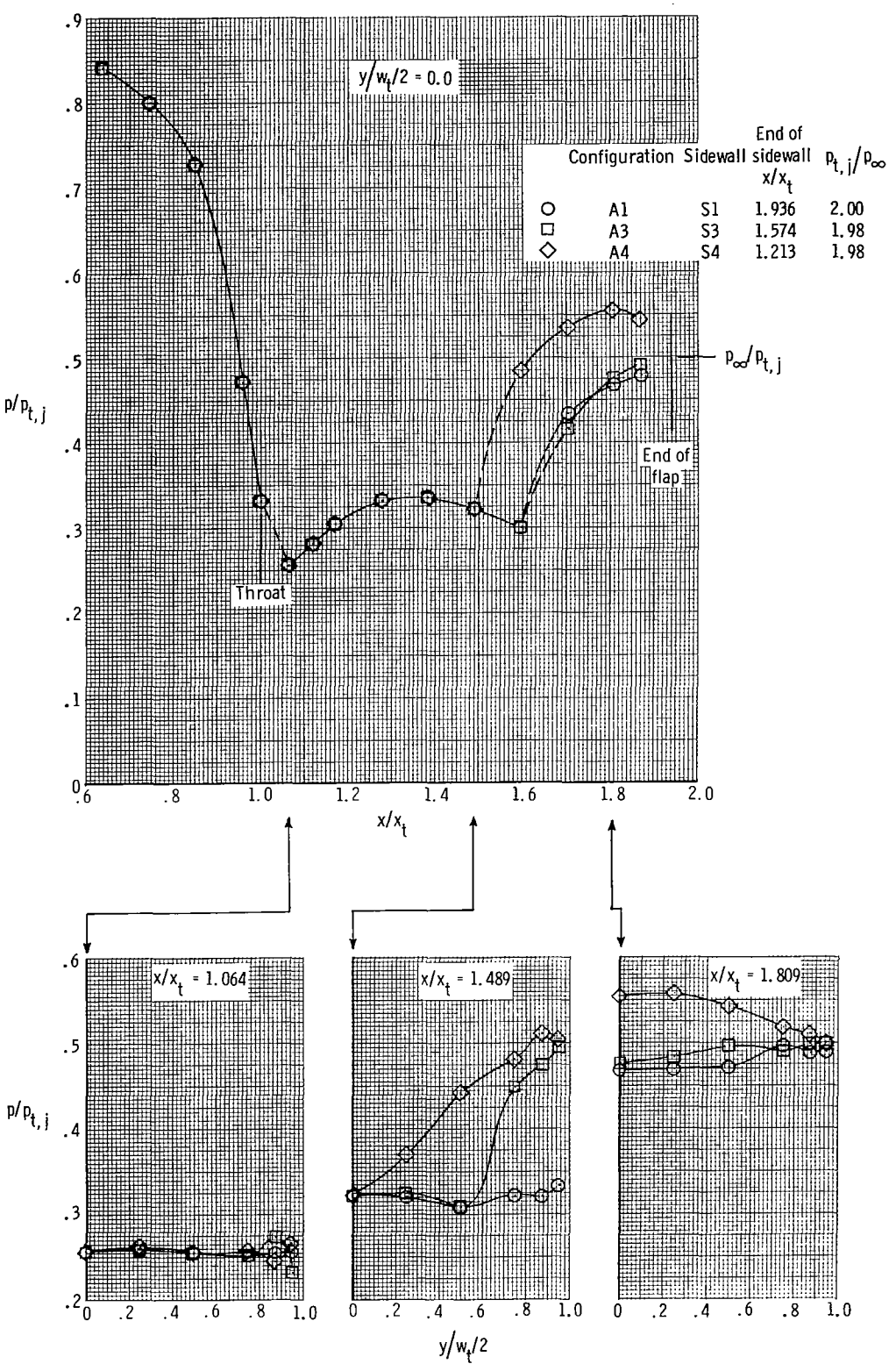

(a) $p_{t,j}/p_\infty \approx 2.00$.

Figure 34.- Effect of nozzle sidewall cutback on flap pressure distribution for an unvectored nozzle with an aspect ratio of 2.012. $A_e/A_t = 1.300$.

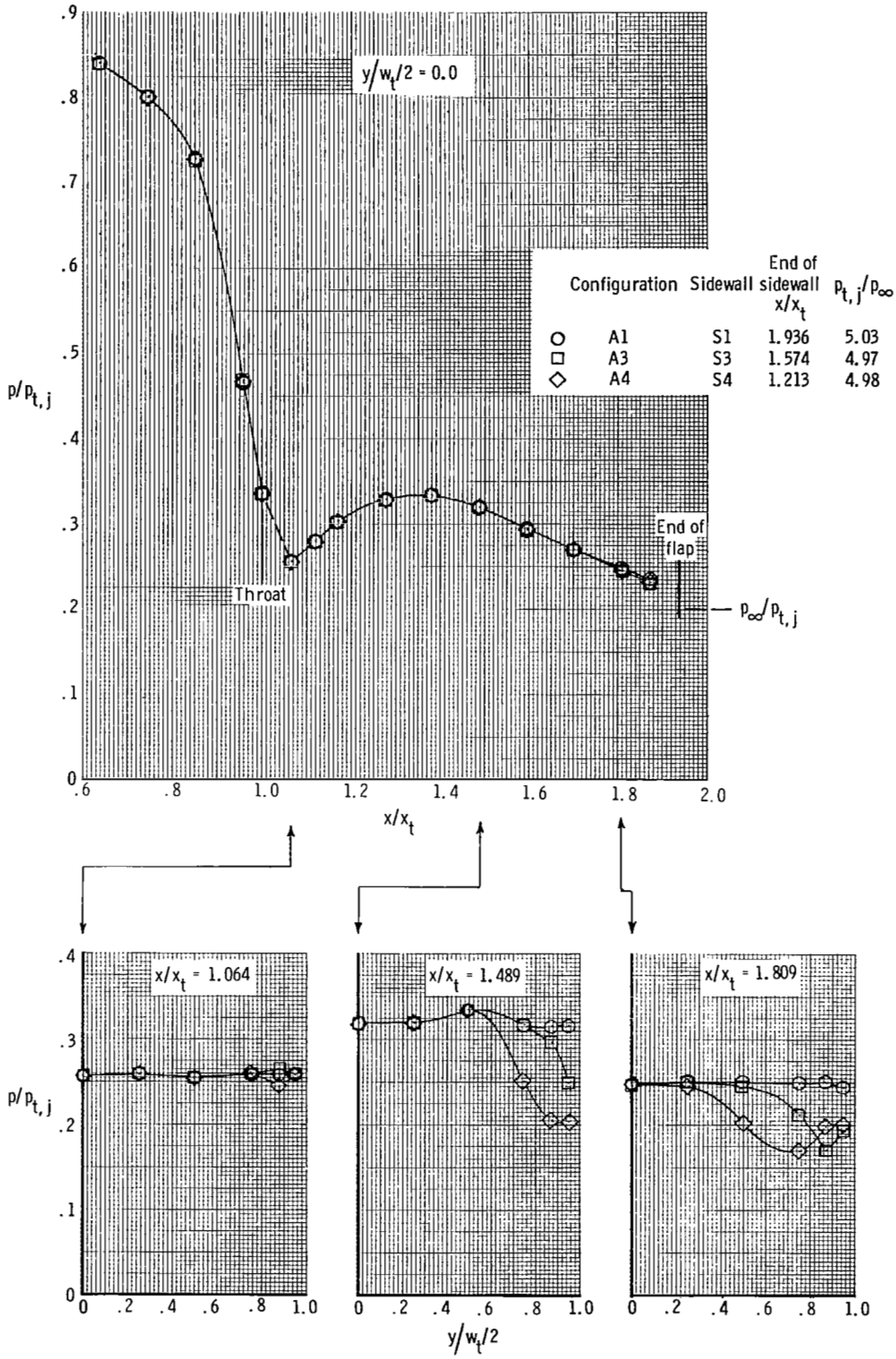

(b) $p_{t,j}/p_\infty \approx 5.00$.

Figure 34.- Concluded.

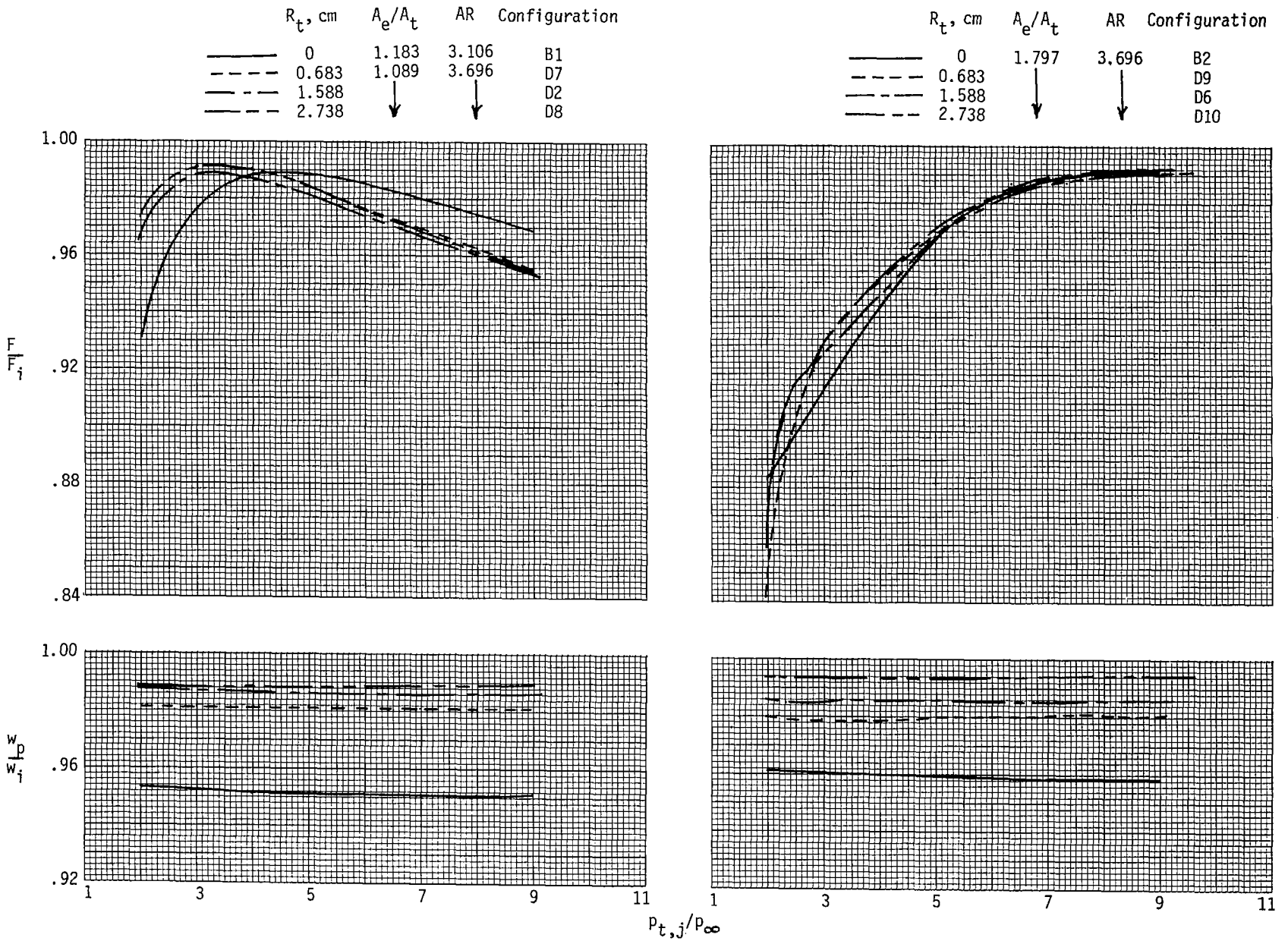

(a) Internal performance comparisons.

Figure 35.- Effect of throat radius on the variation of nozzle thrust ratio and discharge coefficient for low and high expansion ratio nozzles.

$$\Delta\left(\frac{w_p}{w_i}\right) = \left(\frac{w_p}{w_i}\right)_{R_t} - \left(\frac{w_p}{w_i}\right)_{R_t = 2.738\text{cm}}$$

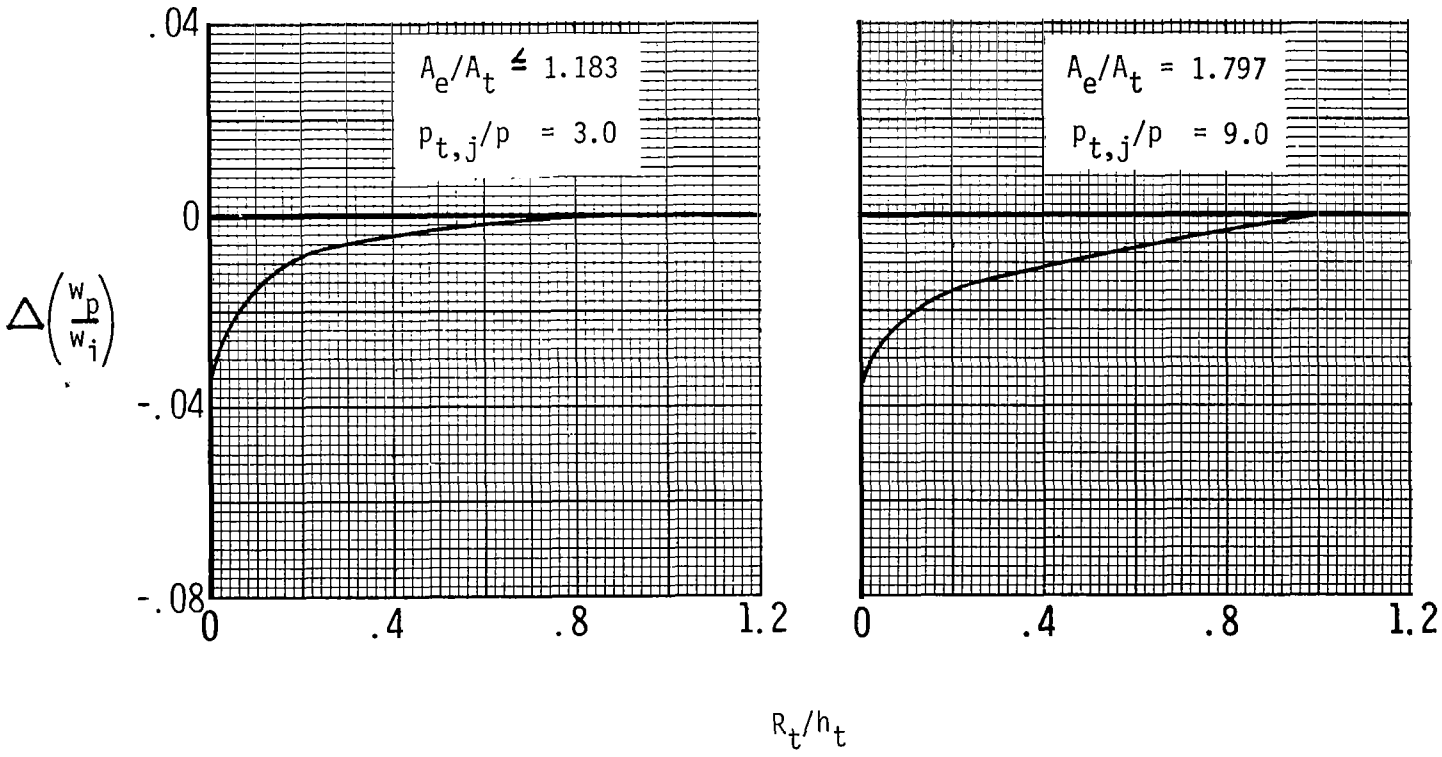

(b) $\Delta\left(\frac{w_p}{w_i}\right)$ due to changes in throat radius.

Figure 35.- Concluded.

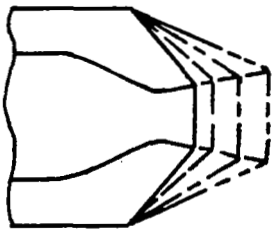

$\frac{A_e}{A_t}$	$\frac{x_e - x_t}{h_t}$	ρ, deg	Configuration	Design $p_{t,j}/p_\infty$
1.250	0.707	10.67	D3	4.25
1.400	1.099	10.83	D4	5.43
1.600	1.621	↓	D5	7.07
1.797	2.100	10.92	D6	8.79

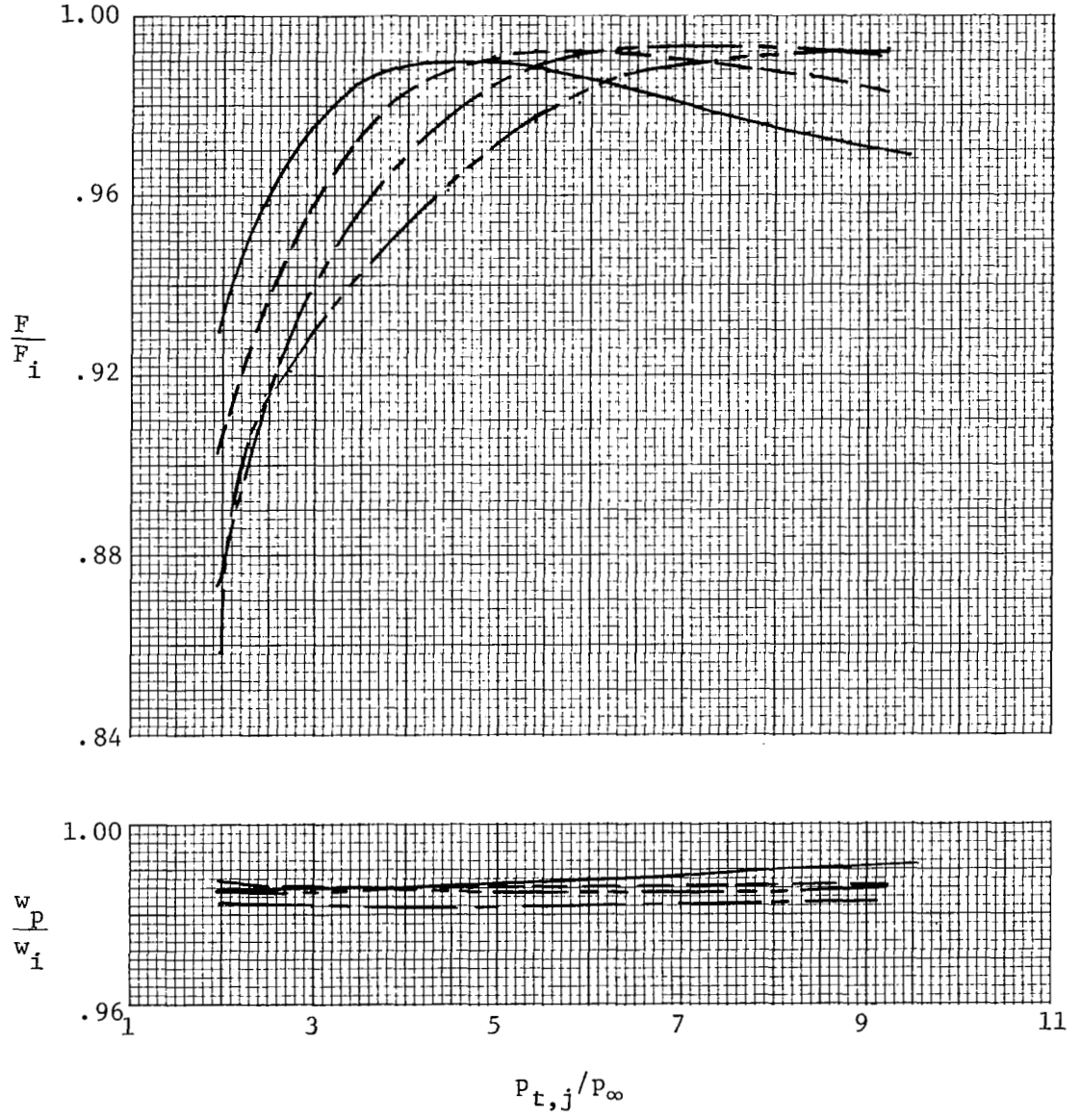

Figure 36.- Variation of nozzle thrust ratio and discharge coefficient with nozzle pressure ratio for four nozzle expansion ratios at approximately the same flap divergence angle (10.8°).

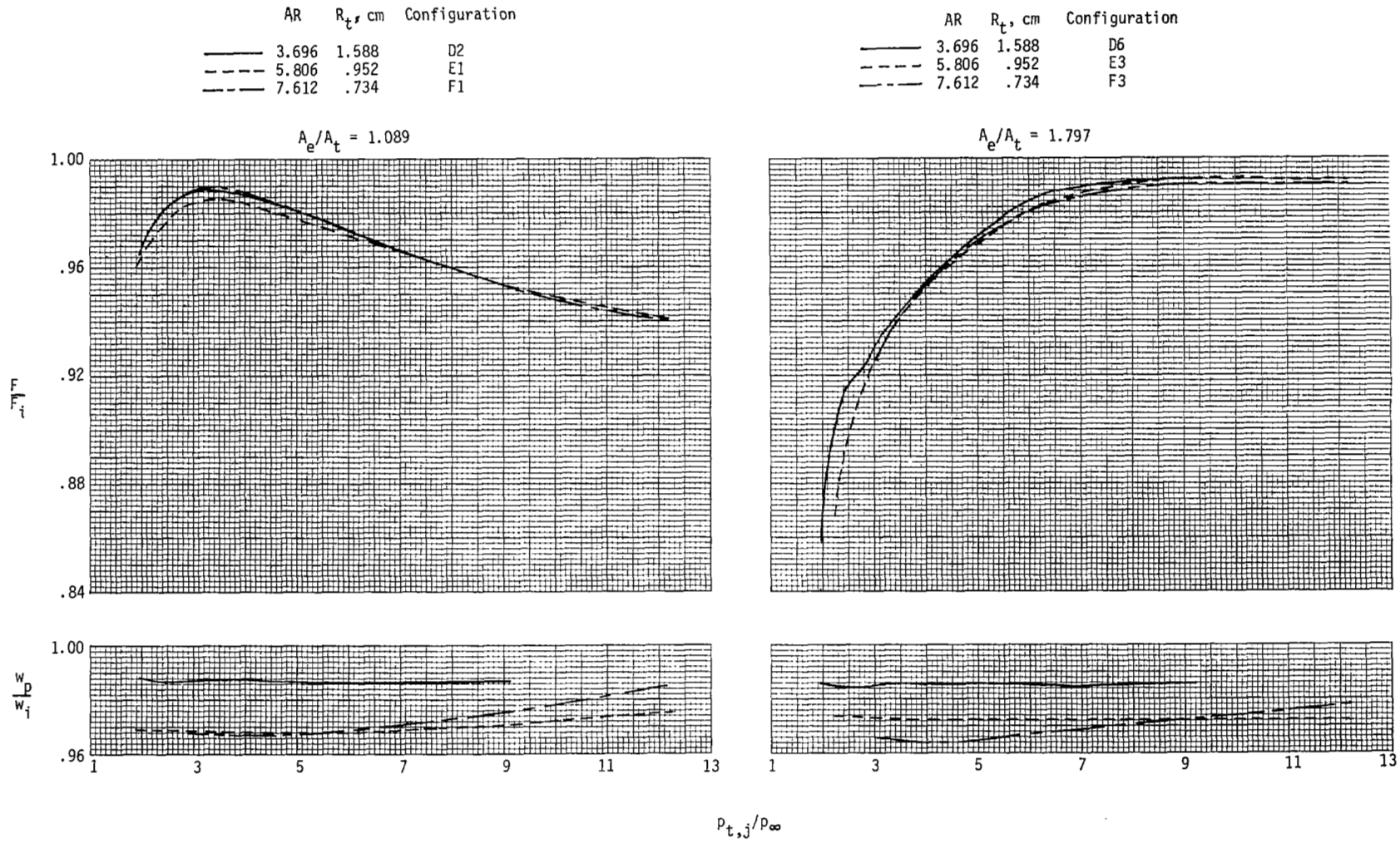

Figure 37.- Effect of throat aspect ratio on variation of nozzle thrust ratio and discharge coefficient with nozzle pressure ratio for low and high expansion ratios.

$$\Delta\left(\frac{F_r}{F_i}\right) = \left(\frac{F_r}{F_i}\right)_{\delta_v \neq 0°} - \left(\frac{F_r}{F_i}\right)_{\delta_v = 0°}$$

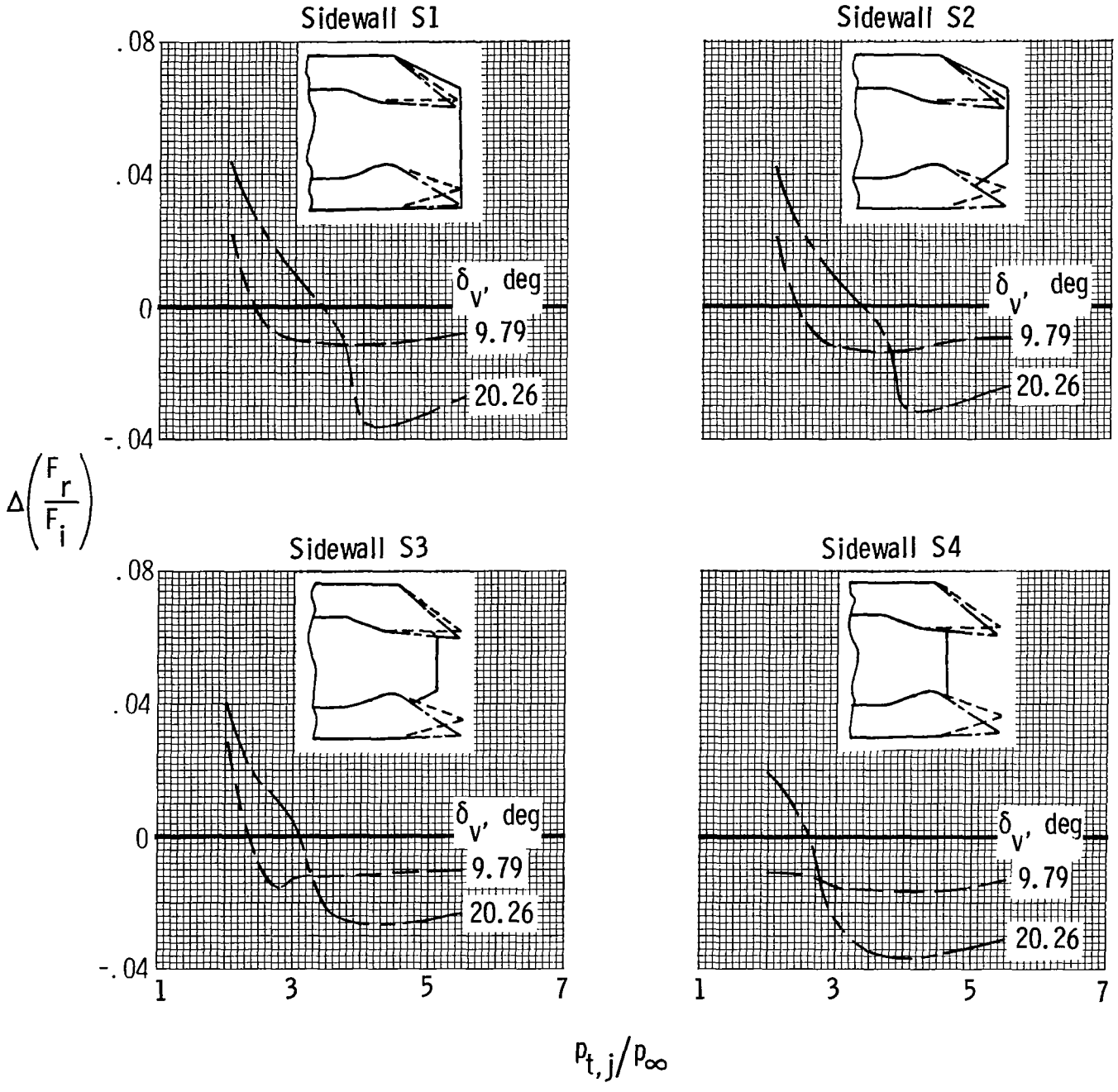

Figure 38.- Variation with nozzle pressure ratio of incremental resultant thrust ratio due to nozzle vector angle for given sidewall configurations. AR = 2.012; A_e/A_t = 1.300.

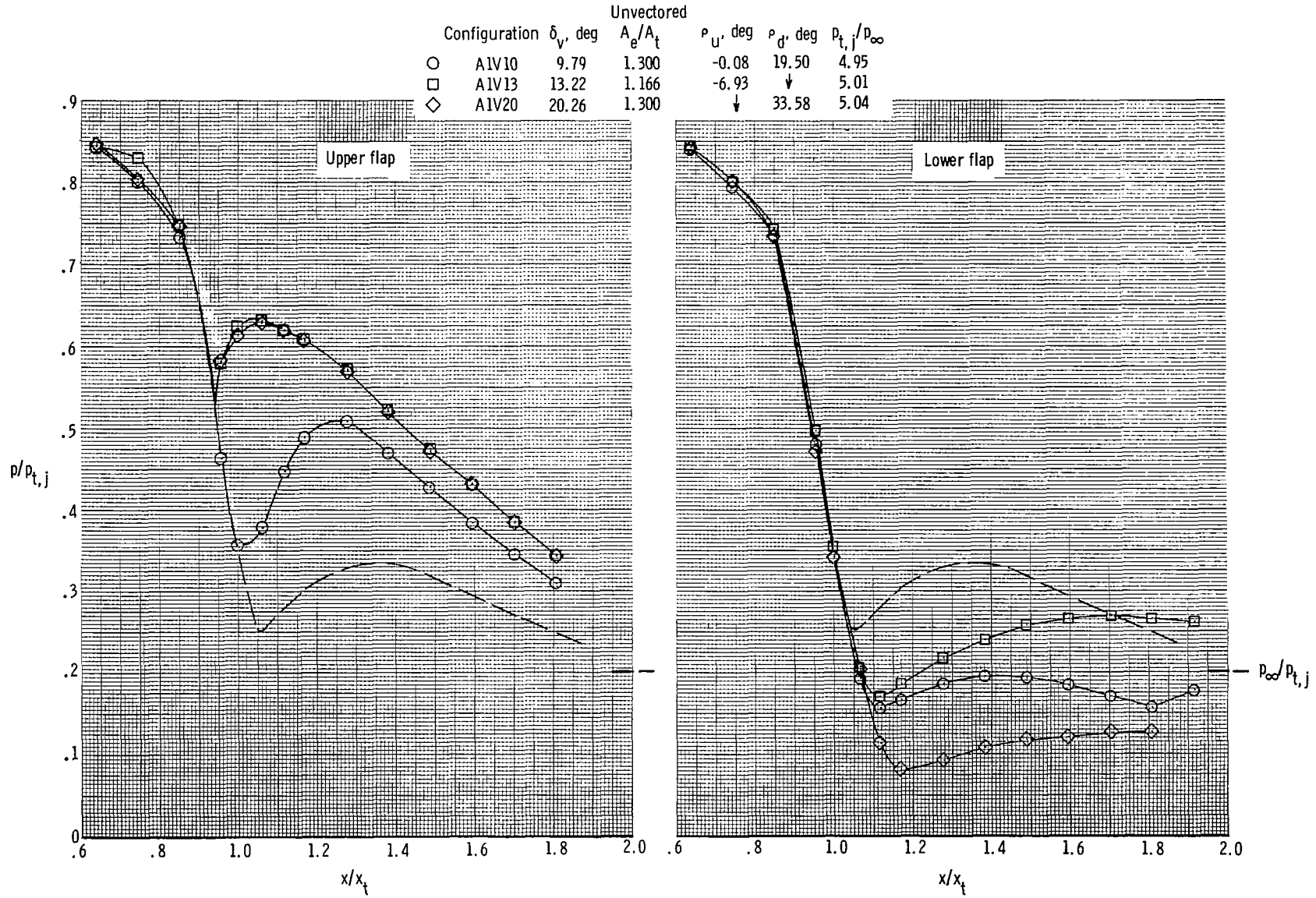

Figure 39.- Effect of nozzle flap angle on flap centerline pressure distribution with full-length sidewalls. Dashed line indicates pressure distribution on flaps with $\delta_v = 0°$ and $\rho_u = \rho_d = 8°$.

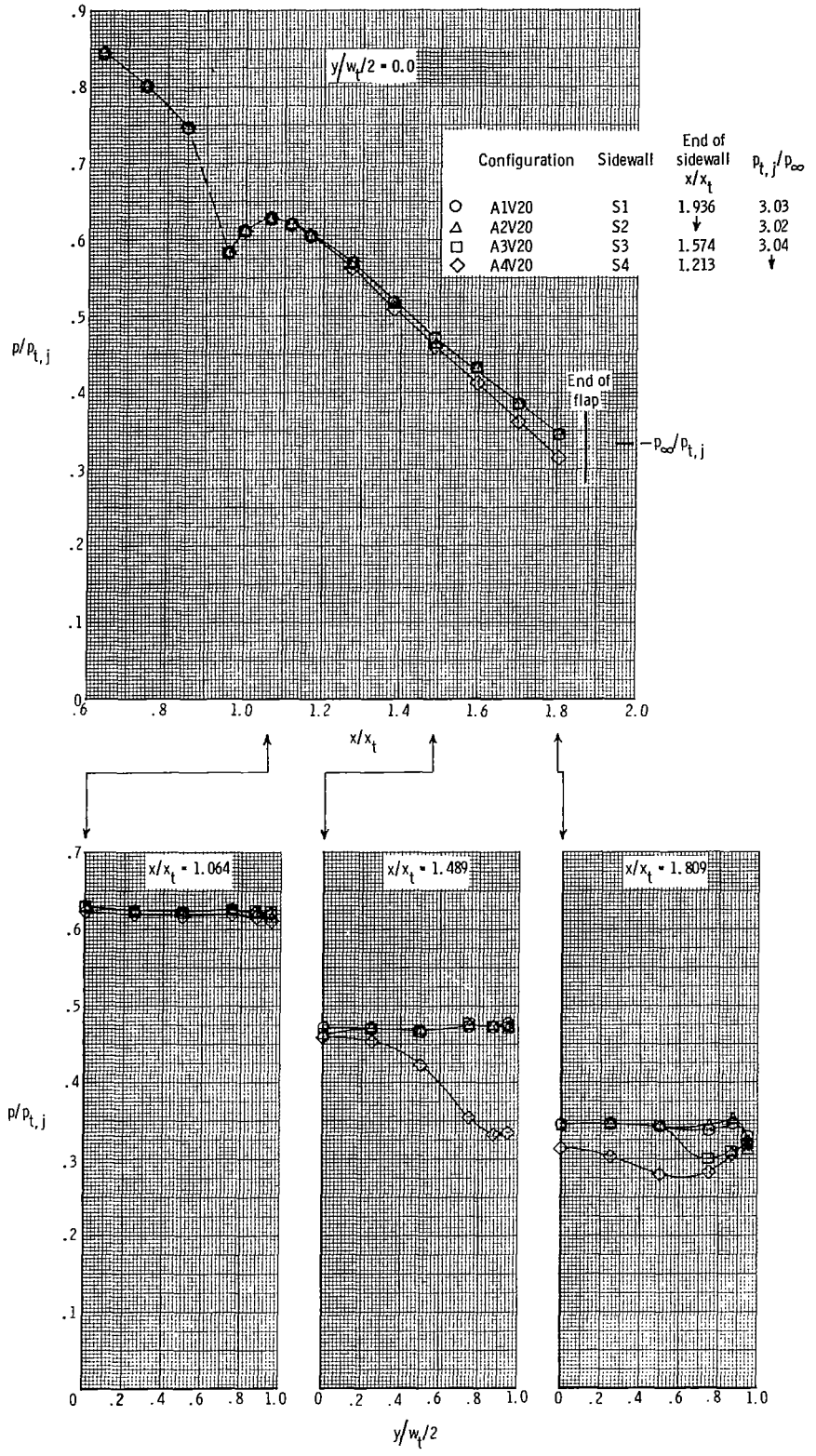

(a) Upper flap.

Figure 40.- Effect of nozzle sidewall length on flap pressure distribution for a nozzle vectored 20.26° at $p_{t,j}/p_\infty \approx 3$. Unvectored $A_e/A_t = 1.300$.

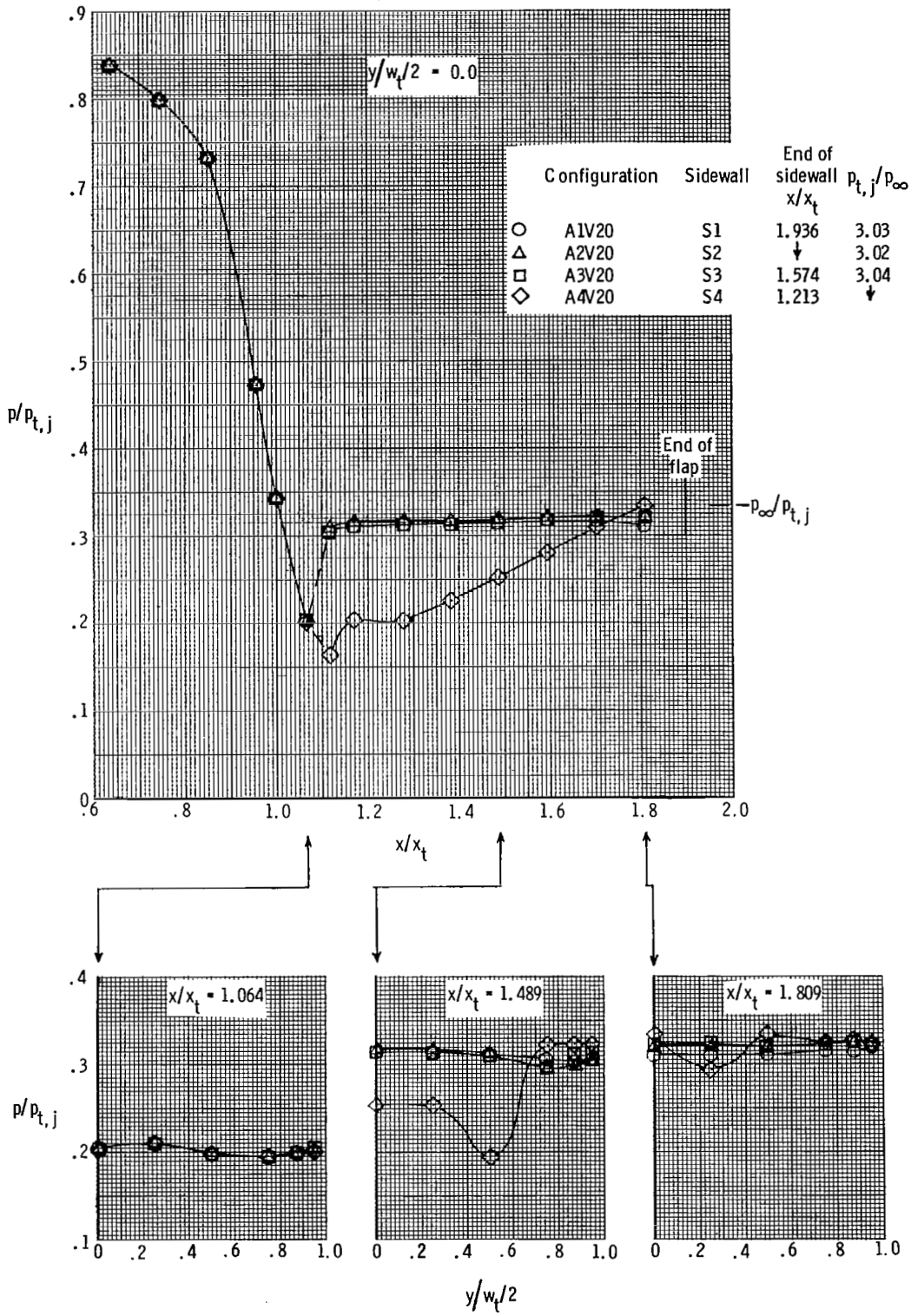

(b) Lower flap.

Figure 40.- Concluded.

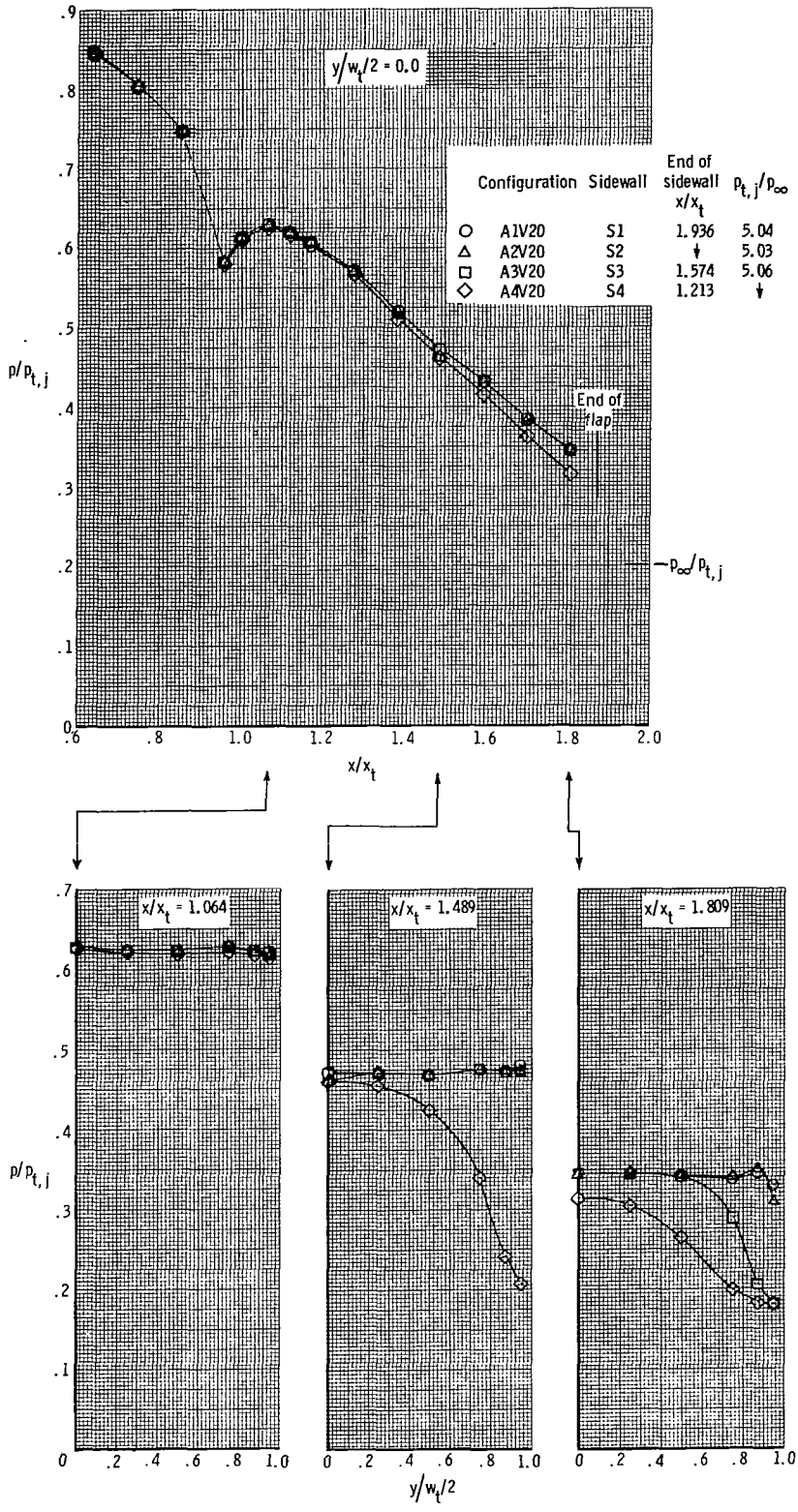

(a) Upper flap.

Figure 41.- Effect of nozzle sidewall length on flap pressure distribution for a nozzle vectored 20.26° at $p_{t,j}/p_\infty \approx 5$. Unvectored $A_e/A_t = 1.300$.

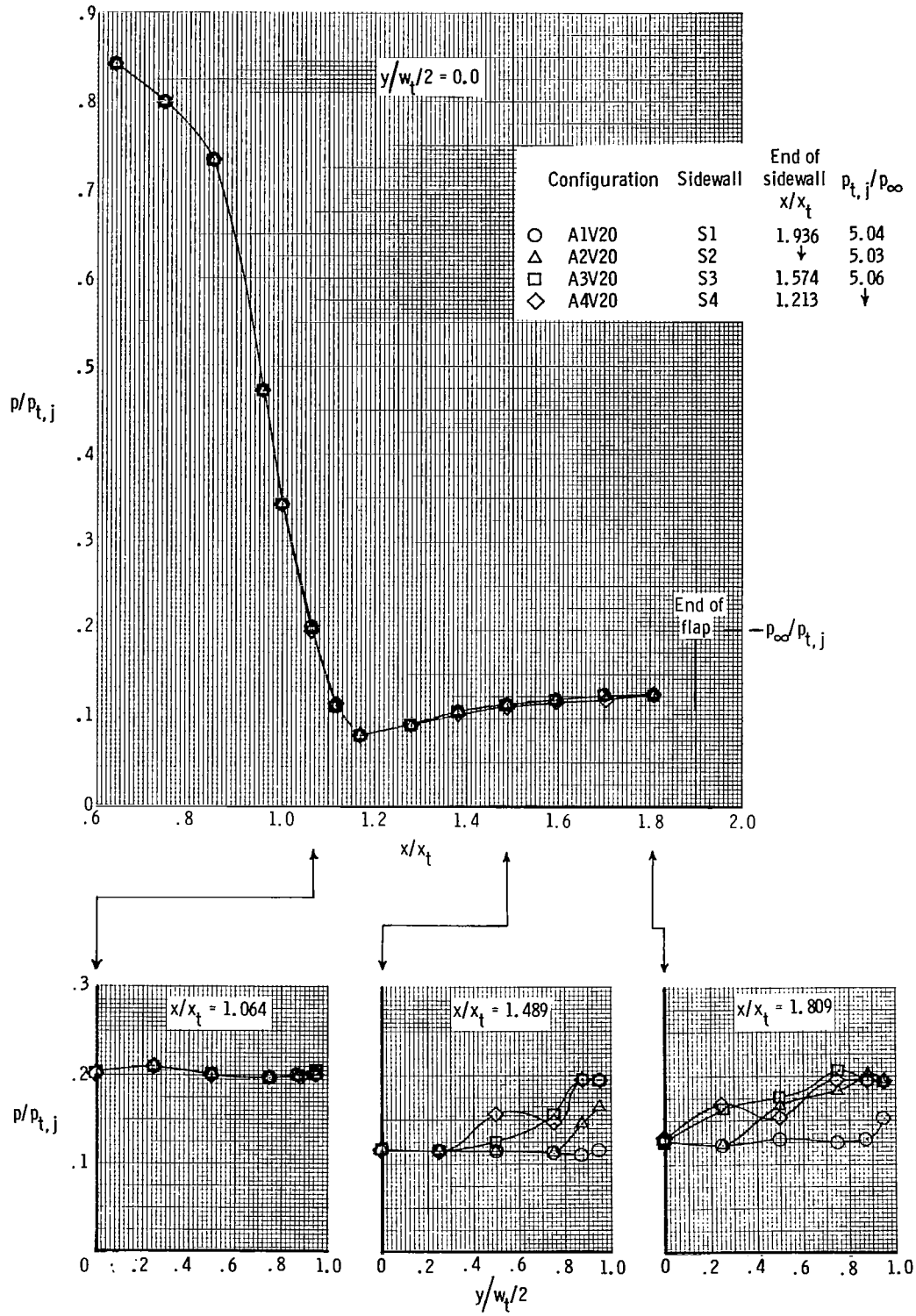

(b) Lower flap.

Figure 41.- Concluded.

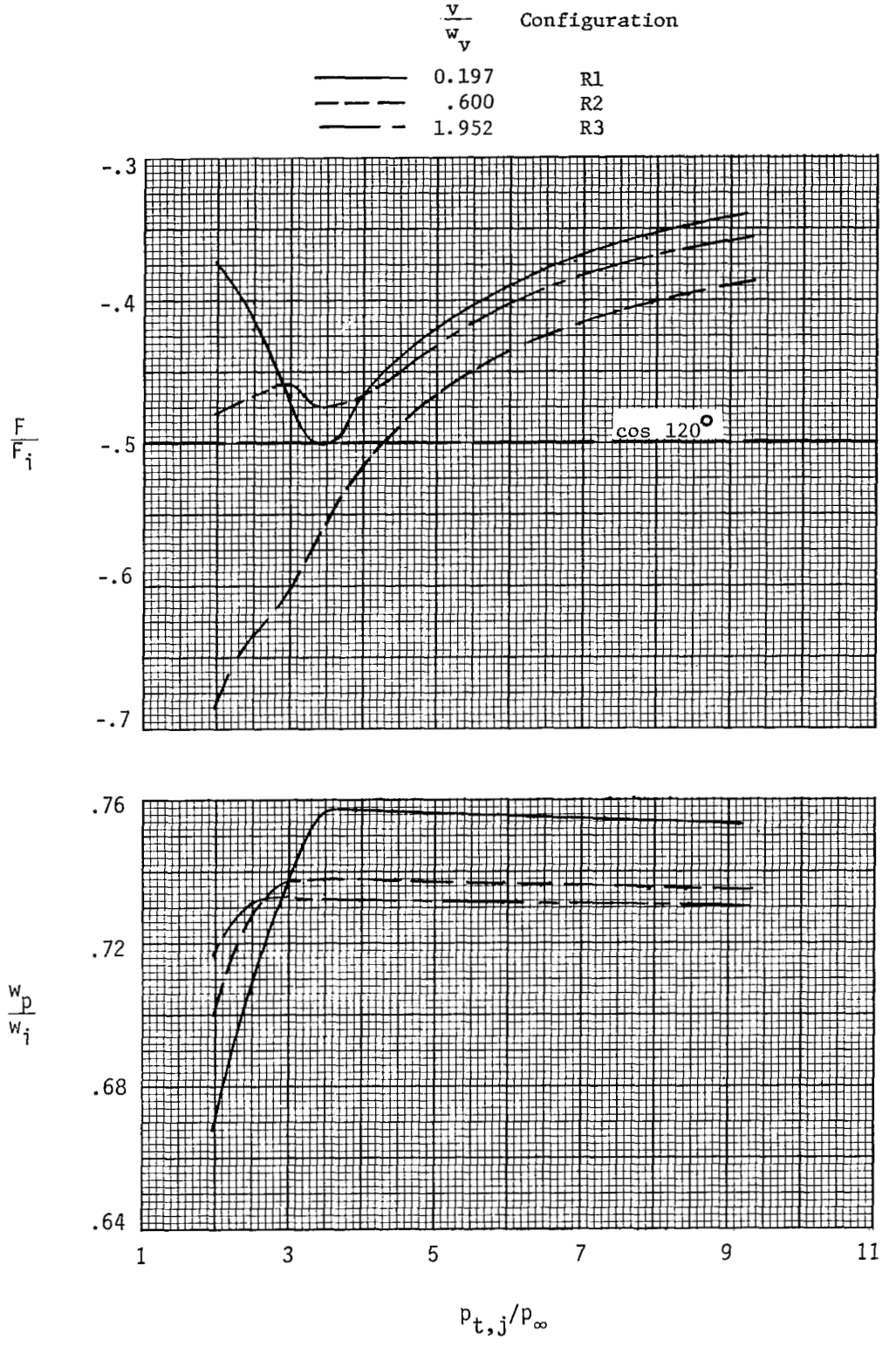

Figure 42.- Effect of thrust-reverser port passage length on variation of nozzle thrust ratio and discharge coefficient with nozzle pressure ratio.

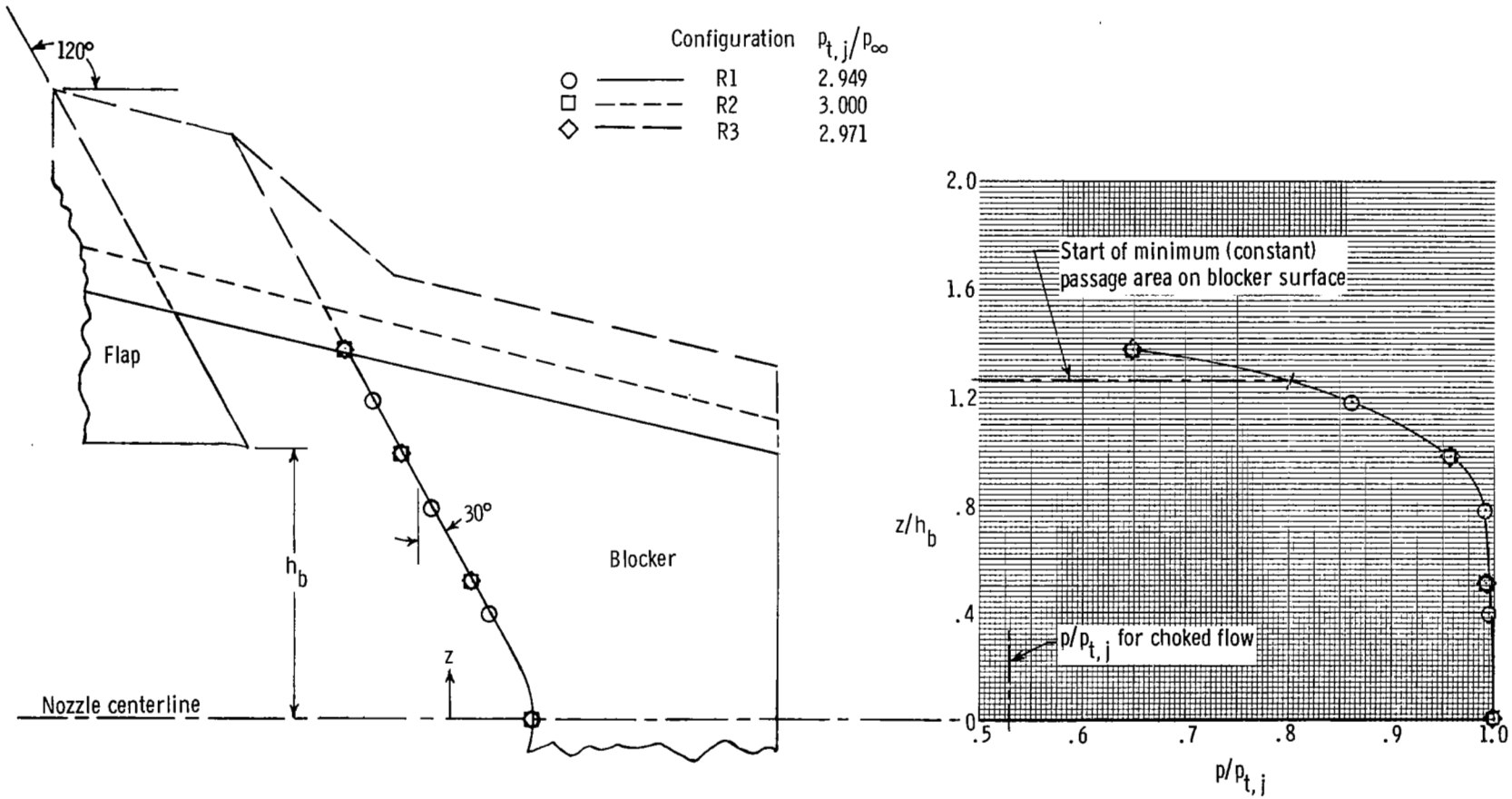

Figure 43.- Comparison of local pressure ratios on surface of thrust-reverser blocker for configurations R1, R2, and R3 at a nozzle pressure ratio of approximately 3.0.

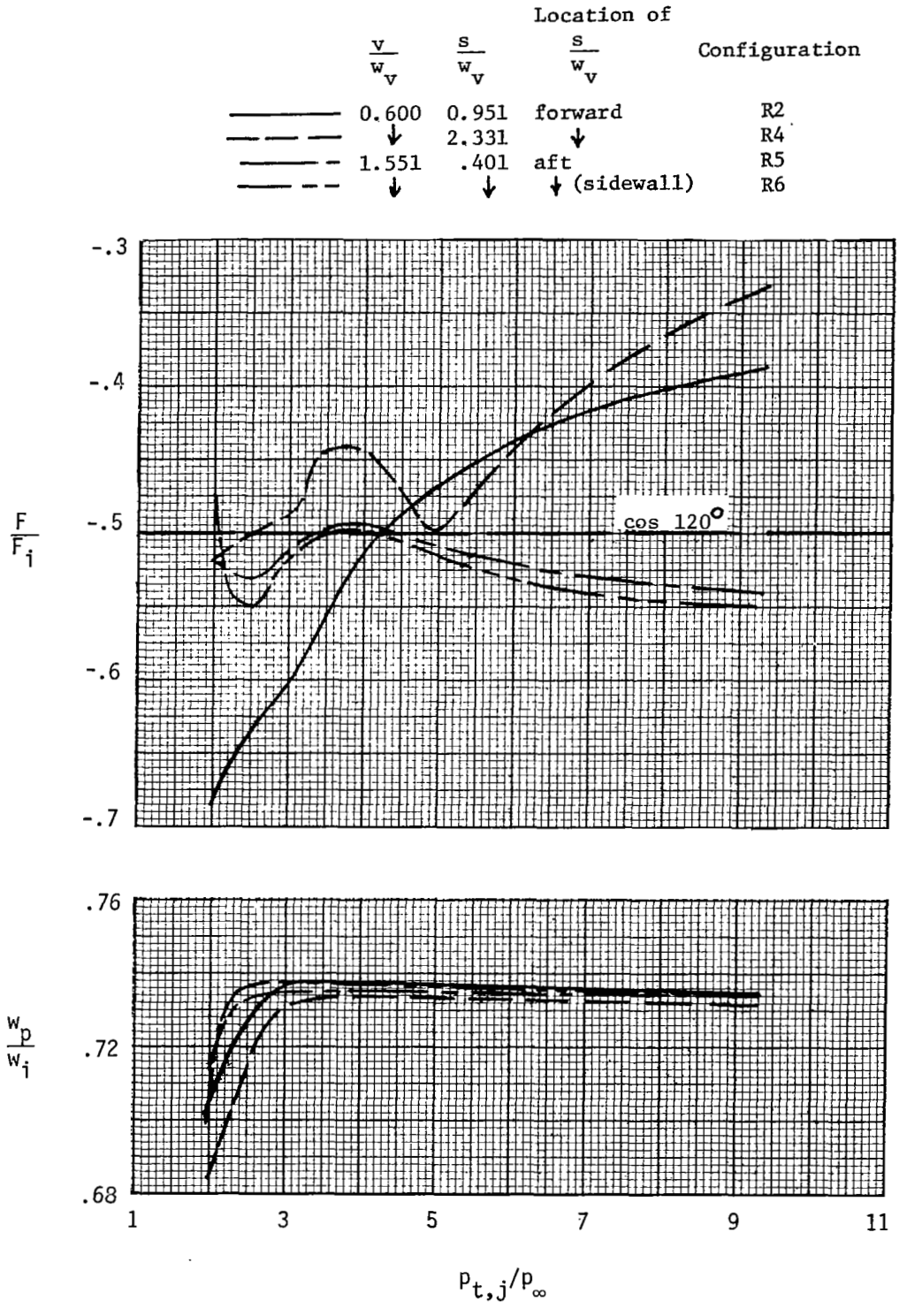

Figure 44.- Effect of thrust-reverser port doors on variation of nozzle thrust ratio and discharge coefficient with nozzle pressure ratio.

1. Report No.	2. Government Accession No.	3. Recipient's Catalog No.
NASA TP-2253		

4. Title and Subtitle	5. Report Date
STATIC INTERNAL PERFORMANCE INCLUDING THRUST VECTORING AND REVERSING OF TWO-DIMENSIONAL CONVERGENT-DIVERGENT NOZZLES	February 1984
	6. Performing Organization Code 505-43-23-01

7. Author(s)	8. Performing Organization Report No.
Richard J. Re and Laurence D. Leavitt	L-15671
	10. Work Unit No.

9. Performing Organization Name and Address	11. Contract or Grant No.
NASA Langley Research Center Hampton, VA 23665	
	13. Type of Report and Period Covered
12. Sponsoring Agency Name and Address	Technical Paper
National Aeronautics and Space Administration Washington, DC 20546	14. Sponsoring Agency Code

15. Supplementary Notes

16. Abstract

The effects of geometric design parameters on two-dimensional convergent-divergent nozzles were investigated at nozzle pressure ratios up to 12 in the static test facility adjacent to the Langley 16-Foot Transonic Tunnel. Forward-flight (dry and afterburning power settings), vectored-thrust (afterburning power setting), and reverse-thrust (dry power setting) nozzles were investigated. The nozzles had thrust vector angles from 0° to 20.26°, throat aspect ratios of 3.696 to 7.612, throat radii from sharp to 2.738 cm, expansion ratios from 1.089 to 1.797, and various sidewall lengths. The results of this investigation indicate that unvectored two-dimensional convergent-divergent nozzles have static internal performance comparable to axisymmetric nozzles with similar expansion ratios.

17. Key Words (Suggested by Author(s))	18. Distribution Statement
Nonaxisymmetric nozzles Internal performance Two-dimensional convergent-divergent Thrust vectoring Thrust reversing	Unclassified - Unlimited Subject Category 02

19. Security Classif. (of this report)	20. Security Classif. (of this page)	21. No. of Pages	22. Price
Unclassified	Unclassified	109	A06

For sale by the National Technical Information Service, Springfield, Virginia 22161